Spontaneous Recombination in Group-III Nitride Quantum Wells

Der Gemeinsamen Naturwissenschaftlichen Fakulität
der Technischen Universität Carolo-Wilhelmina
zu Braunschweig
zur Erlangen des Grades eines
Doktors der Naturwissenschaften
(Dr.rer.nat.)
genehmigte
D i s s e r t a t i o n

von

Jin Seo Im

aus Seoul, Republik Korea

1. Referent:	Prof. Dr. A. Hangleiter
2. Referent:	Prof. Dr. E. O. Göbel
eingereicht am:	31.08.2000
mündliche Prüfung am:	24.11.2000
Druckjahr:	2001

Vorabveröffentlichungen der Dissertation

Teilergebnisse aus dieser Arbeit wurden mit Genehmigung der Gemeinsamen Naturwissenschaften Fakulität, vertreten durch die Mentorin oder den Mentor/die Betreuerin oder den Betreuer der Arbeit, in folgenden Beiträgen vorab veröffentlicht.

Publicationen

- H. Kollmer, J. S. Im, J. Off, F. Scholz, and A. Hangleiter, *Intra- and inter-well transitions in GaInN/GaN multiple quantum wells with built-in piezoelectric fields*, Appl. Phys. Lett. **74**, 82 (1999).
- J. S. Im, H. Kollmer, J. Off, A. Sohmer, F. Scholz, and A. Hangleiter, *Reduction of oscillator strength due to piezoelectric fields in GaN/$Al_xGa_{1-x}N$ quantum wells*, Phys. Rev. B **57**, R9435 (1998).
- A. Sohmer, J. Off, H. Bolay, V. Härle, V. Syganow, J. S. Im, V. Wagner, F. Adler, A. Hangleiter, A. Dörnen, and F. Scholz, *GaInN/GaN heterostructures and quantum wells grown by metal-organic vapor-phase epitaxy*, MRS Internet J. Nitride Semicond. Res. **2**, 14 (1997).
- J. S. Im, A. Moritz, F. Steuber, V. Härle, F. Scholz, and A. Hangleiter, *Radiative carrier lifetime, momentum matrix element, and hole effective mass in GaN*, Appl. Phys. Lett. **70**, 631 (1997).

Tagungsbeiträge

- J. S. Im, A. Hangleiter, J. Off, and F. Scholz, *Sign of the piezoelectric field in asymmetric GaInN/AlGaN/GaN single and double quantum wells on SiC*, (Poster) MRS Fall Meeting, Boston (1999).
- O. Gfrörer, C. Gemmer, J. Off, J. S. Im, F. Scholz, and A. Hangleiter, *Direct observation of pyroelectric fields in InGaN/GaN and AlGaN/GaN heterostructures*, (Vortrag) The Third International Conference on Nitride Semiconductors, Monpellier (1999), phys. stat. sol. (b) **216**, 405 (1999).

- A. Hangleiter, J. S. Im, J. Off, and F. Scholz, *Optical properties of nitride quantum wells: How to separate fluctuations and polarization field effects*, (Poster) The Third International Conference on Nitride Semiconductors, Monpellier (1999), phys. stat. sol. (b) **216**, 427 (1999).

- J. S. Im, H. Kollmer, J. Off, F. Scholz, and A. Hangleiter, *Piezoelectric field effect on optical properties in GaN/GaInN/AlGaN quantum wells*, (Poster) MRS Fall Meeting, Boston (1998), MRS Internet J. Nitride Semicond. Res. **4S1**, G6.20 (1998).

- J. S. Im, H. Kollmer, S. Heppel, J. Off, F. Scholz, and A. Hangleiter, *Piezoelectric fields and optical transitions in GaInN/GaN multiple quantum wells*, (Vortrag) The Second International Symposium on Blue Laser and Light Emitting Diodes, Chiba (1998), Proceedings of the 2nd International Symposium on Blue Laser and Light Emitting Diodes, edited by K. Onabe, K. Hiramatsu, K. Itaya, and Y. Nakano (Ohmsha, Ltd., Tokyo, 1998), pp. 673–6.

- A. Hangleiter, J. S. Im, H. Kollmer, S. Heppel, J. Off, and F. Scholz, *The role of piezoelectric fields in GaN-based quantum wells*, (Vortrag) The Third European GaN Workshop, Jadwisin (1998), MRS Internet J. Nitride Semicond. Res. **3**, 15 (1998).

- J. S. Im, H. Kollmer, J. Off, F. Scholz, and A. Hangleiter, *Carrier confinement in GaInN/AlGaN/GaN quantum wells with asymmetric barriers: direction of the piezoelectric field*, (Vortrag) E-MRS Spring Meeting, Strasbourg (1998), Mat. Sci. Eng. B. **59B**, 315 (1999).

- J. S. Im, H. Kollmer, J. Off, A. Sohmer, F. Scholz, and A. Hangleiter, *Effects of piezoelectric fields in GaInN/GaN and GaN/AlGaN heterostructures and quantum wells* in Nitride Semiconductors, (Vortrag) MRS Fall Meeting, Boston (1997), Vol. 482 of MRS. Symp. Proc., edited by F. A. Ponce, S. P. DenBaars, B. K. Meyer, S. Nakamura, and S. Strite (Materials Research Society, Pittsburgh, 1998), pp. 513–8.

- J. S. Im, S. Heppel, H. Kollmer, A. Sohmer, J. Off, F. Scholz, and A. Hangleiter, *Evidence for quantum-dot-like states in GaInN/GaN quantum wells?*, (Vortrag) The Second International Conference on Nitride Semiconductors, Tokushima (1997), J. Crystal Growth **189-190**, 228 (1998).

- J. S. Im, J. Off, A. Sohmer, F. Scholz, and A. Hangleiter, *Time-resolved spectroscopy on GaN/AlGaN double heterostructures and quantum wells*, (Poster) The 7th International Conference on Silicon Carbide, III-Nitrides and Related Materials, Stockholm (1997), Vol. 264-268 of Materials Science Forum, edited by G. Pensl, H. Morkoç, B. Monemar, and E. Janzén (Trans Tech, Switzerland, 1998), pp. 1299–1302.

- F. Scholz, A. Sohmer, J. Off, V. Syganow, A. Dörnen, J. S. Im, A. Hangleiter, and H. Lakner, *In incorporation efficiency and compostition fluctuations in MOVPE grown GaInN/GaN hetero structures and quantum wells*, (Vortrag) E-MRS Spring Meeting, Strasbourg (1997), Mat. Sci. Eng. B **50**, 238 (1997).

- A. Hangleiter, F. Scholz, V. Härle, J. S. Im, and G. Frankowsky, *Spontaneous and stimulated recombination in the nitrides*, (Vortrag) MRS Fall Meeting, Boston (1996), Gallium Nitride and Related Materials, Vol. 449 of Materials Research Society Symposium Proceedings, edited by F. Ponce, T. D. Moustakas, B. Monemar, and I. Akasaki (Materials Research Society, Boston, MA, 1997), p. 641.

- F. Scholz, V. Härle, F. Steuber, A. Sohmer, H. Bolay, V. Syganow, A. Dörnen, J. S. Im, A. Hangleiter, J. Y. Duboz, P. Galtier, E. Rosencher, O. Ambacher, D. Brunner, and H. Lakner, *Metal-organic vapor phase epitaxial growth of GaInN/GaN heterostructures and quantum wells*, (Vortrag) MRS Fall Meeting, Boston (1996), III-V Nitrides, Vol. 449 of Materials Research Society Symposium Proceedings, Materials Research Society, edited by F. A. Ponce, T. D. Moustakas, I. Akasaki, and B. A. Monemar (Materials Research Society, Pittsburgh, PA, 1997), p. 3.

- J. S. Im, V. Härle, F. Scholz, and A. Hangleiter, *Radiative lifetime of excitons in GaInN/GaN quantum wells*, (Vortrag) The First European GaN Workshop, Rigi (1996), MRS Internet J. Nitride Semicond. Res. **1**, 37 (1996).

- F. Scholz, V. Härle, H. Bolay, F. Steuber, B. Kaufmann, G. Reyher, A. Dörnen, O. Gfrörer, J. S. Im, and A. Hangleiter, *Low pressure metalorganic vapor phase epitaxial growth of GaN/GaInN heterostructures*, (Vortrag) Topical Workshop on III-V Nitrides, Nagoya (1995), Solid State Electron. **41**, 141 (1997).

- A. Hangleiter, J. S. Im, T. Forner, V. Härle, and F. Scholz, *Near-bandgap photoluminescence decay time in GaN epitaxial layers grown on sapphire*, (Poster) MRS Fall Meeting, Boston (1995), Gallium Nitride and Related Materials, Vol. 395 of Materials Research Society Symposium Proceedings, edited by R. D. Dupuis, S. Nakamura, F. A. Ponce, and J. A. Edmond (Materials Research Society, Boston, 1996), p. 559.

Contents

Introduction

The development of semiconductor technology has had a significant impact on almost every sphere of modern life. The prime semiconductors, which have been the origin of this impact, are silicon and gallium arsenide. Despite of their extensive application, electronic devices from those material have shortcomings associated with their narrow bandgaps (1.1 eV for Si and 1.4 eV for GaAs). This makes them unsuitable for high temperature and high power application because valence electrons can be easily excited thermally or by impact ionization to the conduction band [1]. Their optoelectronic applications are also limited to the long-wavelength spectral range.

The group-III nitrides (AlN, GaN, InN) represent promising wide bandgap semiconductor materials, which can potentially overcome the aforementioned bandgap related shortcomings. Wurtzite GaN, AlN, and, InN have direct bandgap of 3.4, 6.2 and 1.9 eV, respectively [2]. When GaN is alloyed with AlN and InN, the group-III nitrides form a series of ternary alloys with bandgap covering the spectral range from red to ultraviolet (UV). Due to the direct bandgap nature of group-III nitrides, they can also generate efficient luminescence in contrast to silicon carbide (SiC) which is another wide bandgap but indirect semiconductor. Those characteristics of nitrides and their alloys make them advantageous for the creation of efficient optoelectronic devices in addition to high power and high temperature application. Over last decade, especially, there has been a breathtaking development in emitters which are active in the previous difficult green and shorter-wavelength part of the spectrum. High-brightness blue, green, and amber light-emitting

diodes (LEDs) [3, 4, 5] are now commercially available, which have applications, for example, in full color display, lighting, indicator lights, and traffic signals [6, 7, 8]. Continuously operating purplish-blue laser diodes (LDs) are also commercialized [9]. Such short-wavelength coherent sources are essential for high-density optical storage systems because the diffraction limited optical storage density increases to a first extent quadratically as the probe laser wavelength is reduced [10].

In the majority of LEDs and LDs, the light-emitting active region consists of a structure containing a thin layer (in the nanometer scale) sandwiched between two barrier layers of dissimilar semiconductors with a larger bandgap. This two-dimensional nanostructure is called a quantum well. Varying structure parameters, for example, bandgap of layers, well width, and bandgap discontinuity, it is possible to tailor carrier confinement and transition energy of quantum wells, which are crucial for the design of devices. The light emitting process in quantum wells is of much interest to help us to understand the characteristics of devices and to improve their performance.

In general, one excites electron-hole (e-h) pairs by an external source of energy in a semiconductor, and they are in non-equilibrium state. In most cases, the electrons and holes will relax to quasi-thermal equilibrium distribution through a thermalization process such as carrier-carrier and carrier-phonon interaction. In the final step, the e-h pairs recombinate, and their energy is released. Radiative recombination produces emission of photons. The radiation produced without presence of external photons is known as spontaneous emission, while stimulated emission requires an external radiative field in order for emission to occur. In non-radiative recombination, the energy of e-h pairs is released to crystal lattice in the form of heat.

Those recombination processes are closely associated with the light emitting mechanism of optoelectronic devices based on semiconductors. Therefore, with the rapid development of light emitting devices from nitrides, the recombination process in group-III nitride quantum wells has been studied actively. Those studies, especially, on the spontaneous emission, have revealed puzzling optical properties, for example, a large shift between emission and absorption [11, 12], an energy and intensity depen-

dent decay time of the emission [13], large emission linewidth [11, 14], and a large spectral shift between spontaneous and stimulated emission [15]. The complexity of the material properties makes it difficult to understand those optical properties and leads to controversial debate. It has been suggested that the observed optical properties can be explained by carrier localization due to composition fluctuation [11] or even phase separation [16] in ternary alloys, in particular, GaInN. On the other hand, wurtzite nitrides are piezoelectric materials [17]. The chemical bond between nitrogen and the group-III atoms has enhanced ionic nature because nitrogen is more strongly electronegative compared with other group-V atoms. Wurtzite nitrides have non-centrosymmetric crystal structure with a polar axis along the c-axis. Those material properties lead to the strong piezoelectric effect in nitrides. Therefore, homogeneously strained quantum wells are subject to a large internal piezoelectric field, which have a strong impact on optical properties [18].

The purpose of this study is to explore the optical properties of the group-III nitride quantum wells and to unveil dominant mechanism of the spontaneous recombination process in these structures. It will be shown that the optical properties of nitrides can be consistently explained by the effects of internal piezoelectric fields. Guided by the fact that the devices are mostly based on the binary compound GaN, together with the ternary alloys AlGaN and GaInN, we concentrate on the optical properties of GaInN/AlGaN/GaN quantum wells.

The structure of this study is as follows. In Chapter 1, key physical properties of group-III nitrides with relevance to this work will be outlined, followed in Chapter 2 by an account of theory, sample structure, and experimental method. This will then be followed by three main chapters containing different experimental concepts. In Chapter 3, single quantum wells will be discussed with emphasis on well-width dependence of transition energies and decay times, which can consistently be explained by the piezoelectric field effect. In Chapter 4, a study on asymmetric quantum well structure will verify this model, giving deep insight into carrier confinement and doping effect. Chapter 5 will include a study on multiple quantum wells, which are important for optoelectronic applications. The results of the above three chapters will be discussed critically

in Chapter 6, followed by a summary of this study in Chapter 7.

Chapter 1

Material properties of group-III nitrides

While the principal concern in this study is the optical properties of quantum wells from nitrides, these cannot be fully understood without reference to the material properties. In this chapter, therefore, a brief account of structural properties and characteristics of epitaxial growth is included. Then, heterostructures which are employed in samples studied in this work will be concentrated on. This will be followed by an account of strain effect.

1.1 Crystal and band structure

The group-III nitrides (AlN, GaN and InN) crystallize preferentially in hexagonal wurtzite structure. The cubic zinc-blende phase of GaN is metastable and observed only for heteroepitaxial layers on a cubic substrate like GaAs. Though cubic nitrides are expected to have possible technical advantages in electrical properties, high crystal quality cannot be easily achieved due to the metastability of the cubic form. The wurtzite nitrides have provided the best results to date for optoelectronic application, and this study is mainly concerned with the material.

The wurtzite crystal structure is shown in Figure 1.1(a). There are two

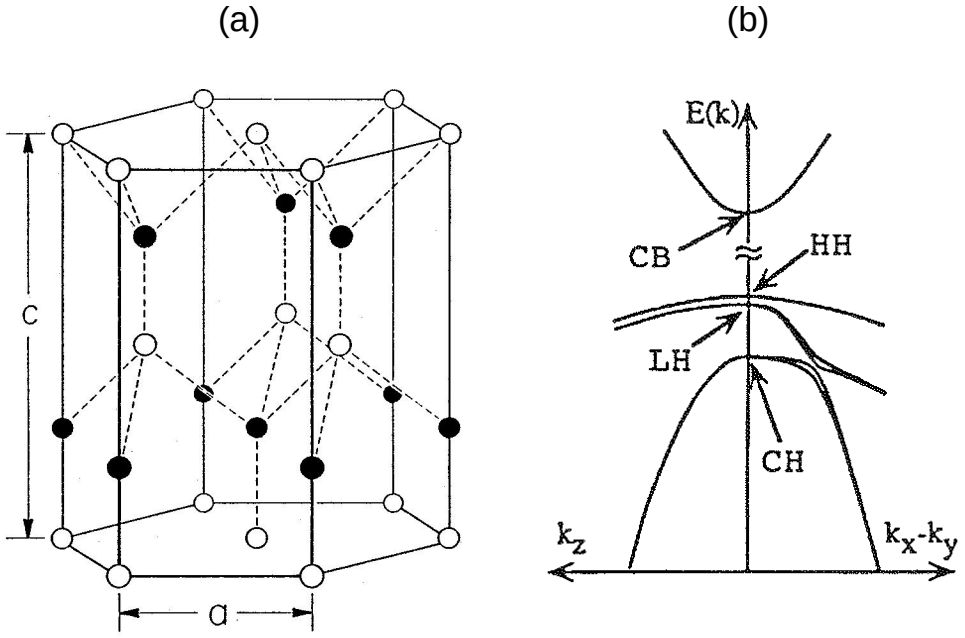

Figure 1.1: *(a) Wurtzite crystal structure [19]. (b) Schematic band structure of wurtzite GaN along the k_z direction and in the $k_x - k_y$ plane near Γ point [20].*

interpenetrating hexagonal close-packed structures, displaced from each other along the c-axis. The lattice constants appropriate to this structure are given in Table 1.1 for nitrides. In contrast to the arsenides, the lattice constants vary strongly with the chemical compositions, leading to a large lattice mismatch for heterojunctions; e.g. 2.5% for GaN/AlN, 11% for InN/GaN.

		AlN	GaN	InN
a	[Å]	3.110±0.002	3.1892±0.0009	3.540±0.008
c	[Å]	4.978±0.002	5.1850±0.0005	5.8±0.10

Table 1.1: *Lattice constant of wurtzite nitrides at room temperature [21].*

The band structures of the group-III nitrides have direct band gaps at the center of the Brillouin zone (Γ point). The band gap energies of wurtzite nitrides at 5 K and room temperature are given in Table 1.2. The band structure over a small k range around band extrema is concen-

		AlN	GaN	InN
E_{g} (5 K)	[eV]	6.28	3.50	1.91
E_{g} (300 K)	[eV]	6.20	3.44	1.89

Table 1.2: *Bandgap energy of wurtzite nitrides at 5 K and room temperature [2, 22, 23]*

trated on because the electric and optical properties are generally governed by this local $E(k)$ relationship. Figure 1.1(b) shows the schematic band structure near Γ point of wurtzite GaN. The low symmetry of the wurtzite structure affects the band structure, in particular, the valence band. The valence bands in hexagonal semiconductors are split into three separate sub-bands, transforming as the irreducible representations Γ_9, Γ_7, and Γ_7 of the C_{6v} point group. The relative energies of the valence band maxima are determined by a combination of spin-orbit splitting and axial crystal field strength. The effective masses of these three hole bands are not isotropic between the k_z direction and the $k_x - k_y$ plane, while the effective mass of electron is quasi-isotropic. The three hole bands are labelled as HH (heavy), LH (light) and CH (crystal-field split-off) based on the feature in the $k_x - k_y$ plane. Table 1.3 shows the calculated effective mass of wurtzite GaN. While the electron mass has been measured by direct cyclotron resonance experiments, which gives a value of m_e = 0.22m_0 [24], the value of the hole mass is so far uncertain. We have estimated the hole mass m_h of about 2.2m_0 based on absorption and lifetime measurements [25], which is slightly higher than the theoretical value [20, 26]. In this work, we apply the value of m_h = 2.0m_0 to theoretical calculations.

	$m_e^{\perp}$	$m_e^{\parallel}$	$m_{hh}^{\perp}$	$m_{hh}^{\parallel}$
Suzuki *et al.* [20]	0.18	0.2	1.61	1.76
Kim *et al.* [26]	0.23	0.19	2.04	2.00

Table 1.3: *Theoretical electron and heavy-hole effective masses (m_0) of bulk wurtzite GaN. m_e and m_{hh} denote electron and heavy-hole effective mass, respectively. The superscripts $\parallel$ and $\perp$ stand for the k_x direction and the k_z direction, respectively.*

1.2 Characteristics of epitaxial growth

The nitrides decompose into the group-III element and nitrogen before they start to melt on account of the extremely high melting temperature. This makes it difficult to grow crystals from the nitrides in the melt. The growth of GaN crystals from gallium solution requires again, high temperature (1400-1500°C) and elevated nitrogen vapor pressure (10 kbar) [19]. The lateral size of bulk single crystals of GaN is therefore limited to up to several millimeters. The difficulty in the growth of bulk substrate material results in epitaxial growth on foreign substrates like sapphire (α-Al_2O_3) and silicon carbide (6H-SiC).

Sapphire substrates have been used widely, but the large discrepancy with nitrides in lattice constants (e.g. 16% to GaN) and in thermal expansion rates (e.g. 36% to GaN) causes problems like high dislocation density and thermal residual strain. The introduction of a low-temperature AlN or GaN nucleation layer has improved the crystal quality reducing the dislocation density to 10^7-10^8 cm^{-2} [27]. This dislocation density is, however, more than several orders of magnitude above any other semiconductors used in the fabrication of LEDs. In spite of the high dislocation density, candela-class LED performance has been presented [3, 4]. The fact that the efficiency of optoelectronic devices based on nitrides is insensitive to dislocations is one of the most surprising characteristics compared with other semiconductors.

Silicon carbide as a substrate offers some potential advantages over sapphire, for example, less lattice mismatch (e.g. 3.1% to GaN), higher thermal conductivity, n- and p-type doping possibility, and easy cleaving. Unlike sapphire, silicon carbide is a polar crystal, and the surface polarity influences the epitaxial growth. Further discussion will be presented later in Section 4.3.

The thin film of nitrides can be grown by various epitaxial techniques: hydride vapor phase epitaxy (HVPE), molecular beam epitaxy (MBE), and metalorganic chemical vapor phase epitaxy (MOCVD). The best device performance and the commercialization of devices have been achieved by the application of MOCVD to the growth of nitrides. The samples studied in this work have also been grown by MOCVD. For

these reasons, interest will be focused on MOCVD, and problems and characteristics involved in this epitaxial technique will be subsequently discussed.

In MOCVD, tri-methyl or tri-ethyl forms of Ga, Al, and In are employed to transfer group-III elements, and ammonia as a source of nitrogen. In general, high growth temperature ($>$1000°C), high V/III ratios ($>$1000) and high gas flow rate are required for the growth of GaN [27]. Due to the mismatch of the thermal expansion rate with the substrate, a thermal strain is introduced after cooling. The thermal strain of GaN epilayers on substrate sapphire tends to be small, with increasing layer thickness, and 0.7-3 μm GaN epilayers are in compressive strain in the range of 0.09-0.16% [28].

The MOCVD growth of the ternary nitride alloys is more complex than that of GaN. In particular, the growth of GaInN alloys is complicated by numerous problems. Due to the thermal instability of InN, In incorporation is expected to be elevated by the reduction of the growth temperature, which can be achieved at the expense of a diminished crystalline quality. Furthermore, the equilibrium vapor pressure of nitrogen is extremely large, which requires a very high V/III ratios ($>$10000) to prevent the formation of In droplets. This will limit the possibility to increase the In-content by simply raising the In partial pressure. The large lattice mismatch between InN and GaN produces considerable internal strain in the GaInN alloy due to a crystalline lattice distortion, which leads to phase separation and immiscibility [29, 30, 31, 32]. The existence of large compositional fluctuation may be encouraged by the miscibilty cap in this system [29].

1.3 Heterostructures

The majority of semiconductor devices are designed and fabricated by using heterostructures which arise when different semiconductor crystals are successively grown in layers. The electronic and optical devices from nitrides are no exception. Those devices available now are principally based on GaN/AlGaN or GaInN/GaN heterostructures and crucially depend on ability to tailor key parameters such as bandgap and carrier or

photon confinement by controlling Al or In composition in ternary alloys AlGaN and GaInN. As seen in Figure 1.2, the bandgap of AlGaN alloys lies above the visible spectral region, which is suited for ultraviolet (UV) detectors [33] or UV light emitters [34]. The bandgap of the GaInN alloys shifts toward the visible region with increasing In content. GaInN alloys are therefore employed in active regions of blue, green, and amber light emitting diodes [5, 35].

Due to the large dissimilarity in lattice constants among nitrides, their heterostructures are subject to significantly large misfit strain or dislocation. Thus, lattice mismatch in these heterostructures is discussed first. This is then followed by discussion of key properties such as band offset and ternary alloy bandgap.

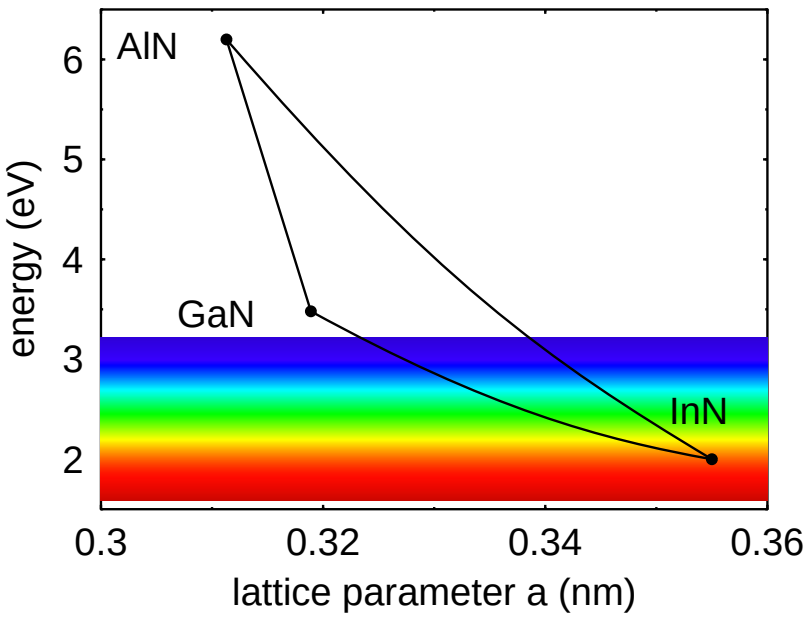

Figure 1.2: *Schematic diagram of bandgaps of wurtzite nitrides in a function of the lattice constant. The shadowed box indicates the visible spectra region.*

Misfit stress and strain

A lattice-mismatched heterostructure can have an ideal interface without forming dangling bonds if the lattice mismatch is accommodated by a

homogeneous strain. A pseudomorphic epilayer grown on a substrate is so distorted that the in-plane lattice constant of the layer is the same as that of the substrate. With increasing layer thickness, the strain energy becomes larger and the strain is partially relaxed by forming misfit dislocations if its thickness exceeds a critical thickness h_{c}.

The in-plane strain ϵ_{xx} due to the lattice mismatch is defined by

$$\epsilon_{xx} = -\frac{a_{\mathrm{epi}} - a_{\mathrm{sub}}}{a_{\mathrm{sub}}}, \tag{1.1}$$

where a_{epi} and a_{sub} are the lattice constants of the epilayer and the substrate, respectively. If the lattice constant of the epilayer is smaller than that of the substrate, the strain is tensile and its sign is positive. The strain is compressive if $a_{\mathrm{epi}} > a_{\mathrm{sub}}$ and its sign is negative. The strain in the growth direction is given by

$$\epsilon_{zz} = -\frac{2\,c_{13}}{c_{33}}\,\epsilon_{xx}, \tag{1.2}$$

where c_{13} and c_{33} are the elastic stiffness constants.

The ternary alloy lattice constant depends linearly on the composition as a good approximation, which is known as Vegard's law. Therefore, the lattice constant of GaInN alloys is given by

$$a_{\mathrm{Ga}_{1-x}\mathrm{In}_x\mathrm{N}} = (1-x)\,a_{\mathrm{GaN}} + x\,a_{\mathrm{InN}}. \tag{1.3}$$

The large lattice mismatch among nitrides puts significant strain on the heterostructure. The growth of the heterostructure with dislocation-free interface depends on the critical layer thickness, which is strongly reduced by increasing misfit strain. The strain of heterostructure can be analyzed by measuring maps in reciprocal space around the asymmetrical X-ray reflex by using triple axis spectrometer, which is known as reciprocal lattice mapping (RLM). Figure 1.3 shows the RLM of a 100 nm GaInN layer grown on a thick GaN layer [36]. The x- and y-axis are inversely proportional to the lattice constants a and c, respectively. The diffraction spots of GaInN and GaN layers are aligned parallel to the y-axis, indicating the fully strained GaInN layer. The RLM measurements reveals that 100 nm GaInN layers are fully strained up to In content of 0.12, which is consistent with the measurement by Takeuchi *et al.* [37].

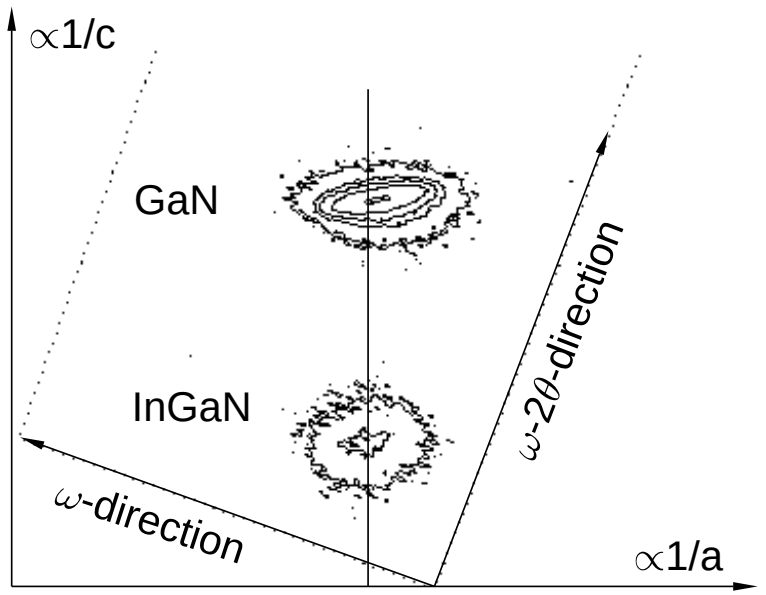

Figure 1.3: *Reciprocal space mapping of a 100 nm GaInN layer on a thick GaN layer [36].*

Ternary alloy band gap

The energy band gap of a ternary alloy such as GaInN is given by the composition-weighted average of the GaN and InN band gaps including a non-linear term described by the bowing parameter b:

$$E_{\mathrm{gap}}(\mathrm{Ga}_{1-x}\mathrm{In}_x\mathrm{N}) = (1-x)E_{\mathrm{gap}}(\mathrm{GaN}) + x\,E_{\mathrm{gap}}(\mathrm{InN}) - b\,x(1-x) \tag{1.4}$$

The measurement of the bowing parameter has been performed usually by studies on the bandgap and the In-content of GaInN epilayers, which is complicated by the strain. The lattice constant along the c-axis measured by x-ray diffraction is used typically for the determination of the In-content. In this case, the elongation of the lattice constant c due to the in-plane strain should be considered to avoid an overestimation of the In-content (see Equation 1.2). On the other hand, the strain deforms the crystal structure and shifts the bandgap (see Section 1.4). Recent studies on strained GaInN epilayers have considered the strain effect and revealed the bowing parameter b in the range between 3.2 eV [37] and 3.8 eV [38], which is much larger than the previously measured

value of 1.0 eV [39, 40, 41]. For a small In-content ($x \leq 0.12$), the bandgap for strained GaInN layers is given in a linear approximation by McCluskey *et el.* [38] as:

$$E_{\mathrm{gap}}(\mathrm{Ga}_{1-x}\mathrm{In}_x\mathrm{N}) = 3.42 - 3.93\,x \qquad (x \leq 0.12, T = 300\ \mathrm{K}) \quad (1.5)$$

where E is in units of eV. For the estimation of the band gap of GaInN alloys, we use the linear relation according to Equation 1.5 or the bowing parameter in the range of 3.2-3.8 eV because the GaInN layers studied in this work are thin enough to be homogeneously strained.

In the case of AlGaN alloys, the compositional dependence of the bandgap appears to be controversial. While Koide *et al.* [42] have yielded b = 1.0 eV, Yoshida *et al.* [43] have observed $b = -0.80$ eV. However, recent studies [44] have suggested a linear relationship indicating b = 0.

Band discontinuity

The heterojunction of two dissimilar semiconductors involves the abrupt change in the energy band structure through the junction, resulting in discontinuities or offsets in the conduction and valence band edges. Electrical and optical characteristics of heterojunction devices, for example, charge transport across the interface and carrier confinement or optical confinement in quantum wells are significantly influenced by the alignment of the band structure between two semiconductors. The knowledge of the offsets is therefore crucial for device design.

Table 1.4 summarize the experimental and theoretical values reported for the ratios of the conduction band offsets (ΔE_{c}) to the valence band offsets (ΔE_{v}) for heterointerface of nitrides. The measurement has been carried out by Martin *et al.* [45] using x-ray photoemission spectroscopy (XPS). The theoretical investigations by Van de Walle *et al.* [46] and Wei *et al.* [47] are based on the pseudopotential density functional method and the linearized augmented plane wave (LAPW) method, respectively. While the experimental estimate of the ratio for the GaN/AlN interface consists with the theoretical values of Van de Walle *et al.* and Wei *et al.*, the investigations of the InN/GaN heterojunction display significant disagreement.

	$\Delta E_c : \Delta E_v$		
	InN/GaN	GaN/AlN	InN/AlN
Martin *et al.* [45]	30:70	75:25	60:40
Van de Walle *et al.* [46]	80:20	75:25	
Wei *et al.* [47]	83:17	70:30	75:25

Table 1.4: *Calculated and measured ratios of conduction-band discontinuities to valence-band discontinuities for GaN, AlN, and InN heterostructures.*

Martin *et al.* have observed a significant forward-backward asymmetry in the heterojunctions and explained it as a piezoelectric strain effect. This effect will be discussed in the following section in detail. The theoretical study by Bernardini *et al.* [48] provides support for the asymmetry in the offset suggesting that the macroscopic polarization requires a non-standard evaluation of band offsets. Van de Walle *et al.* have investigated the effect of strain on the band discontinuities but without consideration of the piezoelectric field effect. It should be noted that the band offset for the alloy cannot be obtained by linear interpolation. Especially, low In-content $Ga_{1-x}In_xN$ alloys ($x < 0.1$) exhibit large and composition dependent bandgap bowing coefficients [38, 49, 50]. According to the theoretical study by Bellaiche *et al.* [50], the ratio of the conduction band offset to the valence band offset for the $Ga_{1-x}In_xN$/GaN heterostructure has a strong composition dependence and can be estimated to be about 35:65 for In content of $x < 0.12$. Considering this, the experimental value of Martin *et al.* is applied to numerical calculations for the GaInN/GaN quantum well with small In contents.

1.4 Effect of strain: bandgap shift and piezoelectricity

As seen in the previous sections, thermal and misfit strains are significantly large in nitrides (see Section 1.2 and 1.3). In this section, the strain effect and its consequences are discussed.

Bandgap shift

The strain changes the lattice constant and modifies the band structure, resulting in the bandgap shift. The dependence of the excitonic transition energy on the strain has been calculated for wurtzite semiconductors [51, 52, 53]. Under biaxial-strain conditions, the shift of excitonic transitions is given by

$$\Delta E = C\epsilon_{zz}, \tag{1.6}$$

where ϵ_{zz} is the strain along the c-axis and C is known as the effective deformation energy. Amano *et al.* [54] has determined the effective deformation energy to be C = 12 eV, which has been confirmed by a cathodoluminescence (CL) measurement [28].

Piezoelectricity

Wurtzite nitrides have a non-centrosymmetric crystal structure with a polar axis along the c-axis. Therefore, the misfit strain in heterostructures grown along the c-axis can generate an electric moment due to the piezoelectric effect. The piezoelectric polarization P_3^{piezo} along the c-axis is simply expressed through the piezoelectric constants e_{33} and e_{13} as

$$P_3^{piezo} = e_{33}\epsilon_{zz} + e_{31}(\epsilon_{xx} + \epsilon_{yy}), \tag{1.7}$$

where ϵ_{zz} and $\epsilon_{xx} = \epsilon_{yy}$ are the strain along the c-axis and the in-plane strain, respectively (see Appendix A). Applying Equation 1.2 and A.7 to Equation 1.7 yields a linear relation of the piezoelectric polarization P_3^{piezo} to the in-plane strain ϵ_{xx}, which is expressed through the piezoelectric coefficient d_{31} as [55]

$$P_3^{piezo} = d_{31}\left(c_{11} + c_{12} - \frac{2\,c_{13}^2}{c_{33}}\right)\epsilon_{xx}, \tag{1.8}$$

where c_{ij} is the elastic stiffness constant. The corresponding piezoelectric field F_3 is given by

$$F_3^{piezo} = -\frac{P_3^{piezo}}{\epsilon_0\epsilon_r}, \tag{1.9}$$

where ϵ_0 and ϵ_r are the permittivity of the vacuum and the static dielectric constant of the material, respectively.

Figure 1.4 shows the magnitude of the strain-induced piezoelectric field for a GaN layer in biaxial strain in a function of in-plane strain using theoretically calculated piezoelectric constants (e_{33} = 0.73 C/m^2, e_{31} = -0.49 C/m^2) [56] and strain ratio $\epsilon_{zz}/\epsilon_{xx} = -0.6$ [57].

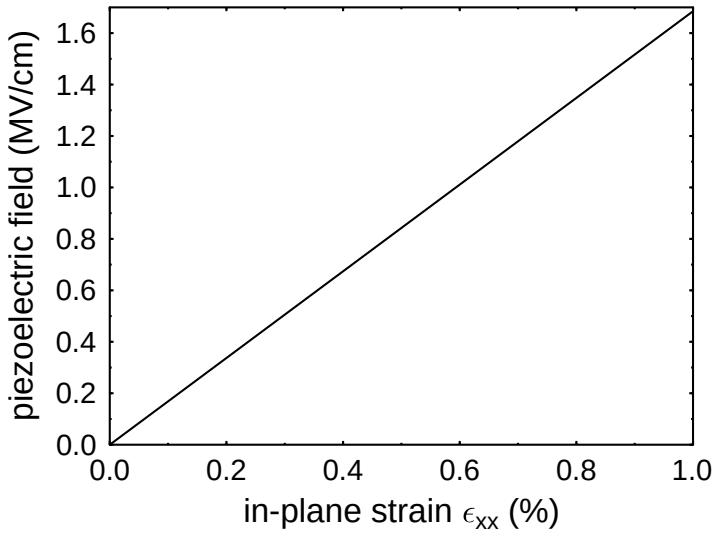

Figure 1.4: *Piezoelectric field F_3^{piezo} along the c-axis for a GaN layer in biaxial strain in a function of in-plane strain ϵ_{xx}.*

In addition to the strain-induced polarization, theory predicts that the **spontaneous polarization**, i.e. the polarization at zero strain, is very large in the nitrides [56]. Indeed, the wurtzite structure has the highest symmetry compatible with the existence of spontaneous polarization (or pyroelectric field with reference to its change with temperature) [58]. The calculated spontaneous polarization for AlN, GaN, and InN is summarized in Table 1.5. According to the calculation, the field resulting from the spontaneous polarization has a fixed orientation which is parallel to the [0001]-direction.

The electric field is usually screened by background carriers or adsorbates which compensate surface charges induced by the spontaneous polarization [59]. In a heterojunction, the discontinuity of the spon-

	AlN	GaN	InN
P^{sp} (C/m^2)	-0.081	-0.029	-0.032

Table 1.5: *Calculated spontaneous polarization for III-V wurtzite nitrides [56].*

taneous polarization causes interface charges σ, which is given by the difference of polarization ΔP^{sp} [60]. Note that the discrepancy in spontaneous polarization between AlN and GaN is large while the difference between GaN and InN is rather small. Therefore, we expect a rather large spontaneous polarization effect on GaN/AlGaN heterostructures. Figure 1.5 shows the magnitude of electric field F^{sp} resulting from heterointerface charges induced by spontaneous polarization of a GaN/AlGaN quantum well in a function of Al content. The inset shows the schematic diagram of a quantum well structure grown along the [0001]-direction indicating the sign of heterointerface charges.

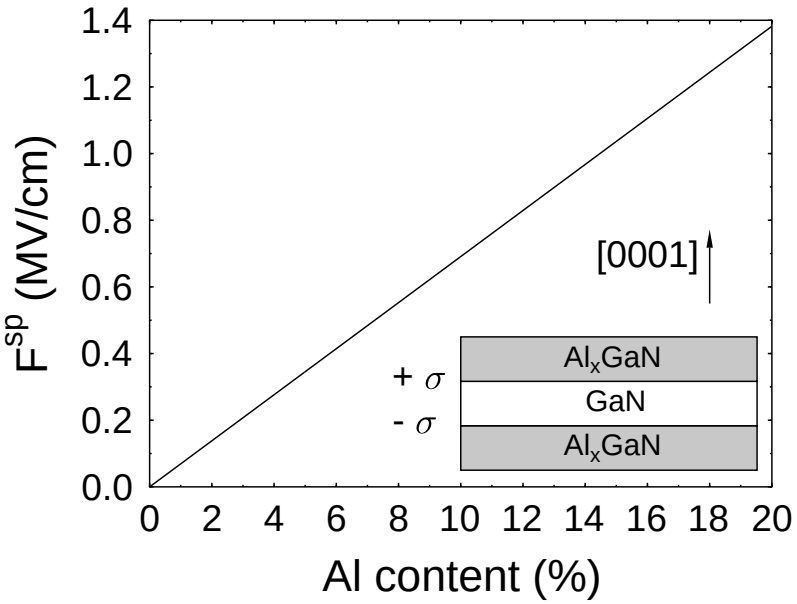

Figure 1.5: *Electric field F^{sp} resulting from heterointerface charges induced by spontaneous polarization of a GaN/AlGaN quantum well in a function of Al content.*

Chapter 2

Theory and experiments

2.1 Optical transition in quantum wells

Radiative lifetime of excess carriers

Electron-hole pairs excited to a non-equilibrium state can be annihilated by emission of photons, which is referred to as radiative recombination. Two fundamental processes involved with radiation are the stimulated and spontaneous emission. The spontaneous emission rate R_{sp} is proportional to the density of occupied state in the conduction band n and the density of empty state in the valence band p [61]:

$$R_{\mathrm{sp}} = \frac{R_{\mathrm{sp}}^{0}}{n_0 p_0} np = Bnp \tag{2.1}$$

where R_{sp}^{0}, n_0, and p_0 are the thermal equilibrium values of R_{sp}, n, and p, respectively. The stimulated emission rate is proportional to the average number of photons per radiation mode $\bar{N}$. The total recombination rate R_{T} is the sum of the stimulated and spontaneous rates:

$$R_{\mathrm{T}} = Bnp(\bar{N} + 1) \tag{2.2}$$

The rate of change in the density of electrons in the conduction band n and in the density of hole in the valence band p are expressed by the total

recombination rate R_{T} and generation rate G_{R} of electron-hole pairs:

$$\frac{dn}{dt} = \frac{dp}{dt} = -(R_{\mathrm{T}} - G_{\mathrm{R}}) \tag{2.3}$$

In thermal equilibrium, R^0_{T} is equal to G^0_{R}. Unless the degree of excitation is large, stimulated emission will be unimportant, then, $R_{\mathrm{T}} \approx R_{\mathrm{sp}}$. External optical excitation normally generates an excess carrier density which is small compared with the number of electrons in the valence band. Thus, the absorption coefficient is not significantly changed by the excitation, and we can take G_{R} equal to its thermal equilibrium value, which gives in a certain approximation

$$\begin{aligned} \frac{dn}{dt} &= -(R_{\mathrm{T}} - G^0_{\mathrm{R}}) \\ &= -B(np - n_0 p_0). \end{aligned} \tag{2.4}$$

The electron and hole densities can be expressed in terms of derivations δn and δp away from the equilibrium values n_0 and p_0. Thus the decay rate of excess carriers is obtained noting $\delta n = \delta p$

$$\frac{d(\delta n)}{dt} = -B(n_0 + p_0 + \delta n)\delta n. \tag{2.5}$$

Under the condition of low injection satisfying $\delta n \ll (n_0 + p_0)$, we obtain an exponential time dependence for the decay of the excess carriers

$$\delta n(t) = \delta n(0)\, e^{-t/\tau} \tag{2.6}$$

with a lifetime τ independent of δn

$$\tau = \frac{1}{B(n_0 + p_0)}. \tag{2.7}$$

Microscopic theory of the matrix element

To describe microscopically the interaction between a radiation field and electrons in a semiconductor, we will use a semi-classical approach. In this approach, the radiation field is treated classically while the electrons

are described by quantum mechanical (Bloch) waves [62]. By applying the results of time-dependent perturbation theory, which are summarized by Fermi's golden rule, the spontaneous emission rate $R_{\rm sp}$ within the frequency interval $\omega, \omega+d\omega$ at the transition of an electron in the conduction band $|{\rm c}>$ to the valence band $|{\rm v}>$ is obtained as [61, 62]

$$r_{\rm sp}(\hbar\omega) = \frac{2\pi}{\hbar} \sum_{\mathbf{k}_c,\mathbf{k}_v} |<{\rm c}|H_{\rm cv}|{\rm v}>|^2 f_{\rm c}(1-f_{\rm v})\delta_{\mathbf{k}_{\rm c},\mathbf{k}_{\rm v}}\delta(E_{\rm c}(\mathbf{k})-E_{\rm v}(\mathbf{k})-\hbar\omega), \tag{2.8}$$

where $|<{\rm c}|H_{\rm cv}|{\rm v}>|^2$ is the matrix element. In Equation 2.8, $f_{\rm c}$ and $f_{\rm v}$ are the Fermi-Dirac distribution function of the conduction band and the valence band, respectively.

We concentrate on the matrix element for the two-dimensional electrons in quantum wells, which have relevance to our experimental study. For the bulk crystal, wave functions $\Psi_{\rm 3D}$ of electrons can be expressed in Bloch function $\Psi_{\mathbf{k}}$ presenting a plane wave whose amplitude is modulated by a periodic function $u_j(\mathbf{r})$:

$$\Psi_{\rm 3D} = \sum_{\mathbf{k},j} c_{\mathbf{k}} e^{i\mathbf{k}\cdot\mathbf{r}} u_j(\mathbf{r}) \tag{2.9}$$

Due to the lack of a translational invariance of the quantum well along the growth direction, the Bloch function of two-dimensional electrons is expressed as [63]

$$\Psi_{\rm 2D} = \sum_{\mathbf{k}_\perp,j} c_{\mathbf{k}_\perp} u_j(\mathbf{r}_\perp) e^{i\mathbf{k}_\perp\cdot\mathbf{r}_\perp} \chi_j(z), \tag{2.10}$$

where $\chi_j(z)$ is the envelope function, which describes the z motion of the electron and $\mathbf{k}_\perp, \mathbf{r}_\perp$ are two-dimensional wave and position vectors, respectively. $u_j(\mathbf{r}_\perp)$ varies rapidly over $k_\perp^{-1}$ or over the characteristic lengths of variation of $\chi_j(z)$. Thus the matrix element can be described approximately by [63]

$$<{\rm c}|H_{\rm cv}|{\rm v}> \approx <u_{\rm c}|H_{\rm cv}|u_{\rm v}><\chi_{\rm c}|\chi_{\rm v}> + <u_{\rm c}|u_{\rm v}><\chi_{\rm c}|H_{\rm cv}|\chi_{\rm v}> . \tag{2.11}$$

The second term in Equation 2.11 vanishes because $|u_{\mathrm{c}}>$ and $|u_{\mathrm{v}}>$ are orthogonal. Assuming that the atomic-like matrix element $<u_{\mathrm{c}}|H_{\mathrm{cv}}|u_{\mathrm{v}}>$ is constant, the matrix element is proportional to the overlap integral between envelope functions $<\chi_c|\chi_v>$. Using Equation 2.1 and 2.7, the lifetime of carriers is reversely proportional to the square of the overlap integral:

$$\tau \propto \frac{1}{|<\chi_{\mathrm{c}}|\chi_{\mathrm{v}}>|^2} \tag{2.12}$$

Therefore, the overlap integral of wave functions of electrons and holes in quantum well can be estimated by measuring the lifetime.

2.2 Fabrication and structure of samples

The samples studied in this work were grown using low-pressure metal-organic vapor phase epitaxy (LP-MOCVD). We use sapphire (α-Al_2O_3) or silicon carbide (6H-SiC) as substrate. A thin AlN nucleation layer (about 15 nm) grown on the substrate at 750-800°C is employed for the improvement of the crystal quality of the upper layers. GaN layers are deposited at 1000°C with a V/III-ratio of 5500 at a growth rate of about 13 nm/min. Under these conditions, single GaN-crystals exhibit a high crystal quality with XRD-linewidth of about 50 arcsecs of [0002] reflection, low-temperature photoluminescence linewidth of 2.7-4 meV for the bound exciton, and room temperature carrier concentration of less than 10^{17} cm^{-3}. As discussed in Section 1.2, the growth of GaInN layer is complicated due to the problems involved in In incorporation. The growth conditions are optimized by lowering H_2 partial pressure and increasing the growth rate in the range of 1.1-5.4 nm/min. Under these conditions, an appreciable In content is obtained at comparably high growth temperature of 700-800°C and low V/III-ratios of 20000-4000 [64, 65, 66]. A further improvement of In incorporation is achieved by the optimization of the AlN-nucleation layer and the GaN-buffer layer [36, 67].

Single quantum well structure

The sample structures of GaN/AlGaN and GaInN/GaN single quantum wells are shown in Figure 2.1. The GaN/AlGaN quantum well structure consists of a 500 nm AlGaN buffer layer followed by a GaN layer and a 50 nm AlGaN cap layer. The AlN mole fraction of the barrier layers is estimated to be 0.15 from the photoluminescence spectra. The thickness of the GaN layers is varied between 1.3 nm and 100 nm. The layers are nominally undoped and grown at 1000°C. The GaInN/GaN quantum well structure is analogous to the GaN/AlGaN quantum well structure. A GaInN layer is grown at 800°C on a 500 nm GaN buffer layer followed by a 65 nm GaN cap layer. The GaN layers are grown at 1000°C. The In-content is estimated as 3-4% by the measurement of the lattice constant along the *c*-axis using x-ray diffraction. The thickness of the GaInN layer lies at 0.4 nm, 0.8 nm, 1.6 nm, 3.3 nm, and 6.5 nm. The thickness is determined by measurement of the superlattice reflection in x-ray diffraction. The layers are also nominally undoped.

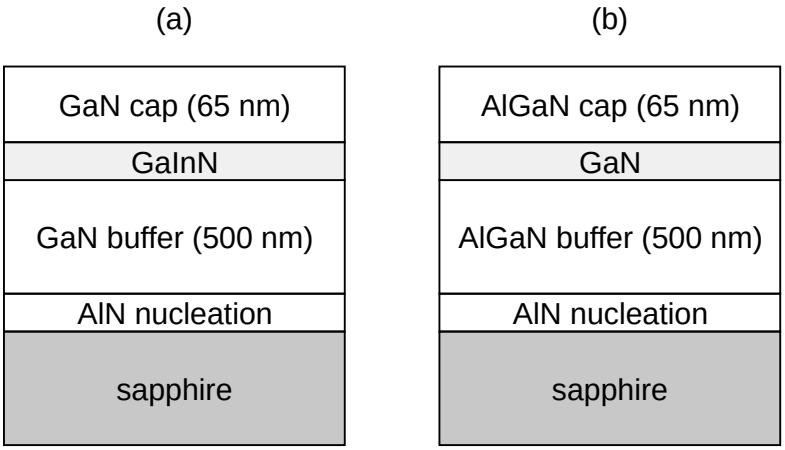

Figure 2.1: *Schematic pictures of sample structure of GaInN/GaN (a) and GaN/AlGaN (b) quantum wells.*

Asymmetric barrier structure

This sample structure has a 6.5 nm GaInN layer embedded in asymmetric barriers, which consists of a GaN layer and an AlGaN layer.

In one sample, the AlGaN layer is grown on the GaInN layer. The other sample has the AlGaN layer above the GaInN layer in reference to the growth direction. The structures of these samples are shown in Figure 2.2. As a reference sample, a simple quantum well structure is grown without the AlGaN layer. The AlN and InN mole fraction of AlGaN and GaInN layers are estimated to be 15% and 6%, respectively. The GaN and AlGaN layers are grown at the same growth temperature to minimize difference in the heterointerface quality of the GaInN layers embedded between the GaN and AlGaN layer. To study the effect of substrate on this structure, two sample series with identical structure are grown on different substrates such as sapphire and silicon carbide. All layers of this structure are also nominally undoped.

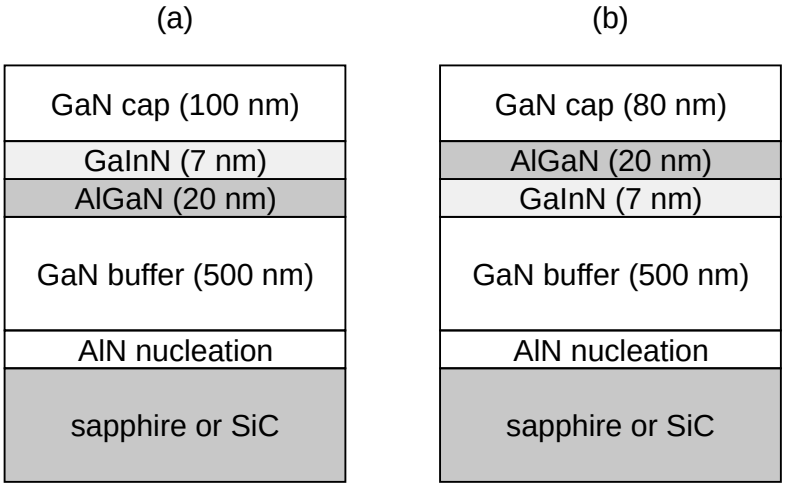

Figure 2.2: *Schematic pictures of sample structure of GaInN/GaN quantum wells with an AlGaN barrier.*

Asymmetrically doped barrier structure

This sample series consists of 6 nm GaInN single quantum wells with doped or undoped GaN barrier layers. In one sample, both the GaN buffer layer and the GaN cap layer are doped with Si. In another one, only the GaN cap layer is doped. The Si-doing level is estimated to be (1-2)$\times 10^{18}$cm^{-3}. As reference samples, we grew a 6 nm and a 3 nm GaInN single quantum well with nominally undoped GaN barrier layers.

Multiple quantum well structure

This sample consists of a single-, double-, and triple quantum well with varying numbers of GaInN quantum wells from one to three. The 3 nm GaInN layers grown on a 500 nm GaN buffer layer and separated by a 3 nm GaN layer. The double quantum well is depicted in Figure 2.3(a).

A GaN/AlGaN asymmetric double quantum well shown in Figure 2.3(b) consists of a 2 nm and a 4 nm GaN layer, which are grown on a 700 nm AlGaN buffer layer and separated by a 2.5 nm AlGaN layer.

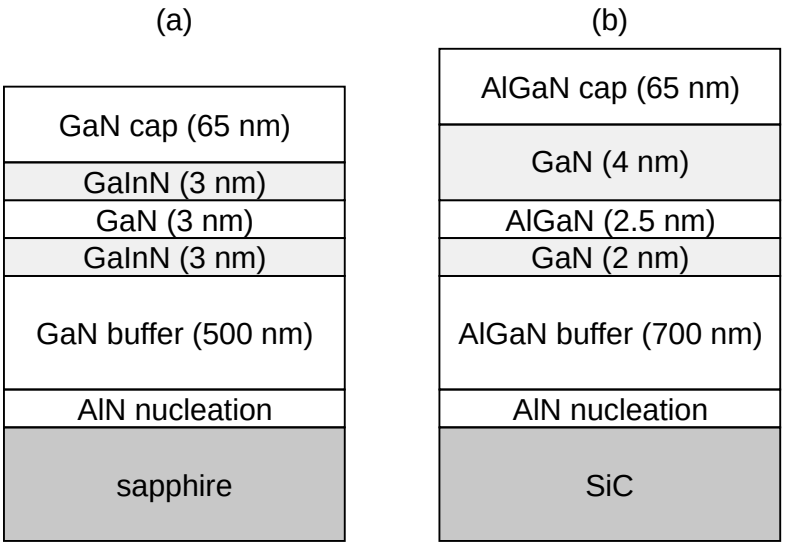

Figure 2.3: *Schematic pictures of a GaInN/GaN double quantum well (a) and a GaN/AlGaN asymmetric double quantum well (b).*

2.3 Characterization methods

Time-integrated spectroscopy

The time-integrated photoluminescence measurement detects the luminescence of a sample excited by a pulsed light source. In contrast to the equilibrium state between recombination and generation under steady excitation, the carriers generated by pulsed excitation are temporally

in non-equilibrium. The time-integrated spectroscopy averages signals detected between pulse intervals temporally.

In regard to the excitation of carriers in double heterostructures, there are two possibilities, those being, resonant and non-resonant excitation (see Figure 2.4). Under the resonant excitation, the photon energy lies between the bandgaps of the barrier and active layer, so that carriers are excited only in the active layer. On the other hand, if the light energy is higher than the bandgap of the barrier layer, carriers are excited not only in the active layer but also in the barrier layers, which is referred to as non-resonant excitation.

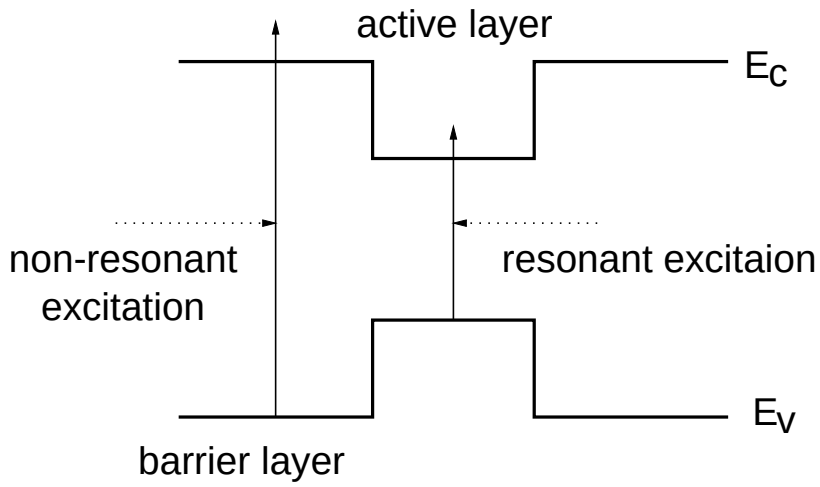

Figure 2.4: *Schematic band diagram of a quantum well under resonant and non-resonant excitation conditions.*

The resonant excitation has advantages such as that the photoexcited carrier density in the active layer is not affected by the diffusion of carriers in the barrier layer and is determined only by the recombination process in the active layer. Secondly, in case of multiple quantum wells, the resonant excitation can generate electron-hole pairs homogeneously in the active layers. Thirdly, the emission lines of the barrier layer can be suppressed by the resonant excitation. Figure 2.5 shows photoluminescence of bulk GaN under resonant and non-resonant excitation condition. The so-called yellow-luminescence is sufficiently suppressed under below-bandgap excitation. Therefore, in the case of GaInN/GaN quantum wells, the resonant excitation excludes the possibility that emission lines originate from GaN barrier layers.

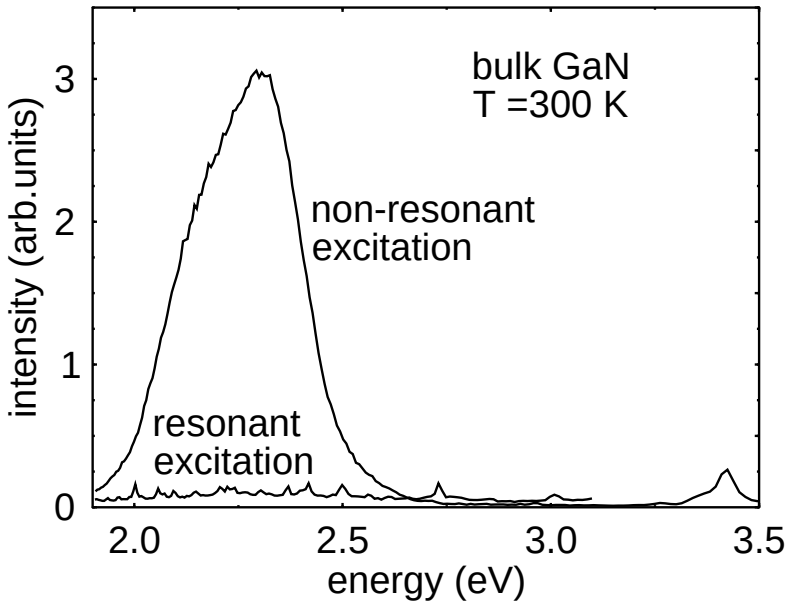

Figure 2.5: *Photoluminescence spectra of bulk GaN at 5 K under resonant and non-resonant excitation conditions.*

Lifetime measurement and time-resolved spectroscopy

The lifetime measurement is performed by using the time-correlated single photon counting technique. The probability of detecting a photon in the time interval between the light pulses is kept much lower than one by reducing exciting power density. This technique allows the sensitivity necessary to measure decay traces over several decades. The measurement of the time delay between the exciting light pulse and the photon detection is repeated with a repetition rate of used laser.

In the time-resolved spectroscopy, the decay curves are measured as a function of detection photon energy giving a photoluminescence spectra at various delay times, which are known as time-resolved photoluminescence (TRPL) spectra.

Photoluminescence excitation spectroscopy

In the photoluminescence excitation spectroscopy (PLE), a luminescence intensity at a particular photon energy is measured as a function of the

excitation photon energy. The advantage of this technique is the sensitivity compared with absorption measurements. For thin epilayers, of which photon absorption is small, PLE measurement is a simple alternative to the absorption measurement. To some extent, PLE spectrum is equivalent to the absorption spectrum. The condition, under which this assumption may be valid, is discussed as follows [62].

The relation between the emission intensity I_{em} and the excitation intensity I_{ex} is given as

$$I_{\mathrm{em}} = P_{\mathrm{abs}} P_{\mathrm{rel}} P_{\mathrm{em}} I_{\mathrm{ex}}. \tag{2.13}$$

Three processes determine this relation: the absorption of the incident photon, the relaxation to the emitting state, and radiative recombination. $P_{\mathrm{abs}}, P_{\mathrm{rek}}$, and P_{em} denote the probability of respective processes. while P_{em} can be assumed to be a constant, P_{rel} depends strongly on the e-h pair energies. When the majority of excited e-h pairs relax via the defect trapping process and/or non-radiative recombination, it is usually not possible to correlate I_{em} with P_{abs}. However, in high quality samples, the non-radiative lifetimes are often long enough to find a good correspondence between the PLE and absorption spectra, particularly at low temperature.

2.4 Experimental set-up

The characterization methods described in the previous section require the following equipment. The schematic experimental set-up is shown in Figure 2.6.

Light Source: Laser system

As sources of continuously turnable picosecond light pulses, we use a cavity-dumped dye laser (Pyridine I) pumped synchronously by a frequency-doubled mode-locked Nd:yttrium aluminum garnet laser. Used with a frequency doubler (BBO), the dye laser system generates a few hundred microwatts of ultra violet in the region of 337-376 nm. Pulse durations are less than 5 ps. The pulse repetition rate can be selected

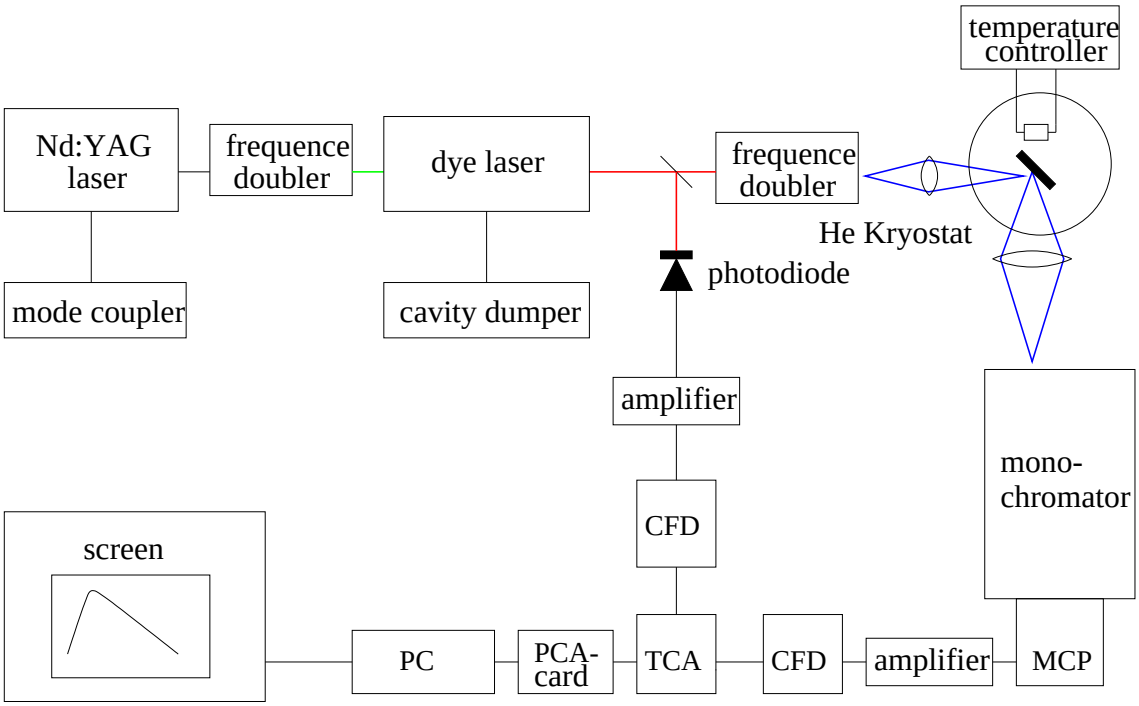

Figure 2.6: *Schematic picture of experimental set-up.*

between 4 MHz and 400 Hz depending on the decay time to avoid multi-excitation.

Detector and Photon-Counting Electronics

Photons emerging from samples are detected by a Hamamatsu R3809 microchannel plate-photomultiplier tube (MCP-PMT). Transit time spread, specified as a full width at half maximum, is less than 25 ps. The dark current of a cooled tube is as low as a few counts per second.

For optimal timing of signals from a MCP-PMT and a photodiode trigger, we use a constant fraction discriminator (CFD). The input signal into CFD is split into two parts. One portion of the signal is delayed and subtracted from a fraction of the input signal. The resulting zero-crossing point is fixed in time and is used to provide a precisely-timed logical pulse for an input signal that spans a wide dynamic range.

Time-to-amplitude converter (TAC) provides a 0 to 10 V output signal proportional to the time difference between the start and stop input signals from the constant fraction discriminator.

A PC with a PCA (personal computer analyzer) card is employed as a multi-channel analyzer with 2014 channels and converts the output signals from TAC to corresponding time channels.

Chapter 3

Study on single quantum wells

From an historical point of view, single quantum wells (SQWs) were adopted for the initial blue/green light emitting diodes (LED) based on nitrides [68]. Furthermore, the SQW structure has been the basis for consequent developmental research into laser diodes [69].

Even through the successful development of optoelectronic devices is based on that structure, the recombination mechanism of carriers in the structure has been unclear and therefore actively discussed. As will be evident in the following sections, the optical characteristics of the simple structure are complicated and puzzling enough to lead to controversial interpretations, which are partly due to the complex material properties and problems involved with the epitaxial growth of nitrides as seen in Chapter 1.

Apart from technological interest in the SQW structure, this structure was chosen as a starting point in the study because understanding this simple structure provides key knowledge for the further study of more sophisticated structures. These will be discussed in Chapter 4 and 5.

In this chapter, we are concerned with GaInN/GaN and GaN/AlGaN single quantum wells, which are mostly employed in the visible and ultraviolet light emitting devices based on nitrides. At first, their optical characteristics will be presented and studied though the use of the experi-

mental techniques described in Section 2.3. This will be followed by an account of controversial models suggested to explain the experimental results. This includes detailed discussion of the piezoelectric field effect, which is able to explain the experimental results consistently.

3.1 Basic optical characteristics

Sample series of GaInN/GaN and GaN/AlGaN single quantum well structure features the well-width variation. The thickness of GaInN and GaN layers are varied in the range of between 1 nm and 10 nm, which allows us to study optical characteristics dependent on the well width.

According to quantum mechanics, carriers confined within a distant L_z (i.e. well width in the case of a quantum well) have an increased momentum by an amount to the order of $\hbar/L_z$ as a consequence of the uncertainty principle. The corresponding kinetic energy is proportional to $(1/L_z)^2$. The increased energy is referred to as the quantum confinement energy. As the well width increases, the confinement energy decreases and converges toward zero due to the diminishing quantum size effect. In addition to shifting the energies, the quantum confinement also modifies the recombination rate of carriers. Electrons and holes are forced to close by the confinement, and the overlap of electron and hole wave functions is increased, which leads to an enhanced transition rate.

Considering this, increased transition energies and enhanced recombination rates of a quantum well would be expected, compared with those of bulk material. With increasing well width, the transition energy of a quantum well would be expected to converge toward the bandgap of bulk material.

Surprisingly, the GaInN/GaN and GaN/AlGaN quantum wells exhibit a significant discrepancy in these expectations. The following sections will present their unusual optical properties in detail.

3.1.1 GaInN/GaN single quantum wells

The bandgap of GaInN alloys depends on InN mole fraction and the bowing parameter as presented by equation 1.4. The InN mole fraction

is estimated to be (3-4)% by using x-ray diffraction with assumption of a Poisson's ratio of 0.27 [67]. The bowing parameter found in relevant literature lies in the range between 3.2 eV and 3.8 eV (see the Section 1.2). We obtain the lower-limit of the bandgap of GaInN alloys as 3.27 eV using the bowing parameter b of 3.8 eV and an InN mole fraction of 4%.

Time-integrated photoluminescence

Figure 3.1 shows time-integrated photoluminescence spectra of GaInN/GaN quantum wells. Measurements are made under non-resonant excitation condition at 5 K. The emission peaks observed in all samples at about 3.48 eV originate from bound exciton recombination in the GaN barrier layer [25, 70]. We also observe emission peaks with a broad linewidth below 3.48 eV. The emission maximum lies at 3.424 eV with L_z = 0.4 nm and shifts up to 3.195 eV with L_z = 6.5 nm. The redshift with increasing well width indicates that the emission lines are correlated with

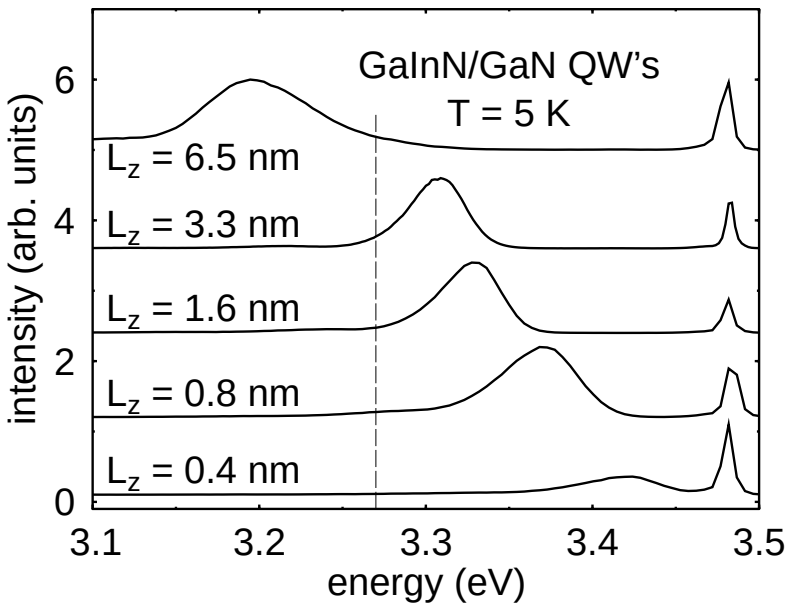

Figure 3.1: *Time-integrated photoluminescence spectra of a series of GaInN/GaN quantum wells under non-resonant excitation at 5 K. The dashed line indicates the position of the GaInN band gap.*

GaInN layers due to the well-width dependence. However, the emission peak of the 6.5 nm quantum well lies at 3.195 eV and clearly lower than the GaInN bulk bandgap of 3.270 eV, which is estimated to be the lower limit. This sub-bandgap emission cannot be explained by a simple square quantum well model, where the emission energy converges towards the bulk bandgap with increasing well width. It is noteworthy that the emission line width of the GaInN layer is fairly large in comparison with that of the GaN barrier layer.

Time-resolved photoluminescence spectroscopy

The emission peaks correlated with GaInN layers are studied with time-resolved measurements. To avoid the trapping process of carriers excited in barrier layers, the quantum wells are excited resonantly: the energy of the exciting photons is below the GaN bandgap. Figure 3.2 shows the decay traces of emission peaks at 5 K. The emission intensity of a 0.4 nm, 0.8 nm, and 1.6 nm quantum well decays mono-exponentially in the nanosecond time scale. With a well width of 3.3 nm, we observe a slight deviation from a monoexponential decay, and the 6.5 nm quantum well shows obviously non-monoexponential decay. In parallel, the decay time scale increases from the range of a few nanoseconds, up to the range of sub-microseconds with increasing well width. The emission line of the 0.4 nm quantum well has a decay time of 0.7 ns. For the 6.5 nm quantum well, the decay time is estimated to be 210 ns at a long delay time after pulsed excitation. The decay time increases by approximately 300 times with a well-width increase of 6 nm.

The temporal behavior of the emission lines are studied in detail by time-resolved spectroscopy. Time-resolved spectra of a 3.3 nm and a 6.5 nm quantum well are shown in Figure 3.3. The spectra are integrated at each time interval, and their intensity is normalized. The emission peaks in these spectra of both quantum wells shift towards lower energy as time evolves. The redshift of the emission peak for a long delay time after pulsed excitation is obtained as 20 meV for the 3.3 nm quantum well and 60 meV for the 6.5 nm quantum well.

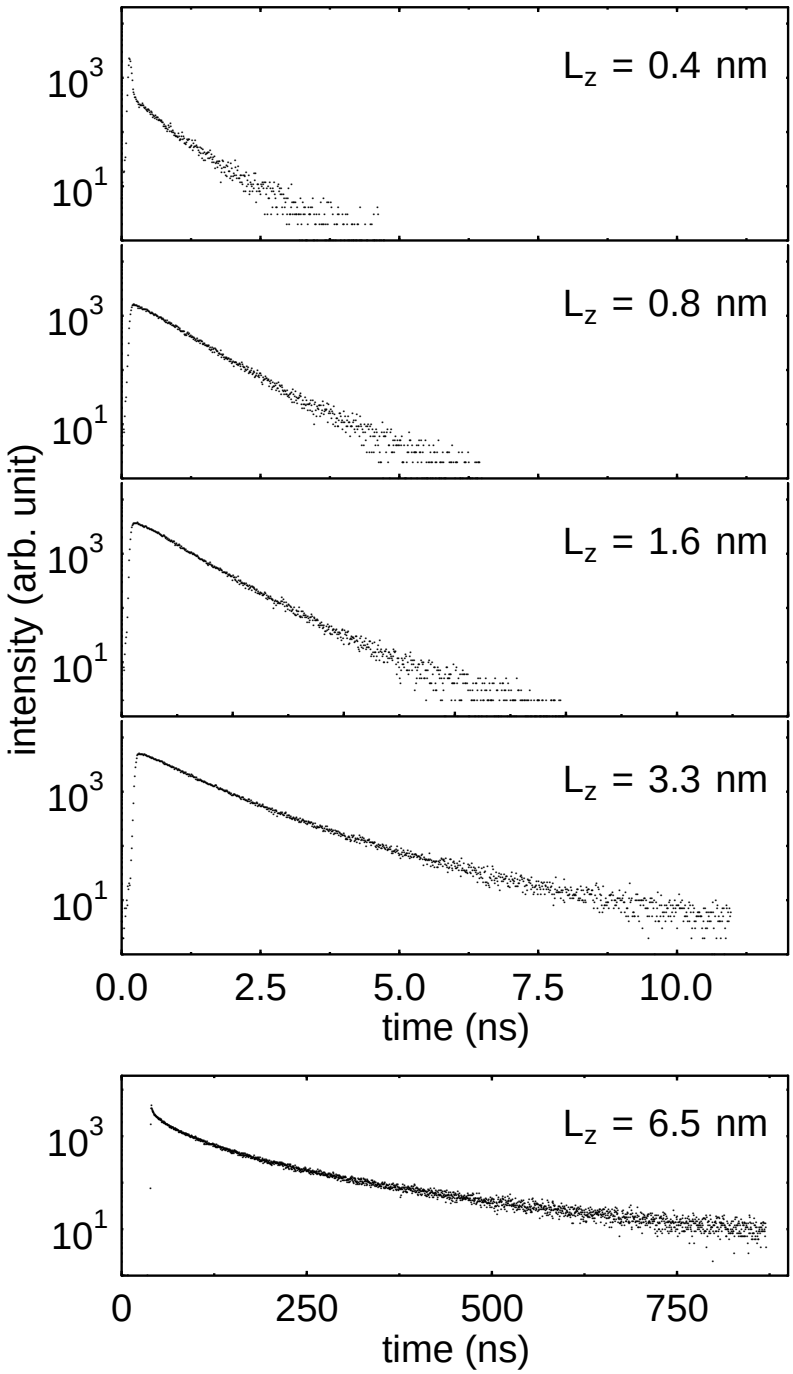

Figure 3.2: *Semi-logarithmic plot of the luminescence decay for GaInN/GaN quantum wells under resonant excitation at 5 K. The signal from the stray light of laser overlaps that of the photoluminescence of the 6.4 nm quantum well and causes the increased intensity at a short delay time after pulsed excitation.*

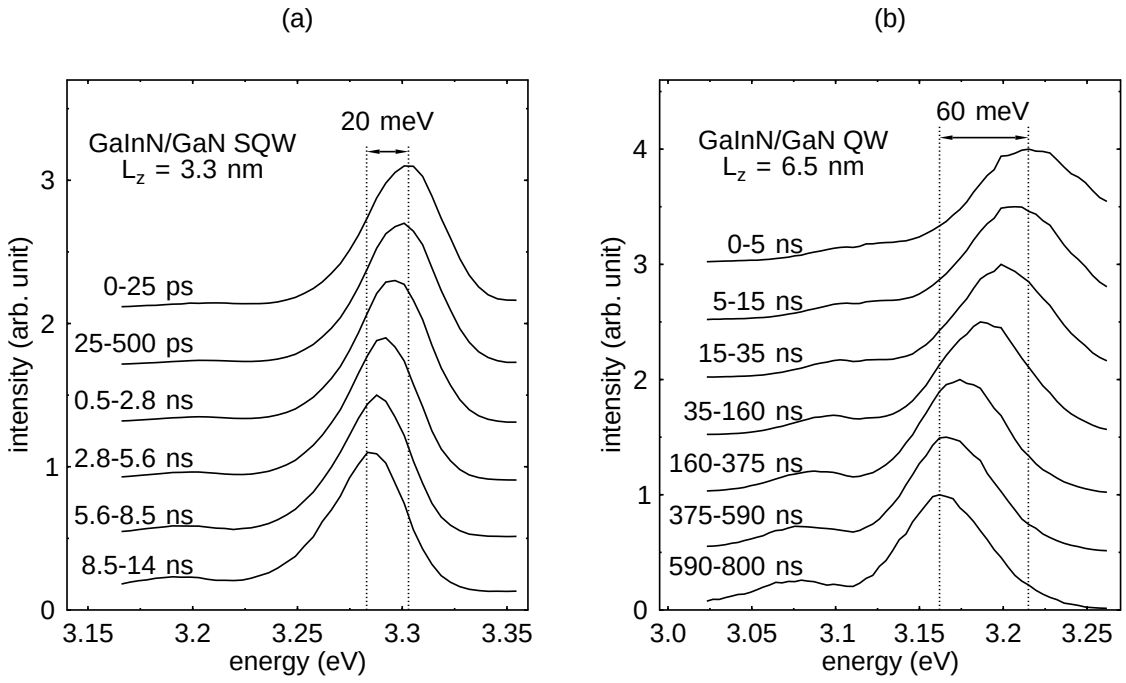

Figure 3.3: *Time-resolved spectra of a 3.3 nm (a) and a 6.5 nm (b) GaInN/GaN single quantum well.*

Photoluminescence excitation spectroscopy

Figure 3.4 shows the photoluminescence and photoluminescence excitation spectra of a 0.8 nm, a 1.6 nm, and a 3.3 nm GaInN/GaN single quantum well structure at 5 K. In all three cases, the most efficient excitation of quantum well luminescence is achieved via the GaN barriers at energies above 3.480 eV. The sharp absorption edge can infer the high quality of the GaN layers.

In the energy range between about 3.3 eV and 3.5 eV, direct excitation of the GaInN quantum well is observed. The signal in this range is much smaller, due to the fact that, at most, a few percent of the excitation of the exciting light is directly absorbed in the quantum well. The absorption edges are broad but clearly shifted to the emission peaks. To have an accurate description of the shift, the absorption edge is defined as the excitation energy where the photoluminescence excitation signal reaches 50% of the signal maximum and is marked by a dotted line in

Figure 3.4. The difference in energy between the emission peak and the absorption edge is known as Stokes shift and is obtained in the range between 54 meV (0.8 nm) and 89 meV (3.3 nm).

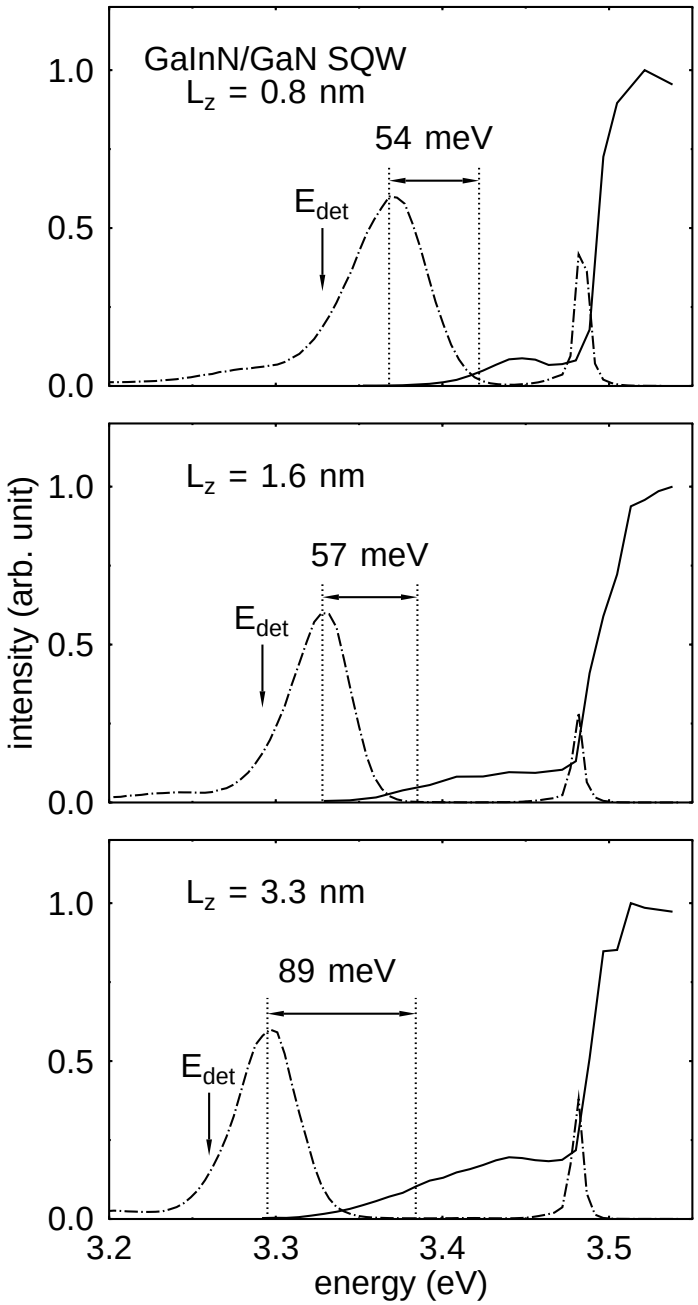

Figure 3.4: *Comparison of PL- and PLE spectra of a 0.8 nm, a 1.6 nm, and a 3.3 nm GaInN/GaN quantum well at 5 K. The arrow indicates the detection energy* E_{det}.

3.1.2 GaN/AlGaN single quantum wells

The GaN layer embedded between AlGaN layers is pseudomorphically in compressive strain. The in-plane strain is estimated to be about 0.4% appropriate to a AlN mole fraction of 0.15. The strain-induced bandgap shift can be estimated to be approximately 36 meV by using Equation 1.6.

Time-integrated photoluminescence

Time-integrated low-temperature luminescence spectra of GaN/AlGaN quantum wells under resonant excitation are shown in Figure 3.5. The 100 nm double heterostructure reveals a spectrum similar to that of bulk GaN, due to the fact that quantum confinement effect is negligible. The emission of excitons at about 3.5 eV dominates the spectrum of the 100 nm double heterostructure, but the peaks originating from donor-acceptor-pair recombination and its phonon replicas are also recognizable. On the other hand, the luminescence spectra of GaN/AlGaN

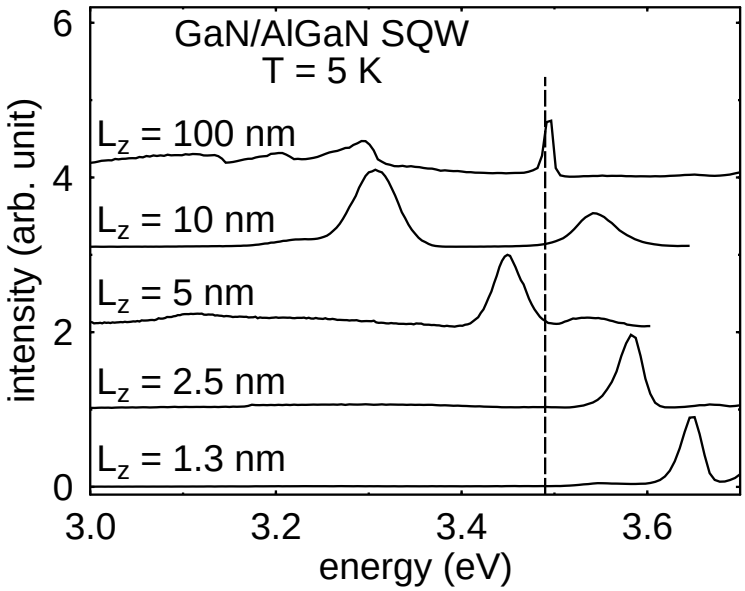

Figure 3.5: *Time-integrated photoluminescence spectra of a series of GaN/AlGaN double heterostructures. The dashed line indicates the position of the GaN bulk bandgap.*

quantum wells exhibit a complex behavior. We observe main emission lines shifting toward lower energy, even below the GaN bulk bandgap as well width increases. The sub-bandgap emission is observed like in GaInN/GaN quantum wells, which can also not be explained by the simple square quantum well model. In thicker layers (5 nm and 10 nm), an additional emission line appears about 70 meV above the GaN bulk bandgap. The photoluminescence linewidth of quantum wells is fairly large compared with that of bulk GaN which usually lies at about 3-4 meV.

Time-resolved photoluminescence spectroscopy

The luminescence decay time is measured at the emission peaks in the spectra, and the typical decay traces are depicted in Figure 3.6. The single emission line in thin quantum wells (1.3 nm and 2.5 nm) as well as the higher-energy line in thicker quantum wells (5 nm and 10 nm) have

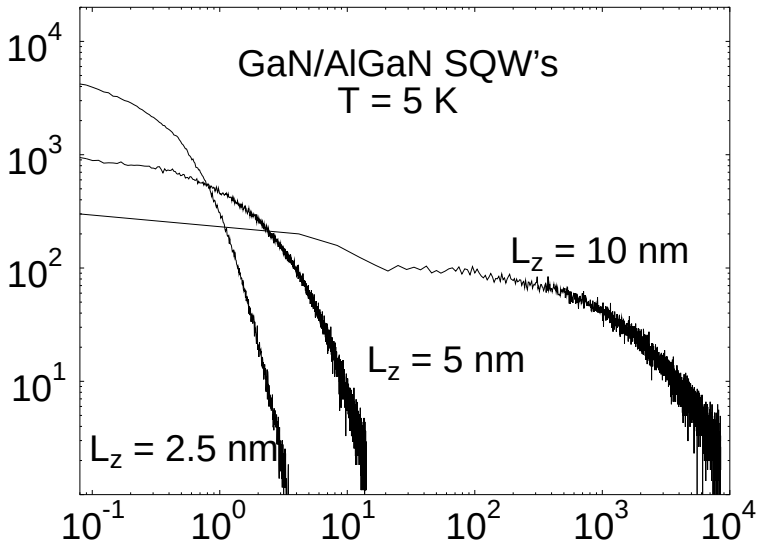

Figure 3.6: *Double-logarithmic plot of the luminescence decay for a 2.5 nm, a 5 nm, and a 10 nm GaN/AlGaN single quantum well. The thickest layer shows a decay in microseconds time scale.*

decay times of 200-300 ps. In contrast, the lower-energy emission lines in thicker layers (5 nm and 10 nm) show a strongly non-exponential decay, and their decay time scale extends into the microsecond range. For the 10 nm QW, the decay time obtained at a long delay time after pulsed excitation reaches 3 μs.

The temporal behavior of the spectrum of the lower-energy line is studied by time-resolved photoluminescence spectroscopy. Time-resolved spectra of the 10 nm quantum well, observed at various time intervals, are shown in Figure 3.7. The spectra are integrated at each time interval, and their intensity is normalized. The emission peaks in these spectra shift towards lower energy as time evolves. The redshift of the emission peak for a long delay time after pulsed excitation is obtained as 27 meV. The shape and linewidth of these spectra are not subject to change with increasing delay time.

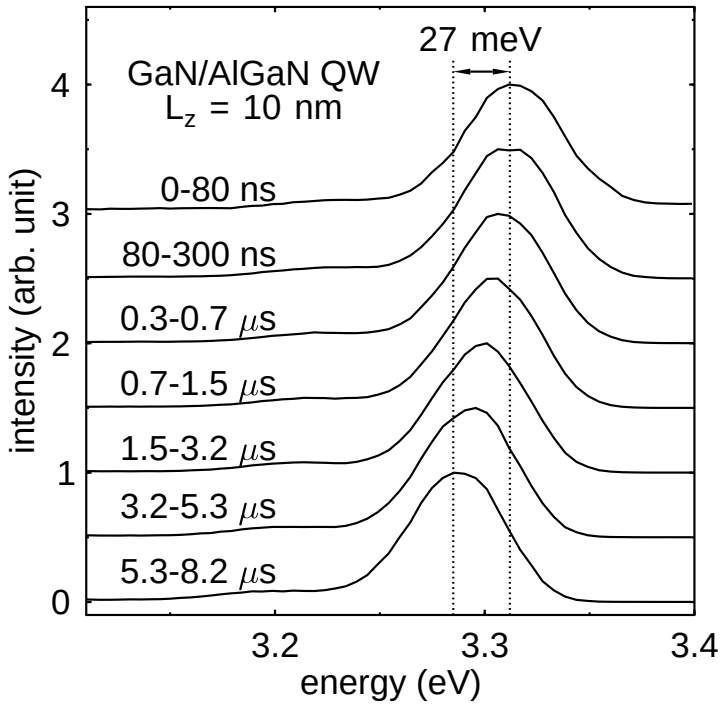

Figure 3.7: *Time-resolved spectra of the lower-energy line of a 10 nm GaN/AlGaN single quantum well.*

3.1.3 Controversial models

As demonstrated in two previous sections, similarities are evident between optical properties of the GaInN/GaN and GaN/AlGaN quantum wells. Main properties are summarized below

- The emission energy $E_{\mathrm{pl}}(L_z)$ of quantum wells shifts toward lower energy even below bulk bandgap with increasing well width.
- The lifetime $\tau(L_z)$ of emission lines increases by several orders of magnitude, and the luminescence tends to decay non-exponentially as well width increases.
- The emission linewidth of the quantum wells is significantly larger when compared with that of bulk GaN.

In order to explain the origin of the sub-bandgap emission, donor-acceptor-pair (DAP) recombination may be a consideration. The strongly non-exponential time decay and the redshift of the emission peaks with evolving time would comply with this model [71]. But, DAP transitions can be excluded because this model cannot account for the well-width dependence of the peak energy and the decay time.

We can attribute the origin of these puzzling features to the complex material properties described in Chapter 1. Particularly, the epitaxial growth of the GaInN layer is subject to problems involved in phase separation due to the large miscibility gap [29, 32, 39] or alloy fluctuation due to the poor In-incorporation. Indeed, several groups have interpreted optical properties of GaInN quantum wells in terms of the localized states at potential minima formed by the composition fluctuation [11] or even quantum-dot-like states due to local segregation [16]. In the context of the localization model, the optically excited carriers diffuse into In-rich areas which act as a recombination region, and the emission energy is reduced by the localization energy resulting in the sub-bandgap energy emission. The large linewidth of photoluminescence spectra is explained by inhomogeneous broadening due to the formation of the band tail states, resulting from a disorder-like fluctuation of alloy composition [11, 72]. The redshift of the time-resolved photoluminescence spectra with evolving

time has also been observed by other groups, and an exciton relaxation process to the localized lower-energy states has been suggested to account for the temporal behavior [13, 72]. The energy difference of emission peak and absorption edge, referred to as Stokes shift, has been discussed also in terms of the localization of excitons [12, 13, 72].

The localization model however fails to explain our experimental observation completely. The highly analogous optical properties of GaInN/GaN and GaN/AlGaN quantum wells cannot be accounted for by this model. The GaN/AlGaN quantum wells use a binary semiconductor as an active layer and localized states due to composition fluctuation are therefore excluded. The sub-bandgap emission of GaN/AlGaN quantum wells cannot be explained by the localization model, and these evident similarities should have another origin. Furthermore, the well-width dependence of the lifetime and the emission energy cannot be understood by the localization model. With an increase of well width by a few nanometers, the lifetime increases dramatically by two or three orders of magnitude to the microsecond time scale. This indicates the increasing large localization energy with increasing well width, which is not plausible. Additionally, the very slow decay could be explained by a strong localization in Å range, which is also not feasible.

An alternative model is based on the strain-induced piezoelectric field discussed in Section 1.4. In the next section, this model will be focused on.

3.2 Piezoelectric effect on optical transitions

3.2.1 Piezoelectric field in quantum wells

Following the study of critical thickness discussed in Section 1.2, the active layers of the GaInN/GaN and GaN/AlGaN quantum wells are pseudomorphically strained. The quantum well structure is grown along the [0001]-direction, which is a polar axis for the wurtzite semiconductors. Considering that the nitrides are piezoelectric material, of which the piezoelectric coefficients are about 10 times larger than those of other III-V semiconductors [17], a large strain-induced piezoelectric

field is expected to be built in quantum wells of wurtzite nitrides.

To illustrate how the built-in electrical field modifies the electric structure and optical properties of quantum wells, a schematic picture of the potential profile of GaN/AlGaN quantum well with the piezoelectric field is shown in Figure 3.8. The AlGaN barriers are assumed unstrained and have no piezoelectric field, while the GaN layer is under a biaxial compressive in-plane strain, which induces a piezoelectric field parallel to the growth direction (see Section 1.4).The broken line and solid curve in the valence and the conduction band indicate the calculated energy level of the ground state and the corresponding wave function, respectively. The electric field pulls the electrons and holes towards opposite sides of the GaN layer. Due to the potential drop over the well, the difference of the energy level of the electron and hole are reduced resulting in a redshift of the transition energy, which is known as the Stark shift. If the well width is thick enough ($L_z \times F_{\mathrm{piezo}} > (E_{\mathrm{g}}^{\mathrm{AlGaN}} - E_{\mathrm{g}}^{\mathrm{GaN}})$), the transition energy shifts towards even lower energy than the GaN bandgap energy leading to a sub-bandgap emission, which we have observed. At

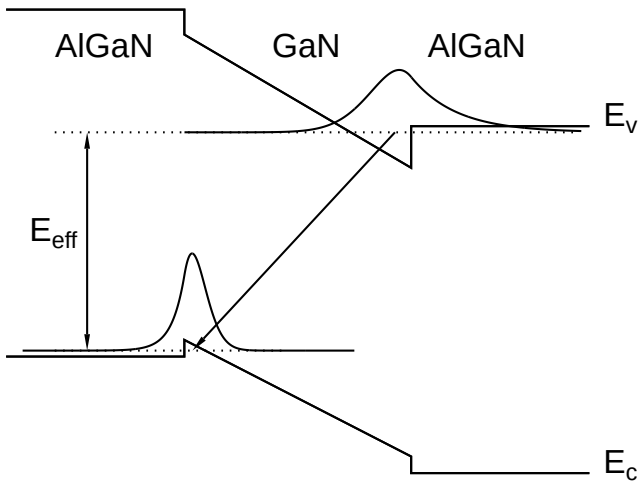

Figure 3.8: *Schematic picture of the energies and wave functions of electrons and holes in a strained quantum well with a piezoelectric field.*

the same time, the electron and hole ground-state wave functions are spatially separated by the electric field, which results in a reduction of oscillator strength congruous to a small overlap of wave functions. It is notable that the piezoelectric field effect can explain both the redshift of transition energy [18] and the reduction of oscillator strength with increasing well width. Furthermore, the redshift of the time-resolved photoluminescence spectra with evolving time can be explained by using this model. The spatial separation of optically created carriers induces electrostatic potential screening the piezoelectric field. Decreasing carrier density with time evolution results in the recovery of the screened piezoelectric field and in redshift of the transition energy. The screening effect due to photogenerated carriers can be corroborated by blueshift of photoluminescence energy with increasing excitation intensity, which has been observed by several groups [18, 73].

This electric field effect on quantum wells is known as quantum-confined Stark effect (QCSE). In contrast to the Franz-Keldysh effect observed in bulk semiconductors, the shift in band-edge absorption of quantum wells for an external electric field can exceed the exciton binding energy as a consequence of the quantum confinement of carriers [74, 75]. The corresponding lifetime enhancement has verified the quantum-confined Stark effect [76].

The quantum-confined Stark effect due to the strain-induced piezoelectric field has been shown in strained quantum wells and superlattices using zinc-blende compounds such as GaAs/GaInAs grown along the [111]-direction [77, 78, 79, 80] or the wurtzite II-VI semiconductors like CdS/CdSe grown along the c-axis [81].

The piezoelectric field model based on the quantum-confined Stark effect provides a possibility to explain the well-width dependence of the emission energy and lifetime, which cannot be explained by the other models such as the localization model. To prove the validity of the piezoelectric field effect, numerical calculations of transition energy and lifetime will be made using the model. An explanation will then be given about the linewidth and Stokes shift on the base of the model.

3.2.2 Numerical calculation of transition energy and decay time

For a quantitative calculation, an effective-mass Schrödinger equation was solved for the conduction and valence band using a spatially linearly varying potential energy in the quantum well. In this simple model, the quantization energy, the wave function, and the matrix elements are calculated at various well widths. The matrix elements are proportional to the square of the overlap integral between electron and hole wave function (see Section 2.1). For the material parameters such as the band offset and the effective mass of electrons and holes, we use the values given in Section 1.1. Due to the small mole fraction of AlN and InN, we assume no difference of the effective mass between layers and use that of GaN.

A comparison of the calculated energies and oscillator strengths with the experimental data is shown in Figure 3.9 for GaN/AlGaN quantum wells. For this figure, the energetic positions were taken from time-resolved photoluminescence spectra at the longest possible delay time after excitation, i.e. with screening of the field being as small as possible. For the same reason, the decay time in the strongly non-exponential decay was also determined at a long delay time. The strained bulk bandgaps of the active layers, which are applied to the calculation, are indicated by dashed-dotted lines. The calculated curves include only a single adjustable parameter, which is the magnitude of the electric field. In the present case, the well-width dependence of the emission peaks and the decay times can be consistently explained by a field of 350 kV/cm for GaN/$Al_{0.15}Ga_{0.85}N$ quantum wells.

It should be noted that spontaneous polarization has a significant influence on the electric field in the quantum well. Large discontinuity of the spontaneous polarization across AlGaN/GaN heterointerfaces induces interface charges which establish an electric field in the quantum well. Therefore, the electric fields in the quantum well F_{QW} is the sum of the piezoelectric and spontaneous contributions

$$F_{\mathrm{QW}} = F_{\mathrm{spon}} + F_{\mathrm{piezo}}, \tag{3.1}$$

where F_{piezo} is the piezoelectric field induced by strain and F_{spon} is the electric field resulting from spontaneous polarization. Guided by

the theoretical calculation [56], the magnitude of the electric field F_{spon} and F_{piezo} in GaN/$Al_{0.15}Ga_{0.85}N$ quantum wells is estimated to be about 900 kV/cm and 670 kV/cm, respectively (see Figure 1.4 and 1.5). Furthermore, the theory predicts that F_{spon} and F_{piezo} have the same sign in the compressively strained GaN layer and point to the $[000\bar{1}]$-direction [56]. The direction of the piezoelectric field will be discussed

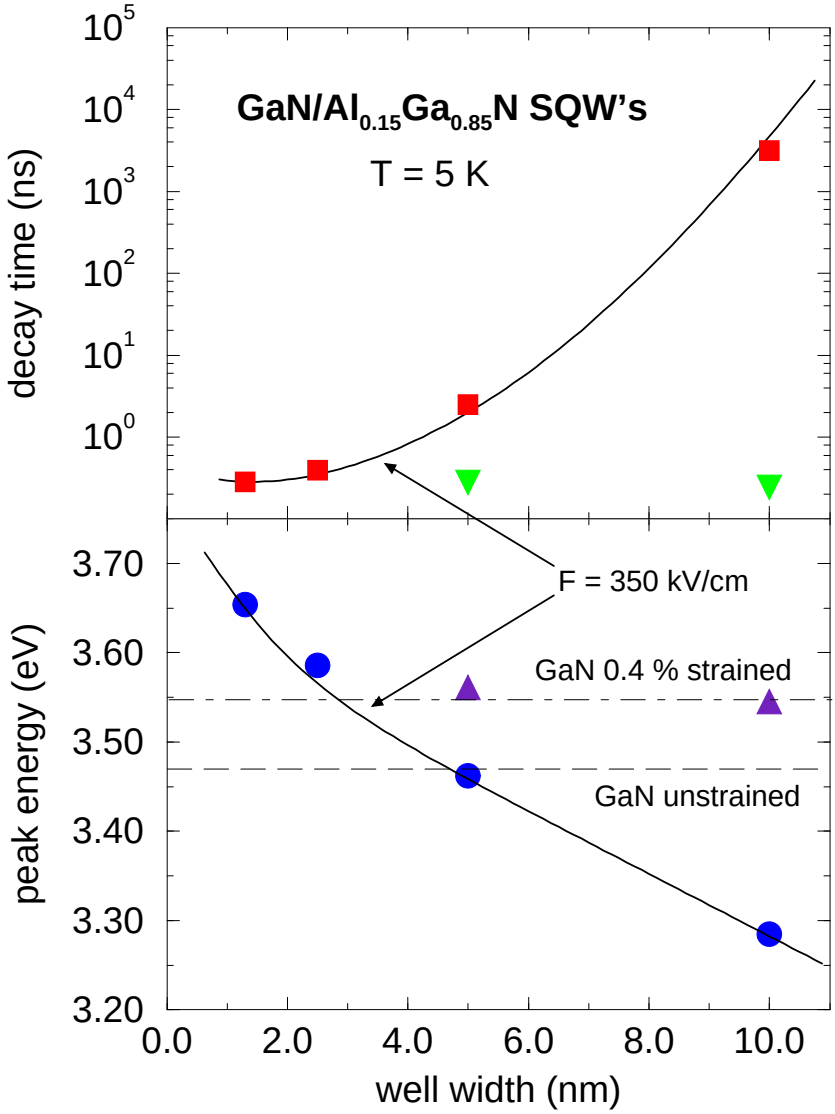

Figure 3.9: *Comparison of the measured energy position (dots) and decay times (squares) of lower-energy emission lines in GaN/AlGaN quantum wells with a numerical calculation using a piezoelectric field of 350 kV/cm. The energy position of higher-energy emission lines (triangles) coincides well with the bandgap of 0.4% strained bulk GaN indicated by dashed-dotted line.*

in the following chapters in more detail. The electric field in the quantum well estimated theoretically is much larger than that attained by a fit of the experimental data to numerical calculations. The discrepancy is partially attributed to screened field due to background carriers. This effect will be discussed in Chapter 4.

Spontaneous polarization also induces charges on the surface of samples. The surface charges are normally compensated by charged surface adsorbates. Gfrörer *et al.* [59] has shown that the surface adsorbates can be removed by electron irradiation, and uncompensated surface charges establish an electric field. The macroscopic electric field always points to the [0001]-direction (see Section 1.4). In case of GaN/AlGaN quantum wells, it reduces the internal electric field F_{QW} in quantum wells given by Equation 3.1. This results in a compensation of the internal electric field and consequently leads to a blueshift of the luminescence energy [59, 82, 83].

Considering this, the higher-energy line in the thick layers can be originated from regions where the internal electric field is compensated. Figure 3.9 shows that the transition energy of the higher-energy line coincides with the bandgap of GaN under 0.4% compressive strain (dashed-dotted line). This indicates that the higher-energy line is associated with spatially direct transitions observed in a nearly flat-band case. The short decay time of these higher-energy lines is consistent with the nature of the spatially direct transitions. Furthermore, with increasing electron irradiation time, enhanced luminescence intensity of the higher-energy line has been observed [82], which is associated with the increased oscillator strength due to the compensated internal electric field. Due to the large radius of the optically excited region (about 100 μm), surface regions which are compensated differently by adsorbates are excited simultaneously, and both the higher- and lower-energy lines are observed in photoluminescence spectra. This is supported by the fact that electron irradiation of a few small areas leads to the observation of both lines [59].

Figure 3.10 summarizes our results for a series of $Ga_{0.96}In_{0.04}N$/GaN single quantum wells. In this case, the analysis of the emission peaks yields a piezoelectric field of 300 kV/cm. From x-ray diffraction data we estimate the strain to be about 0.3%. Unlike the case of the GaN/AlGaN

structures, for the thickest quantum wells, the numerical calculation of the decay times does not correlate to the experimental value. A larger decay time is observed for the 6.5 nm quantum well than that of the theoretical value. This discrepancy could be partly due to the simple model neglecting, for example, global band bending in equilibrium band structures. On the other hand, the rather weak electron confinements in the GaInN/GaN quantum well could account for it. The ratio between

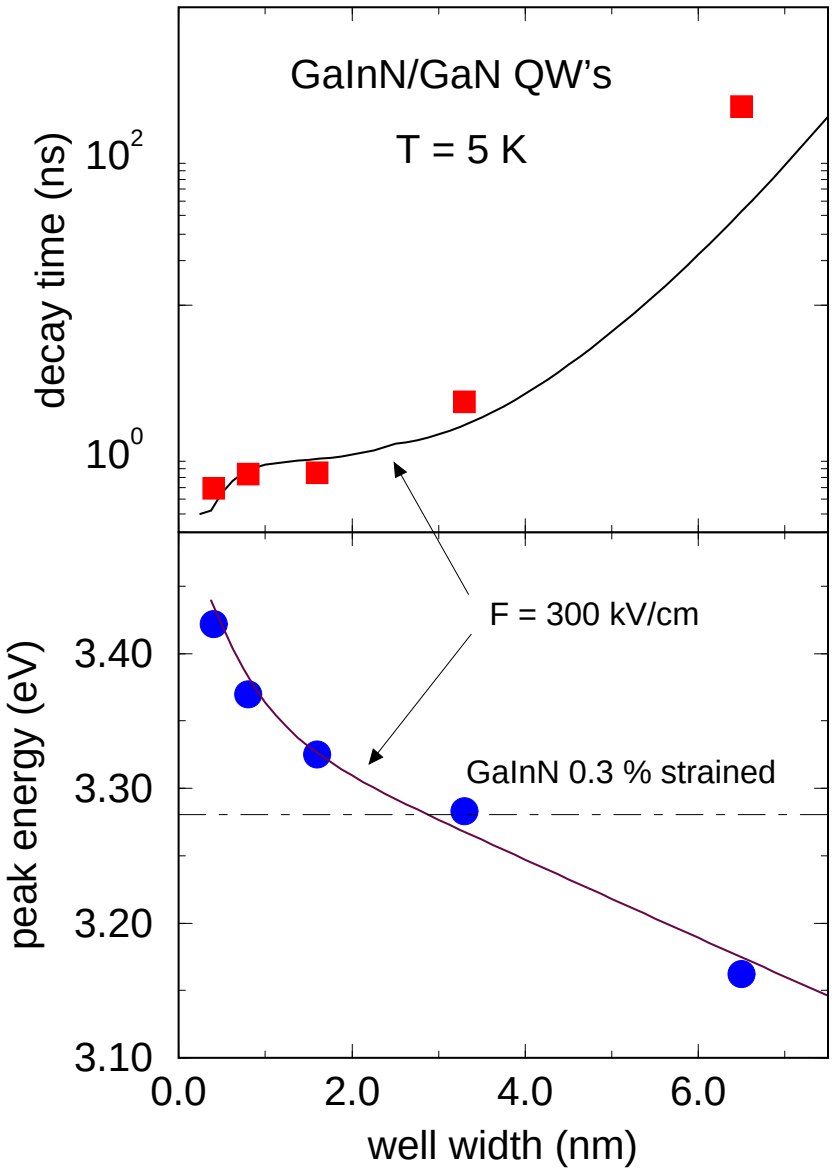

Figure 3.10: *Comparison of the measured energy position (dots) and decay times (squares) of emission lines in GaInN/GaN quantum wells with a numerical calculation using a piezoelectric field of 300 kV/cm.*

the conduction band offset and the bandgap difference is determined to be only 0.3 for GaInN/GaN quantum wells and in contrast 0.75 for GaN/AlGaN quantum wells (see Section 1.3). Thus the wave function of electrons in GaInN/GaN quantum wells penetrate more strongly into the barrier due to the small conduction band offset, which leads to a weak electron confinement. With increasing well width the potential drop over the quantum well is enlarged, and electrons are more strongly pushed into the barrier, which can lead to critical electron confinement and enhancement of decay time.

3.2.3 Origin of Stokes shift

In order to address the Stokes shift, we perform calculations of the absorption spectra of quantum wells with a strong built-in field. These are based on numerical calculations of the energies and wave functions of electrons and holes in piezoelectric quantum wells. Typical results for these are depicted in Figure 3.11, showing that the electron and the hole are localized at opposite sides of the quantum well. As shown from time-resolved photoluminescence measurements, this leads to a dramatic reduction of the oscillator strength by many orders of magnitude. It is most important here to note that this reduction of oscillator strength also means that there is almost no absorption due to the lowest-energy transition. Only higher excited states, particularly in the valence band, provide a large enough wavefunction overlap to allow for significant absorption. Such transitions become possible only for tilted wells, whereas for square wells they would be forbidden due to the higher symmetry of the wave functions.

By adding up the contributions of the various states we calculate absorption spectra for GaInN/GaN quantum wells of different well width, assuming a built-in field of 1 MV/cm typical for about 9% In, as shown in Figure 3.12. In this figure, the photoluminescence position is indicated by a Gaussian line with a linewidth as observed in typical experiments. The results show that significant absorption sets in only at photon energies around the bandgap of the bulk well material. Since the photoluminescence due to the quantum well ground state is shifted down

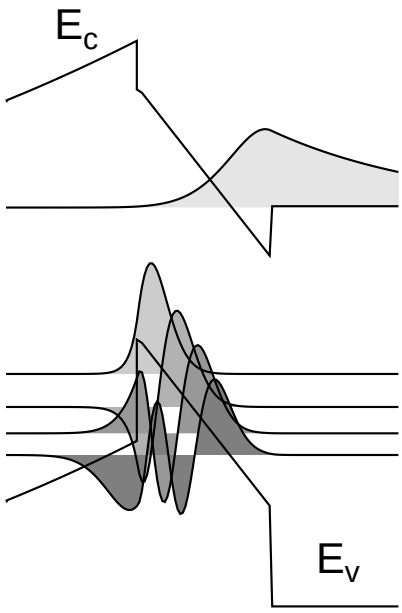

Figure 3.11: *Schematic view of optical transitions in a piezoelectric quantum well.*

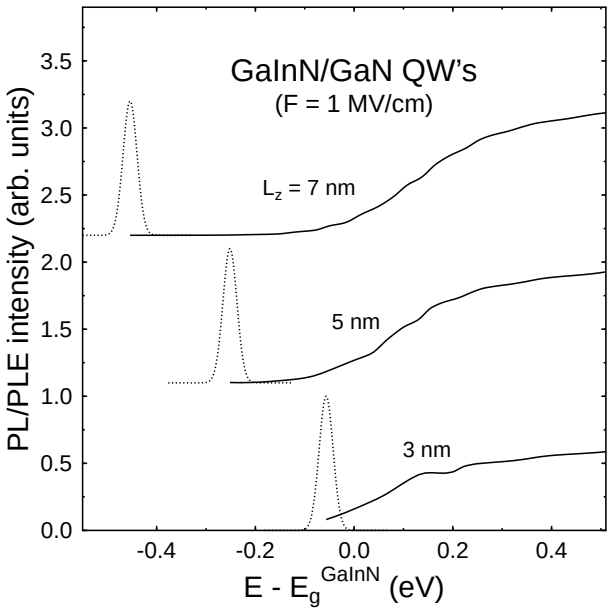

Figure 3.12: *Calculated photoluminescence excitation spectra of piezoelectric quantum wells.*

in energy by the polarization field, this results in a large Stokes shift as observed experimentally (see Figure 3.4). It is interesting to note that the Stokes shift increases with increasing well width in Figure 3.12, which consists with experimental results.

3.2.4 Inhomogeneous broadening and piezoelectric field

As noticed in Section 3.1 that the photoluminescence linewidths of GaInN/GaN and GaN/AlGaN quantum wells are fairly large compared to that of bulk GaN. The broad linewidth of GaInN/GaN quantum well has been explained in terms of In composition fluctuation [11, 72]. However, for GaN/AlGaN quantum wells using a binary semiconductor as the active layer, the origin of linewidth broadening cannot be clearly explained by the composition fluctuation model. Now, the piezoelectric field is taken into account when analyzing the linewidths of quantum wells.

The effective bandgap energy in a piezoelectric quantum well is given by

$$E_{\mathrm{g}}^{\mathrm{eff}} = E_{\mathrm{g}}^{0} + E_{\mathrm{q}} - e \times F \times L_z, \tag{3.2}$$

where E_{g}^{0} is the bulk bandgap of the well material, E_q is the quantization energy, and $e \times F \times L_z$ is the field-induced redshift of the gap.

In a first approximation, the variation of the effective gap, i.e. the linewidth, is given by the sum of fluctuation terms due to the bulk gap, the quantization energy, the field, and the well width.

$$\delta E_{\mathrm{g}}^{\mathrm{eff}} = \delta E_{\mathrm{g}}^{0} + \delta E_{\mathrm{q}} + e \times L_z \times \delta F + e \times F \times \delta L_z \tag{3.3}$$

To estimate terms in Equation 3.3 quantitatively, we assume a relative In fluctuation of 10% and a well fluctuation of a monolayer, i.e. about 0.3 nm. We consider for example a typical 3 nm GaInN/GaN quantum well with a piezoelectric field of about 1 MV/cm appropriate to an In content of 10%. We can neglect the variation of the quantization energy δE_{q} in case of quantum wells which are thicker than the Bohr radius of excitons (i.e. about 2 nm). Using Equation 1.5, the bulk gap fluctuation is estimated to be about 40 meV. The field fluctuation δF

is induced by the In fluctuation and estimated therefore to be about 0.1 MV/cm. The third and fourth terms of Equation 3.3 are approximately 30 meV. In this rough estimation, the total effective bandgap fluctuation of 100 meV is found, which is comparable to the experimental results. This estimation exhibits that the linewidth is significantly broadened in the presence of the piezoelectric field.

We can divide the terms in Equation 3.3 into two groups according to dependence on well width as follows:

$$\delta E_{\mathrm{g}}^{\mathrm{eff}} = (\delta E_{\mathrm{g}}^{0} + e \times F \times \delta L_z) + (e \times \delta F) \times L_z \tag{3.4}$$

This equation reveals a linear relation between the linewidth and the well width. The field fluctuation δF can be expressed as a function of the composition fluctuation δx using composition bandgap dependence given by Equation 1.4. Thus the slope of the linear relation yields the composition fluctuation δx.

Figure 3.13 shows photoluminescence spectra of $Ga_{0.88}In_{0.12}N$/GaN quantum wells at 5 K. We can observe the linear increase of the linewidth of $Ga_{0.88}In_{0.12}N$/GaN quantum wells with increasing well width.

The analysis of photoluminescence linewidth for GaInN/GaN and for GaN/AlGaN quantum wells is summarized in Figure 3.14. The straight line is a linear least-squares fit to the data. Interestingly, the slope of this straight line gives, directly, the composition fluctuation. Knowing this, the well width fluctuation from the constant term is extracted, thereby separating the two contributions quantitatively.

In the case of $Ga_{0.88}In_{0.12}N$ quantum wells, a relative In fluctuation is found to be well below 10% and a typical thickness fluctuation about 0.29 nm, i.e. 1 monolayer. For GaN/$Al_{0.85}Ga_{0.15}N$ quantum wells, there is a fluctuation of barrier height and strain of 10% and a thickness fluctuation of 0.43 nm. With moderate composition and well-width fluctuation, the large linewidth of both quantum wells can be well explained by a piezoelectric field.

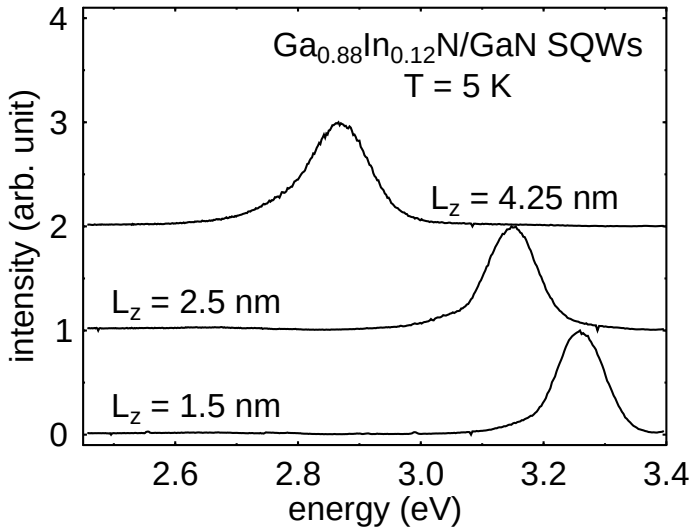

Figure 3.13: *Photoluminescence spectra of $Ga_{0.88}In_{0.12}N/GaN$ quantum wells at 5 K.*

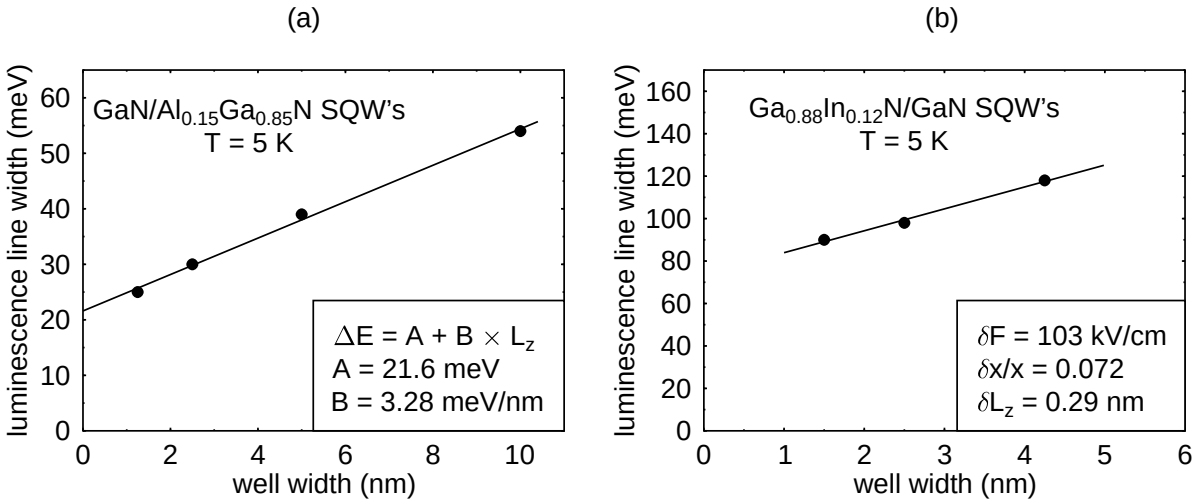

Figure 3.14: *Measured luminescence linewidth for GaInN/GaN quantum wells (a) and for GaN/AlGaN quantum wells (b). The strain line is a linear least-square fit to the data.*

Chapter 4

Study on asymmetric quantum well structures

Based on the knowledge acquired in Chapter 3, the piezoelectric field effect will be studied in more detail, approaching this from a new prospective, that being, that the piezoelectric field breaks the inversion symmetry of single quantum wells. In the presence of the piezoelectric field, the band structure of the single quantum well is not invariant under the inversion symmetry operation with respect to the center. Therefore, the lack of inversion symmetry is unambiguous evidence for the existence of the piezoelectric field.

To investigate this, samples employing asymmetric quantum well structures were designed, which feature two different barriers on the two sides of the quantum well. Samples studied are classified by two groups. First, an additional AlGaN barrier is introduced to a GaInN/GaN single quantum well, so that the GaInN active layer is asymmetrically sandwiched by the barrier layers. Secondly, we dope only one of the GaN barrier layers, and the quantum well is embedded in asymmetric doped barriers.

In the following sections, it will be demonstrated how the asymmetry introduced to single quantum wells can unveil the lack of inversion symmetry and verify the existence of the piezoelectric field. Furthermore, asymmetric structures enable us to determine the sign of the piezo-

electric field based on the asymmetry, and we will also discuss the relation between the piezoelectric polarity and the crystallographic polarity.

4.1 Asymmetric barrier structure: GaInN/AlGaN/GaN single quantum wells

Single GaInN/GaN quantum wells with an additional AlGaN barrier will be studied. The structure of these samples is shown in Section 2.2. The thickness of the GaInN layers is chosen to be 7 nm, which is large enough so that the piezoelectric field effect dominates optical transitions.

4.1.1 Basic concept: carrier confinement

For GaInN/GaN quantum wells, electrons are confined less strongly than holes due to the small band offset in the conduction band (see Section 1.3). Additionally, due to the small effective mass of electrons, the wave function of electrons penetrates more strongly into the barrier layer. Thus, the additional barrier affects particularly the electron confinement.

Figure 4.1 shows, schematically, the effect of an one-sided increase of barriers on the conduction band. In case there is no internal field in the quantum well, the electron confinement is not dependent on the position of the additional barrier. The samples with the additional barrier on the right or left side of a quantum well are equivalent in the potential

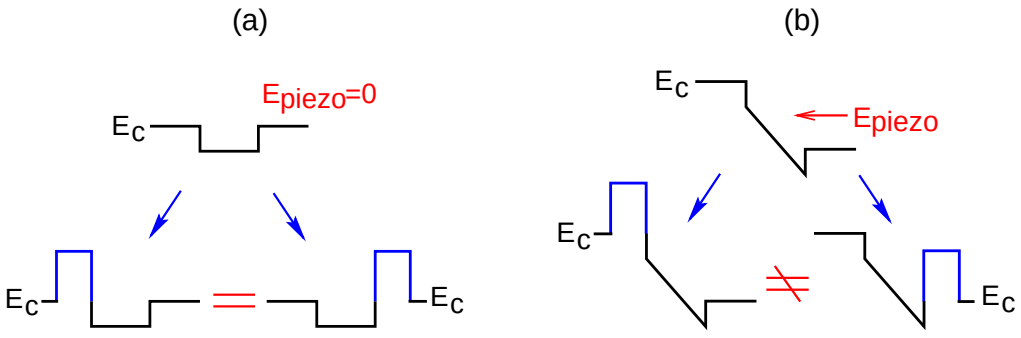

Figure 4.1: *Schematic picture of the conduction band structure with an additional barrier without a piezoelectric field (a) and with a piezoelectric field (b).*

profile and display no difference in optical properties. In the presence of an internal field in the quantum well, the inversion symmetry is broken, and the electron confinement depends strongly on the position of the additional barrier. As shown in Figure 4.1(b), the electron confinement is enhanced if the additional barrier is placed at the side to which the internal field pushes electrons (in this case at the right-hand side of the well). We can therefore expect a difference in the transition energy and the recombination rate with the introduction of an additional barrier. Based on this concept, two GaInN/GaN quantum wells with an additional AlGaN barrier layer below or above the quantum well were grown and studied. As a control sample, a 7 nm GaInN/GaN single quantum well without an additional barrier is also studied.

4.1.2 Optical transition and location of the AlGaN barrier

Low-temperature photoluminescence spectra of these GaInN/GaN quantum wells with asymmetric barrier structure are summarized in Figure 4.2. As shown in time-integrated spectra (dotted curves), the sample with an AlGaN barrier below the quantum well has an emission maximum at 3.060 eV, below the emission line (dot-dashed line) of the reference sample without the AlGaN barrier. In contrast, the other one exhibits a broad emission band with two maxima at 3.146 eV and 3.236 eV, above the emission line of the reference sample. A more detailed picture is given by time-resolved spectra (solid curves). At short delay times, both samples show an emission line near 3.245 eV, but their temporal behaviors are clearly different afterwards: in the sample with the AlGaN barrier on top of the quantum well, an additional lower-energy emission line emerges with increasing time and finally reaches 120 meV below the emission line at early times, but the other sample with the AlGaN-barrier below the quantum well shows a dramatic redshift by about 220 meV, even 65 meV below the emission maximum of a simple GaInN/GaN quantum well without the AlGaN layer.

A closer look is taken at the emission lines which dominate at long delay times and measurements of the decay traces of each sample are made at luminescence maxima in the late time interval. What is found is

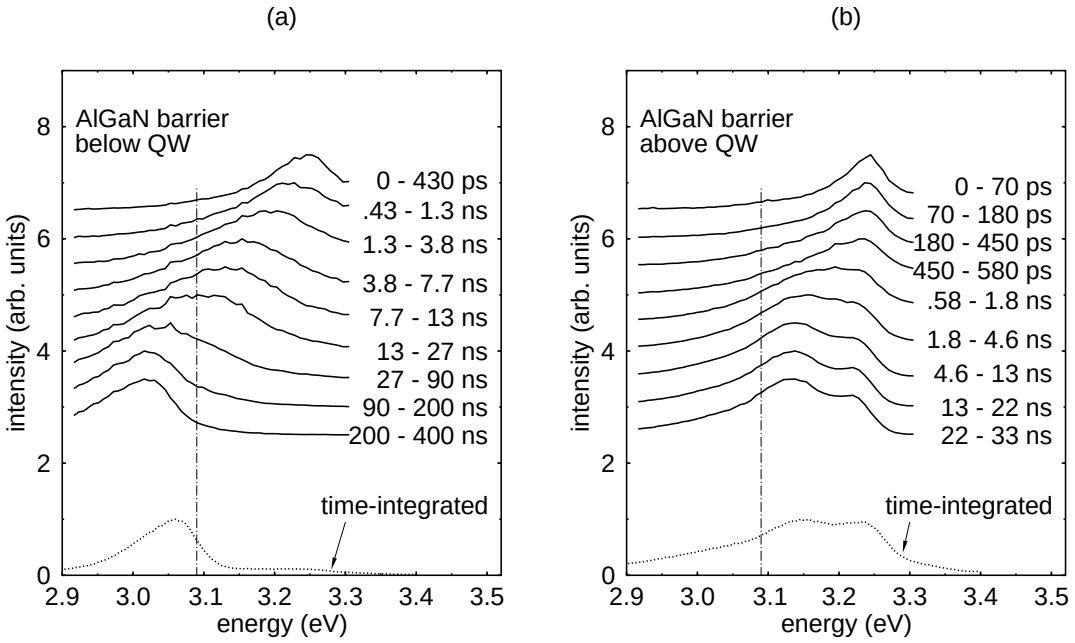

Figure 4.2: *Time-integrated (dotted curves) and time-resolved (solid curves) low-temperature spectra of GaInN/GaN quantum wells with an additional AlGaN barrier below (a) or above (b) the quantum well. The dot-dashed lines indicate the emission energy of a simple GaInN/GaN quantum well without the AlGaN barrier.*

that the luminescence intensity of the sample with AlGaN barrier above the quantum well decays much faster than that of the other one with AlGaN barrier below the quantum well (see Figure 4.3). At long delay times, a decay time of 77 ns is obtained for the former, which is about 500 times smaller than that of 34 μs for the latter.

Figure 4.4 depicts the decay traces of the emission maxima at 3.245 eV, which are observed in time-resolved spectra of both samples at a short delay time after pulsed excitation. In addition to the similar energetic position of the emission lines, the luminescence intensities decay in a comparable time scale. Compared with the decay of the emission lines at long delay time, those emission lines show a fast decay in the nanosecond range.

As considered in the previous section, the differences in the transition energy and the luminescence decay, indicate the lack of inversion

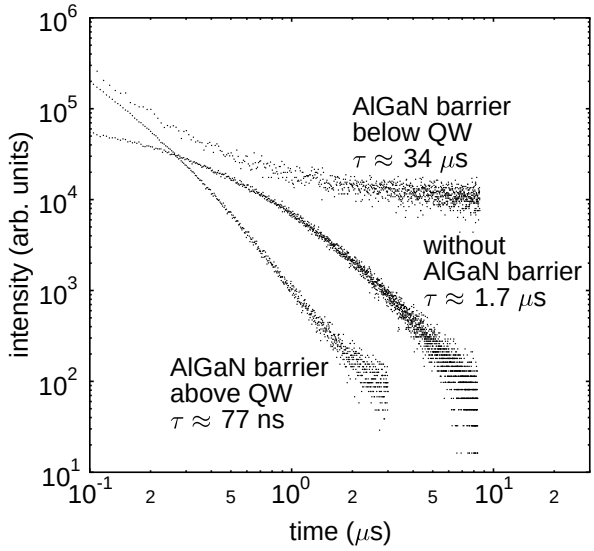

Figure 4.3: *Double-logarithmic plot of the luminescence decays for asymmetric structures at emission maxima in the late time interval.*

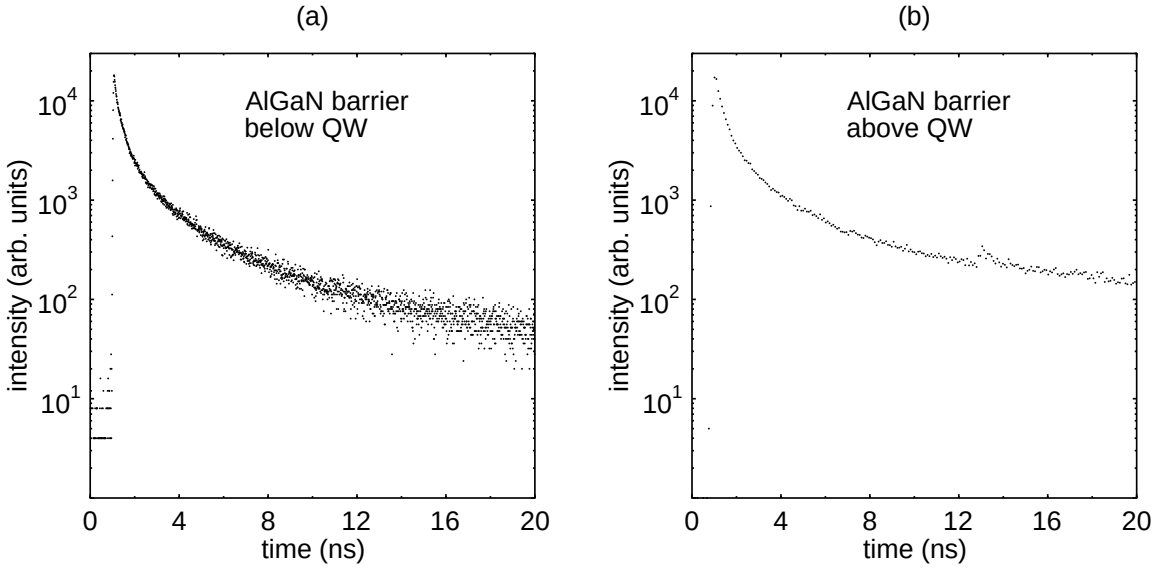

Figure 4.4: *Semi-logarithmic plot of the luminescence decays of emission maxima at 3.245 eV, which are observed in time-resolved spectra of both samples at a short delay time.*

symmetry in quantum wells. This asymmetrical behavior observed in the optical properties is indeed unambiguous evidence as to the existence of the piezoelectric field. If there were to be no electric field in the quantum well, both samples would be identical in their optical properties.

The temporal redshift of the emission lines is due to the recovery of the piezoelectric field partially screened by photoexcited electron-hole pairs. The similar emission energy and the comparable decay traces observed at a short delay time support the assumption that the piezoelectric field is screened at this time interval, which results in such similar optical properties.

Our principal interest is in the optical properties at a long delay time when the piezoelectric field has almost recovered. At this time region, the sample with the AlGaN layer on top of the quantum well exhibits the shortest decay time when compared with the other samples. As considered in Section 4.1.1, this indicates enhanced oscillator strength due to increased electron confinement as can be seen in the rightmost diagram in Figure 4.1. Thus we can reach the conclusion that the piezoelectric field points towards the substrate. In the other case where the AlGaN barrier is placed below on the quantum well, the electron confinement is reduced by the additional barrier leading to a longer decay time.

However, the above qualitative explanation is not sufficient enough to understand the experimental results completely. Particularly, the energetic position of the emission lines cannot be explained easily. The emission energy of the sample with an AlGaN layer above the quantum well may be higher than that of the simple quantum well because of increased quantum confinement energy. But the reason why the emission line of the other asymmetric sample lies 65 meV lower than that of the reference sample is still unclear. Deeper insight will be provided by numerical calculations of band structure in the next section.

4.1.3 Numerical calculation of band structures: screening effect

Bearing in mind the direction of the field determined in the previous section, self-consistent calculations of the equilibrium band structure

were performed as described in Appendix B. At first, the conduction band of a simple 7 nm GaInN/GaN quantum well was calculated with a piezoelectric field of 300 kV/cm. The GaN barrier layers are assumed relaxed and have no piezoelectric field. A background carrier density of 5×10^{16} cm^{-3}, which is estimated in nominally undoped samples, is applied. The result of the calculation of the equilibrium band diagram, which is depicted in Figure 4.5, reveals a strong global band bending. The band in the GaN buffer layer is bent upward, and electrons are depleted. The positive space-charge in the GaN buffer layer and electrons accumulated in the quantum well and the GaN cap layer build an electrostatic field (F_{scr}) which points in the opposite direction to that of the piezoelectric field (F_{piezo}) and screens it. Therefore, the effective field (F_{eff}) in the quantum well is smaller than the strain-induced piezoelectric field, and this calculation results in F_{eff} of 240 kV/cm, which is reduced by approximately 20 % from F_{piezo}.

The calculated band structures with an additional AlGaN barrier are more complex (see Figure 4.6). The AlGaN and GaInN layer are assumed

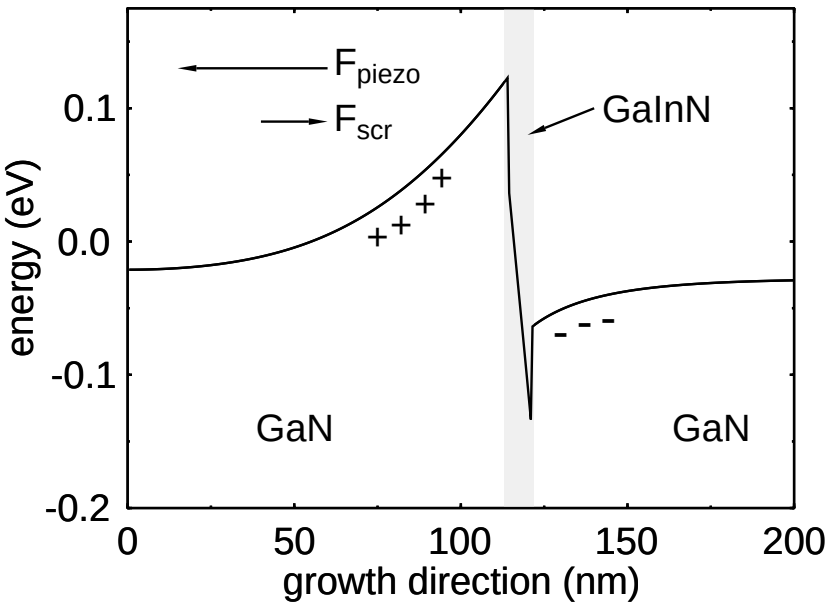

Figure 4.5: *Calculated equilibrium conduction band diagram of a GaInN/GaN single quantum well with a piezoelectric field.*

to be in tension and compression, respectively. Strain-induced piezoelectric fields are estimated as 350 kV/cm for the former and 300 kV/cm for the latter with an opposite direction. To have a close look at conduction bands, the enhanced electron confinement with an AlGaN barrier above the GaInN quantum well is clearly recognizable as expected previously. A further comparison between the band structures reveals that the potential energy drop over the quantum wells is not equal. In the case of an AlGaN barrier above the quantum well, a depletion region is established in the GaN buffer and cap layer. The electrons accumulated in the quantum well screen the piezoelectric fields both in the quantum well and in the AlGaN barrier. With an AlGaN barrier below

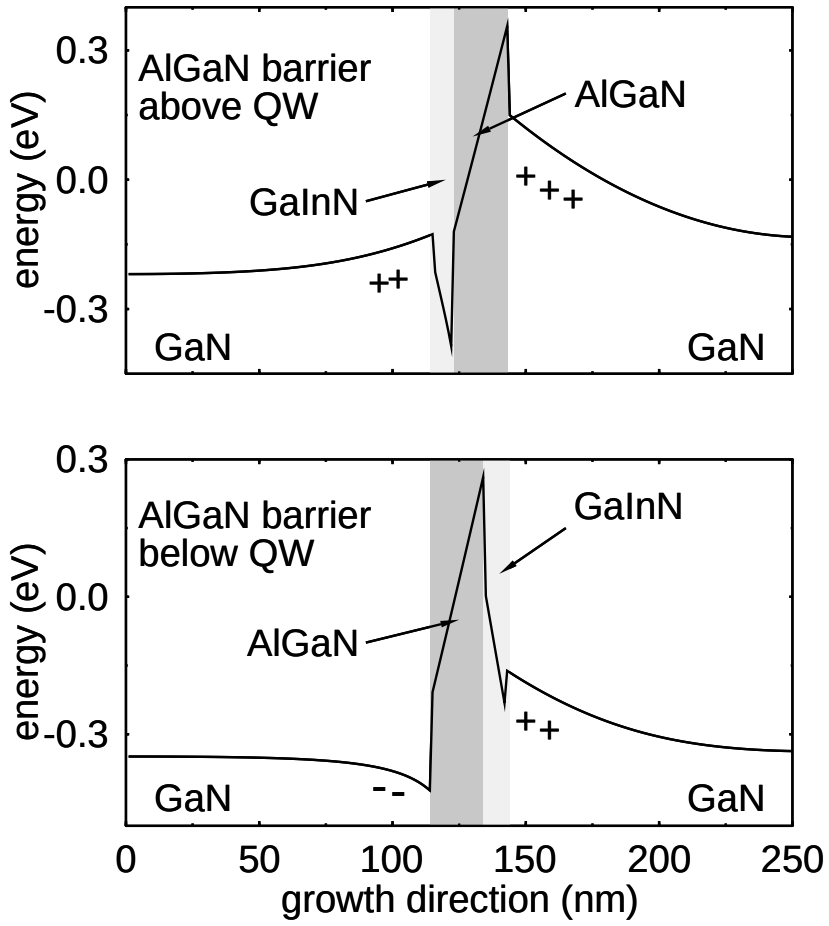

Figure 4.6: *Calculated conduction band structures of samples with an additional AlGaN barrier.*

the quantum well, electrons are accumulated in the GaN buffer layer, and the depletion region in GaN cap layer screens the piezoelectric field in the AlGaN barrier but reinforces it in the quantum well. The screening effect, therefore, depends on the placement of the AlGaN barrier: F_{eff} is calculated as 240 kV/cm and 330 kV/cm for the AlGaN barrier above and below the quantum well, respectively.

At this point, the energetic position of the emission lines can be well understood. The emission line of the sample with the AlGaN barrier below the quantum well lies about 65 meV below the emission line of the simple quantum well without AlGaN barrier. The different effective field (ΔF_{eff}) accounts for this emission energy difference (ΔE): $\Delta E = \Delta F_{\text{eff}} \times L_{\text{z}}$. The calculated effective field difference results in an energy shift of about 60 meV, which is quite comparable to the experimental results if considering unknown parameters, e.g. the electron concentration. On the other hand, the AlGaN barrier above the quantum well enhances the electron confinement, and therefore the increased confinement energy leads to an emission energy higher than that of the simple quantum well.

4.1.4 Alternative substrate: silicon carbide

Until now, we have studied samples grown on sapphire substrate. In this section, we study samples with the same asymmetric barrier structure grown on silicon carbide substrate to test the influence of the substrate on the piezoelectric effect. Unlike sapphire, silicon carbide is a polar crystal, and the surface polarity influences the epitaxial growth.

Figure 4.7 shows the low-temperature photoluminescence spectra of two quantum wells with asymmetric structure and a simple quantum well without the AlGaN barrier. The simple quantum well has an emission maximum at 3.08 eV, and phonon replica are recognizable. The sample with an AlGaN barrier below the quantum well exhibits no emission related to the GaInN layer but a broad emission band around 2.67 eV emitted by the SiC substrate [84]. In contrast, the sample with an AlGaN barrier above the quantum well shows an emission, and its maximum lies higher than that of the simple quantum well.

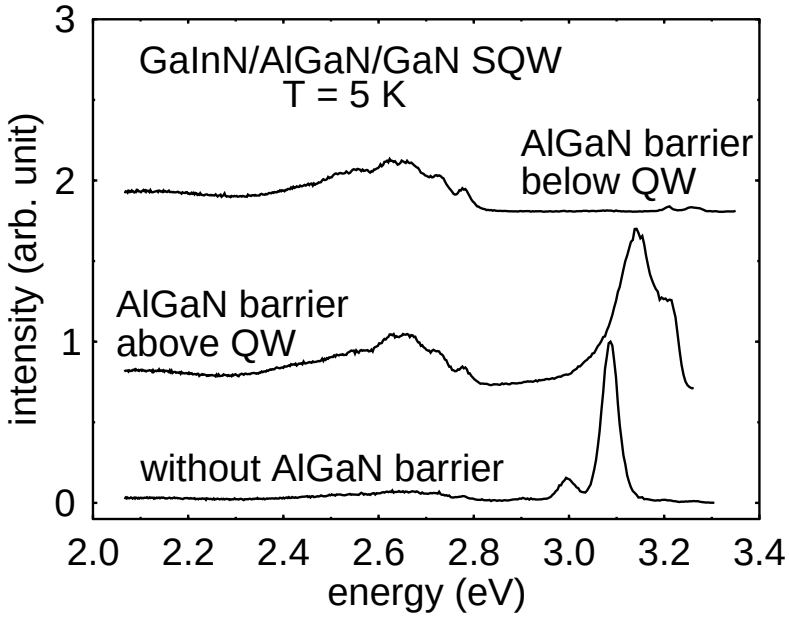

Figure 4.7: *Time-resolved low-temperature photoluminescence spectra of GaInN/GaN quantum wells grown on substrate SiC with and without an additional AlGaN barrier.*

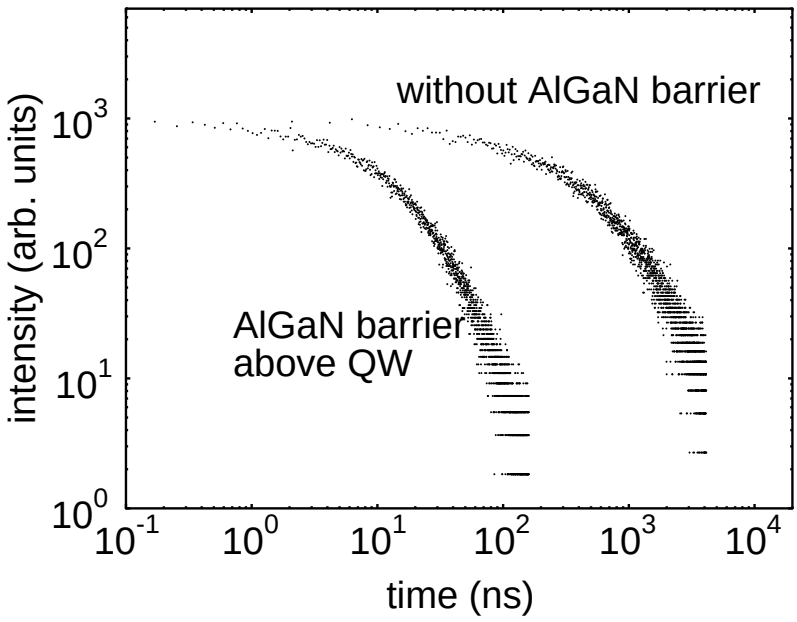

Figure 4.8: *Photoluminescence decay of GaInN/GaN quantum wells grown on substrate SiC with and without an additional AlGaN barrier.*

A more detailed picture is given by decay traces at the respective luminescence maximum (see Figure 4.8). It is found that the luminescence intensity of the sample with an AlGaN barrier above the quantum well decays much faster than that of a simple quantum well without an AlGaN layer. At long delay time, a decay time of 25 ns is obtained for the former and 100 ns for the latter.

The differences among the samples in optical properties indicates again the existence of a piezoelectric field. The sample with an AlGaN layer above the quantum well exhibits increased oscillator strength and blueshift, which can be interpreted as enhanced electron confinement, as discussed in the previous sections. While we have earlier observed that a decay time decreases by 2-3 orders of magnitude if the AlGaN layer is grown on the other side of the quantum well, the sample with the same structure grown on substrate SiC shows quenched optical transitions indicating an extreme decrease in electron confinement.

It is interesting to note that the AlGaN layer above the quantum well increases electron confinement in the both sample groups, which are grown on silicon carbide and sapphire substrate, respectively. Thus we can conclude that the direction of the piezoelectric field is not dependent on the choice of silicon carbide or sapphire substrate for epilayers grown by the use of MOCVD.

4.2 Asymmetrically doped structure

To proceed investigating the lack of inversion symmetry in GaInN/GaN single quantum wells, asymmetry is introduced to the single quantum wells by one-sided asymmetrical doping of the GaN barriers. As seen in the detailed study on the asymmetric barrier structure, the background carriers are expected to screen the piezoelectric field built in the quantum well and in turn affect the optical properties. Thus, an asymmetrically doped structure may confirm the presence of the piezoelectric field again and furthermore provide a deeper understanding of the screening effect.

In this section, we study 6 nm GaInN/GaN quantum wells sandwiched between selectively doped or undoped GaN barriers. In one sample, both the lower and upper cladding GaN layer are doped with

Si. Another sample adopts one-sided asymmetrical doping of the GaN barrier: only the upper GaN cap layer is doped while the lower GaN buffer layer is nominally undoped. The Si-doping level estimated as (1-2)$\times 10^{18}$ cm^{-3}. 6 nm and 3 nm single GaInN/GaN quantum wells are also studied as reference samples.

4.2.1 Influence of doping on optical transitions

The low-temperature photoluminescence spectra of these samples are shown in Figure 4.9. It is noted that the spectral width of the emission lines is about 60 meV, which is rather small for GaInN/GaN quantum

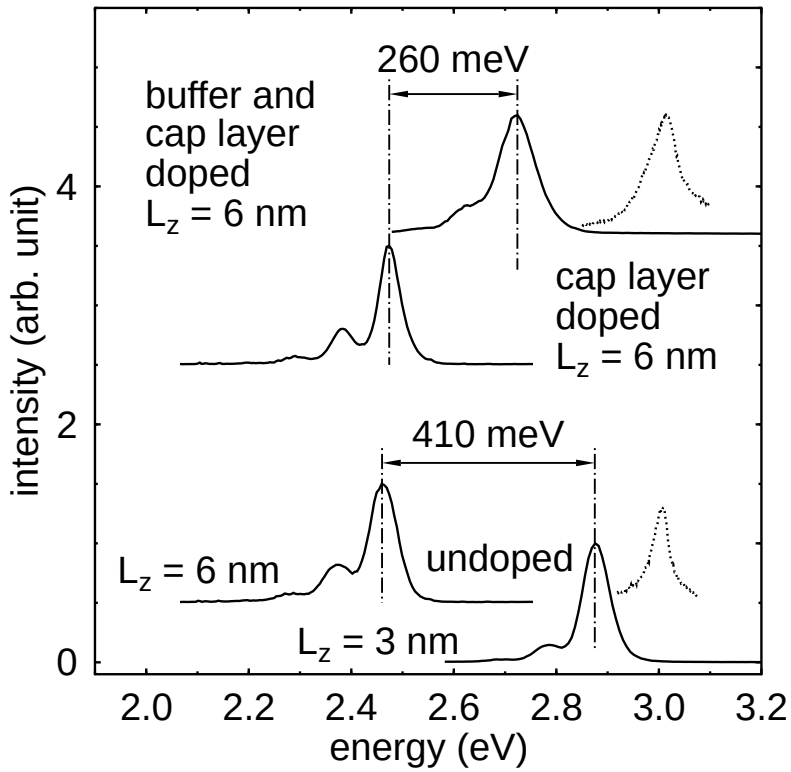

Figure 4.9: *Photoluminescence spectra of GaInN/GaN single quantum wells with and without Si-doping in the GaN barriers. The stimulated emissions are indicated by dotted curves.*

wells and indicates high sample quality. Clearly resolved phonon replicas are also observed, with an energy spacing equal to the LO phonon energy of 92 meV [85]. Moreover, the fact that the stimulated emission (dotted curves) appears at the same position confirms that there is no significant variation of In content or well width fluctuation. Under the high-power excitation condition, the piezoelectric field is almost screened by photo-excited carriers. Therefore, the In content can be estimated to be 11% from the stimulated emission energy using Equation 1.5.

The emission maximum of the 3 nm GaInN quantum well with nominally undoped GaN barrier layers lies at 2.875 eV and shifts toward 2.460 eV with increased well width of 6 nm. This energy difference allow us to estimate an effective field of about 1.4 MV/cm in the quantum well. The emission energy of the sample when only a GaN cap layer is doped is almost the same as that of the sample with undoped GaN barrier layers. In contrast, the sample doped in both the GaN buffer and cap layer shows a blueshift of about 260 meV. Obviously, the blueshift is due to the screening of the piezoelectric field by electrons supplied by the n-doping. The energy shift of 260 meV corresponds to a change in the electric field of 430 kV/cm for a 6 nm quantum well. However, it is not immediately clear why the screening takes place only if electrons are supplied by the lower cladding layer.

The explanation is provided by considering the calculated band structure shown in Figure 4.5. In the band diagram, a space-charge region is established in the lower GaN cladding layer and induces an electrostatic field screening the piezoelectric field together with electrons accumulated in the heterointerface between the quantum well and upper GaN layer due to the piezoelectric field. The doping level of the lower GaN cladding layer, therefore, has a dominant influence on the screening effect but not on that of the upper GaN cap layer. This asymmetric behavior is exactly what was observed experimentally.

It should to be noted that the issues discussed here are directly related to the question of the sign of the piezoelectric field. If the field had the opposite sign, the doping of the upper GaN cap layer would be effective for screening, and the emission line of the sample where the upper GaN cap layer is doped would shift toward lower energy. Therefore, the piezo-

electric field points towards the substrates, which is consistent with the earlier determination of the sign of the field (see Section 4.1).

Several groups have discussed the effect of doping on optical properties of nitride quantum wells in terms of the carrier localization at potential fluctuation [15, 86, 87]. It was noted that increasing the doping level led to a blueshift of the luminescence peak [86] and decreasing carrier lifetime [87]. This was attributed to an increased homogeneity of the wells. However, due to the screening effect, the presence of background carriers is also expected to have a considerable impact on the optical properties of those samples. Furthermore, the asymmetric behavior of the doping effect cannot be completely explained by the localization model, which confirms a dominant effect of the piezoelectric field on the optical properties of nitride quantum wells.

4.2.2 Analytical calculation of screened electric field

To calculate the screening field analytically, we develop a simple model as follows. Under the abrupt approximation, the depletion-region width l below the quantum well can be expressed as $l = (2\epsilon_0\epsilon_\mathrm{r}\Phi/eN_\mathrm{D})^{1/2}$ with a potential drop $\Phi = F_\mathrm{eff} \times L_\mathrm{z}$ over the quantum well [88]. The doping density N_D is assumed as spatially homogeneous, and the electron concentration in the depletion region is neglected. Integrating over the depletion-region width gives the resultant electric screening field $F_\mathrm{scr} = eN_\mathrm{D}l/\epsilon_0\epsilon_\mathrm{r}$. The effective field $F_\mathrm{eff} = F_\mathrm{piezo} - F_\mathrm{scr}$ is therefore given by

$$F_\mathrm{eff} = F_\mathrm{pizeo} + \frac{eN_\mathrm{D}L_\mathrm{z}}{\epsilon_0\epsilon_\mathrm{r}}\left\{1 - \sqrt{1 + \frac{2F_\mathrm{piezo}}{eN_\mathrm{D}L_\mathrm{z}/\epsilon_0\epsilon_\mathrm{r}}}\right\}. \tag{4.1}$$

For a doping density of $5 \times 10^{16}\mathrm{cm}^{-3}$, an intrinsic piezoelectric field of 300 kV/cm, and a well width of 7 nm, an effective field is given by this equation as 243 kV/cm in agreement with the previous result from the numerical calculation in Section 4.1.3. The effective fields can therefore be well calculated by this simple analytical model in a good approximation.

Now, we apply this model to the experimental results. A doping level of (1-2)$\times 10^{18}$ cm^{-3} results in blue-shift of about 260 meV in a 6 nm quantum well, which means a reduction of the effective field by 440 kV/cm ($\approx$ 260 meV/6 nm) to 940 kV/cm. Figure 4.10 shows the values of F_{eff} as a function of the doping density with a piezoelectric field of 1500 kV/cm according to Equation 4.1. Both the difference of the effective field strength and the corresponding doping density can be clearly explained by the model.

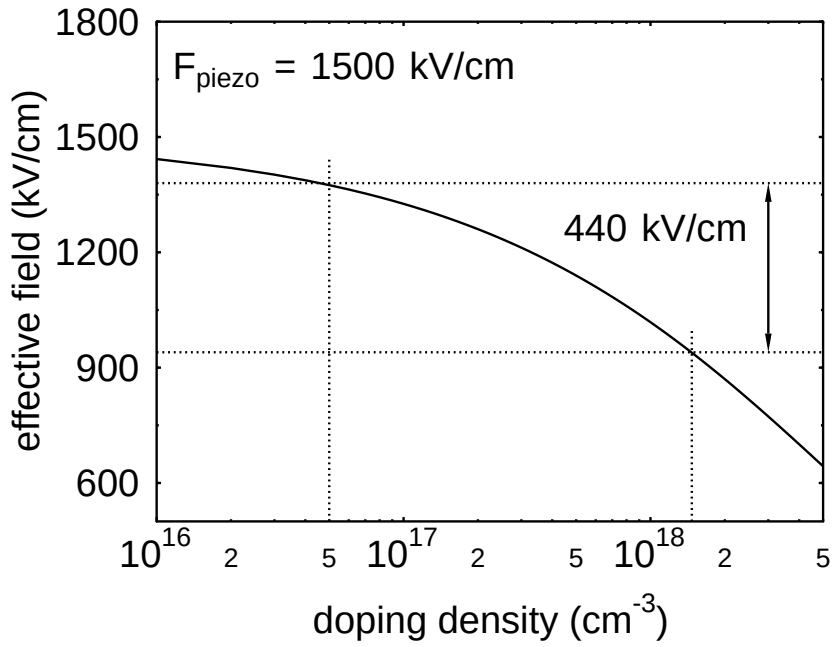

Figure 4.10: *Effective electrostatic field in a 6 nm quantum well versus doping density for a intrinsic piezoelectric field of 1500 kV/cm.*

4.3 Crystallographic polarity and sign of piezoelectric field

The crystallographic polarity of epitaxial grown nitride layers is a key parameter in obtaining smooth surface morphology and low defect density, on which the optimization of optoelectronic devices depends crucially. The determination of the polarity has therefore attracted a

lot of interest and has been studied using various techniques such as ion channeling, convergent beam electron diffraction (CBED) [89], x-ray photoelectron spectroscopy (XPS), transmission electron microscopy (TEM) [90] and etching method [91]. In this study, the possibility of using the sign of the piezoelectric field is considered as a way to determine the crystallographic polarity. First the sign convention is discussed to avoid confusion in the use of terminology [92, 93] .

Wurtzite-type compound semiconductors have a non-centrosymmetrical structure. The stacking sequences of atomic planes are reversed along [0001] and [000$\bar{1}$] directions. Consequently, the [0001] and [000$\bar{1}$] directions are non-equivalent. Ga-N bonds aligned along the *c*-axis are oriented in one direction, and the vector, which starts on Ga and points to N, defines the positive direction of *c*-axis (see Figure 4.11). The epitaxial growth of the nitrides is typically done along the polar axis. The polarity of the epitaxial nitrides films is defined by the orientation of *c* with respect to a vector which points outward normal to the surface of the film. The epilayer has a Ga-polarity or N-polarity and is called a Ga-face or N-face, when its surface normal vector is

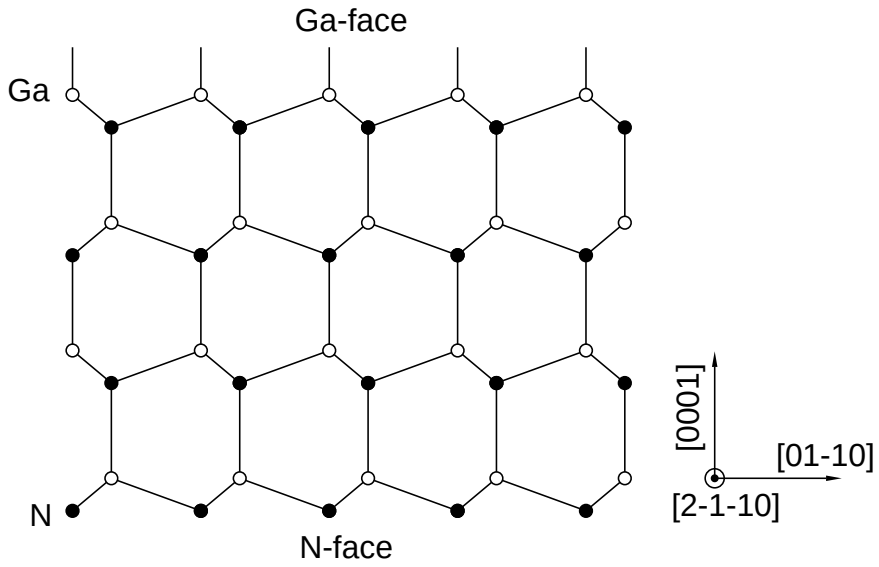

Figure 4.11: *[2-1-10] projection of wurtzite GaN. Considering the GaN bonds along the c-axis, the* **c***=[0001] vector starts on Ga (white) and points to N (black).*

parallel or antiparallel to **c** = [0001], respectively. The above polarity definitions do not refer to a surface property as like surface termination. However, the polarity can influence the termination type. If there is no special reconstruction of the bonds at the surface, a Ga-face surface has potentially a Ga termination to minimize the number of dangling bonds.

In a typical GaInN/GaN quantum well, a GaInN layer is grown on a thick GaN layer along the c-axis. Because of the 11% lattice mismatch between GaN and InN, a pseudomorphic GaInN film is formed under biaxial compressive strain in the growth plane, resulting in tensile strain along the c-axis. These strains induce an electric field that can be simply expressed via the piezoelectric coefficient d_{31} (see Equation 1.8). The sign of the piezoelectric field is determined by the sign of the coefficient. Principally, there is no conclusive relationship between the crystallographic polarity and the piezoelectric polarity. Bernardini *et al.*'s calculation of the piezoelectric coefficients suggested that piezoelectric coefficients have the same sign as in II-VI compounds, and opposite to III-V compounds [56]. Guided by the theoretical sign of piezoelectric coefficients, the direction of the piezoelectric field in a compressively in-plane strained quantum well is the opposite of the [0001]-direction. Because we find that the piezoelectric field in GaInN/GaN quantum wells points towards the substrate, the epilayers are grown in [0001]-direction and are Ga-face. N-face GaN epilayers are generally found to have a rough surface morphology comprising pyramidal grains and extended defects such as inversion domains [91, 93]. Conversely, Ga-faces GaN epilayers tend to have a smooth surface morphology and low defect density. Thus, the high epitaxial quality of the samples used here complies well with the Ga-polarity assumed by using the sign of the piezoelectric field and the theoretical calculation of the piezoelectric coefficients.

The GaInN/GaN quantum wells on sapphire and SiC substrates display the same orientation of the piezoelectric field. Therefore, we can conclude that the crystallographic polarity of epilayers on sapphire and SiC substrate both are Ga-face. But, it should be noted that the polarity selection can be obtained by the pretreatment of the substrate surface [91]. It is well known that GaN layers grown on the polar substrate like SiC assemble the polarity of the substrate: Ga-face GaN grows on Si-face

SiC and N-face GaN grows on C-face SiC.

It is interesting to compare the results here with other measurements to determine the piezoelectric polarity. Studies on pseudomorphically strained AlGaN/GaN heterojunction device structure showed an enhanced two-dimensional electron density at AlGaN-on-GaN interfaces due to the band bending effect of the piezoelectric field [55, 94, 95]. This result indicates that the in-plane tensile strain in the AlGaN layer induces a piezoelectric field parallel to the growth direction, which agrees conclusively with the results of this study.

Chapter 5

Study on multiple quantum wells

Until now the optical properties of single quantum wells have been concentrated on. In this chapter, multiple quantum wells will be studied to investigate the optical properties of neighboring quantum wells. For this purpose, two sample groups are investigated. Firstly, the number of neighboring quantum wells is varied to study the dependence of optical properties on the number of quantum wells. Secondly, a double quantum well with different well widths is studied, which is referred to as asymmetric double quantum well (ADQW).

5.1 GaInN/GaN multiple quantum wells

The sample series studied consists of a single, a double, and a triple GaInN/GaN quantum well with a well width of 3 nm. In the case of the multiple quantum wells, the quantum wells are separated by a 3 nm GaN barrier layer. The structure of the samples has been shown in Section 2.2. A 6 nm single quantum well is adopted for estimation of the internal field. The PL spectra of the 3 nm and 6 nm single quantum well, which have been shown in Section 4.2, are presented again to compare with those of the multiple quantum wells.

5.1.1 Experimental results

Figure 5.1 summarizes the time-integrated photoluminescence spectra of the 3 nm single, double and triple quantum well and the 6 nm single quantum well under resonant excitation. Following the main emission line for the one-to-three well series, one observes an energy shift from 2.87 eV for the 3 nm single quantum well to 2.52 eV for the double quantum well (DQW) and to 2.1 eV for the triple quantum well (TQW). In comparison, the main emission of the 6 nm single quantum well is 400 meV lower than that of the 3 nm single quantum well and at about the same energy level as the dominant emission peak of the double quantum well. Besides the main emission lines, the spectra of both the double

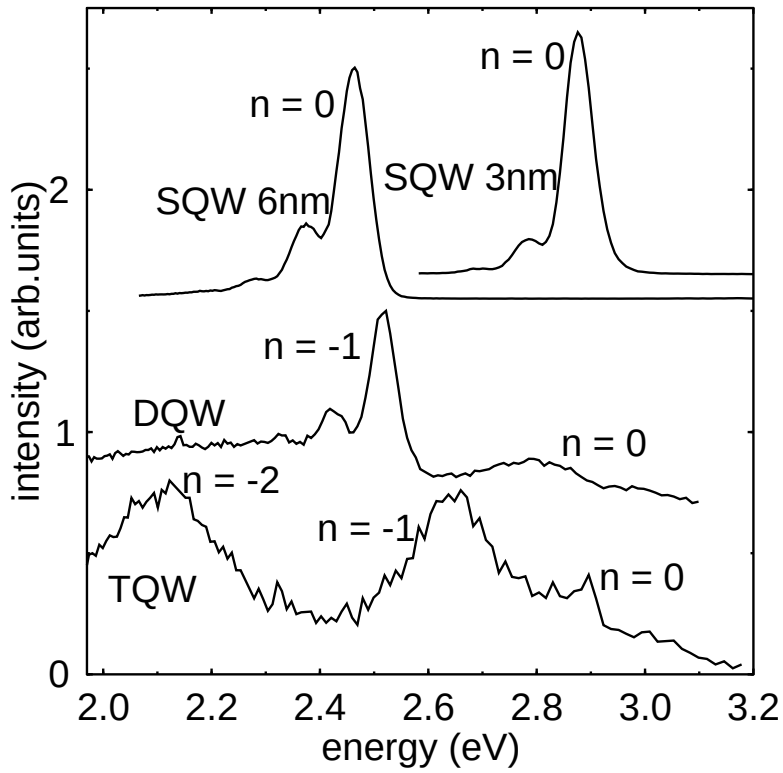

Figure 5.1: *Time-integrated photoluminescence spectra of single and multiple GaInN/GaN quantum wells of different thickness and well number at 5 K.*

quantum well and the triple quantum well show additional features at higher energies.

Time-resolved measurements reveal a more detailed picture. Figure 5.2 shows normalized photoluminescence spectra of the triple quantum well at increasing delay times. One can clearly distinguish three peaks in the high-, the middle-, and the low-energy region dominating the spectrum for different delay times. Within the first 70 ns after excitation the high-energy peak intensity decays almost completely and the middle-energy peak takes over the maximum position. During this time, the transition line in the high-energy region exhibits a red-shift of about 40 meV while the peak in the middle energy region shifts about twice

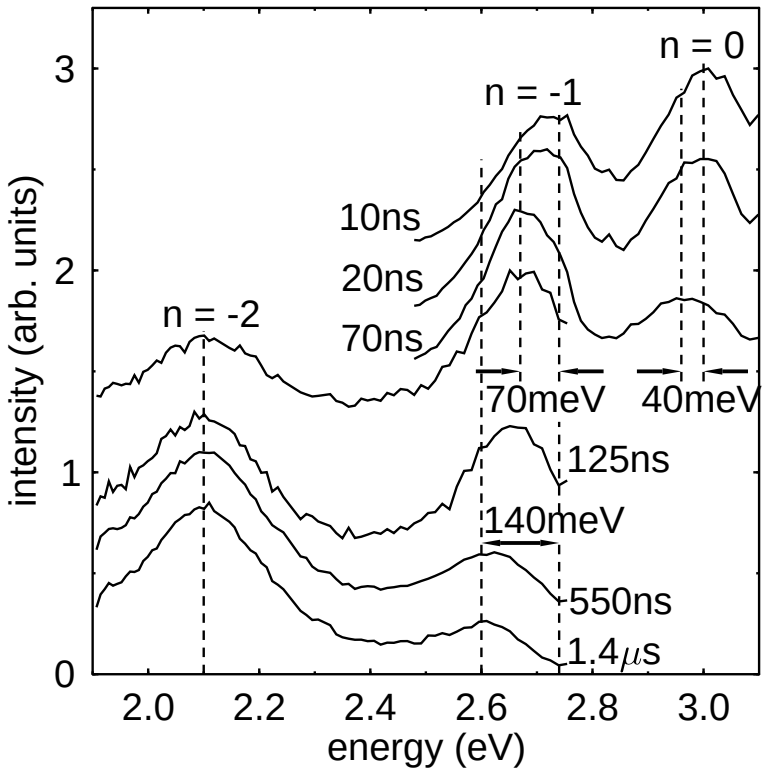

Figure 5.2: *Time-resolved photoluminescence spectra of the triple quantum well at 5 K for delay times up to 1.4 μs. For long delay times the spectrum is dominated by the low-energy line at 2.1 eV.*

that much by 70 meV. With passing time, the middle-energy peak shifts down to about 2.6 eV. Finally, for delay times over 100 ns the spectrum is dominated by the lowest-energy line at approximately 2.1 eV.

A comparison of the decay times of the different emission lines in the one-to-three well series is given in Figure 5.3. The 3 nm single quantum well shows a slightly non-exponential time dependence with a lifetime of about 100 ns. In contrast, the main emission lines of the double and triple quantum well in the low-energy region decay on a time scale in the upper microsecond range which can not be measured at practical pulse

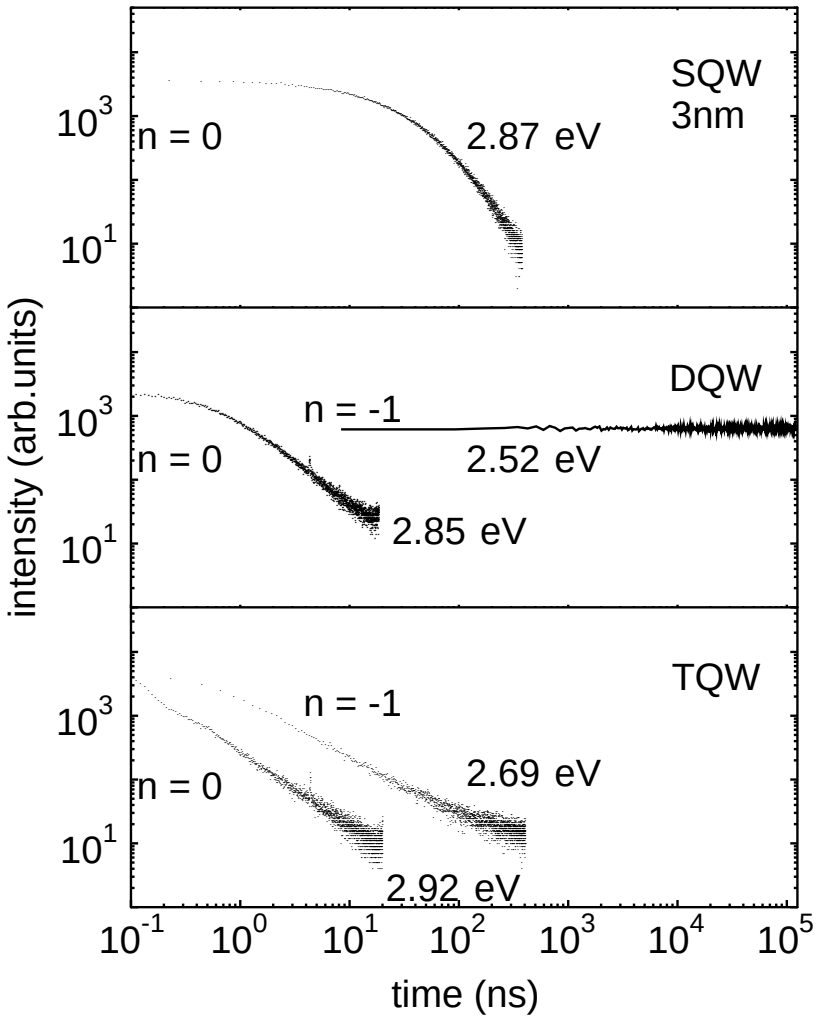

Figure 5.3: *Photoluminescence decay of the one-to-three well series at their respective emission peaks at 5 K. No decay is observed for the low-energy line if the double quantum well at 2.52 eV within 125 μs.*

repetition rates. For the double quantum well, the plotted time dependence of the emission line at 2.52 eV was measured at a repetition rate of 8 kHz. No decay is observed within 125 μs. Actually, we observe the same drastic increase of the lifetime for the 6 nm single quantum well. However, it is also interesting to note that for the higher-energy transitions in the multiple quantum wells we find a non-exponential time dependence with a faster decay time than in the case of the 3 nm single quantum well.

5.1.2 Discussion

For the two single quantum well samples, as has been discussed in the previous chapters, the strain-induced piezoelectric field explains the increased decay time and the redshift of emission lines with increasing well width. An estimate of the field strength is given by the energy shift between the 3 nm and 6 nm single quantum well emission peak divided by the difference in well thickness. Thus, we arrive at a field of about 1.4 MV/cm. Taking this field into consideration, the emission lines of a 6 nm and of a 6.5 nm single quantum well may exhibit an energy difference of about 70 meV. This order of magnitude should be kept in mind as a margin of error when absolute peak energies of different quantum well structures are compared.

In the case of the multiple quantum wells, our experimental results suggest that inter-well transitions between nearest and next-nearest neighbors play a significant role in the emission spectra. For the double quantum well this situation is depicted schematically in Figure 5.4. The intra-well transition is labelled with $n = 0$ and the inter-well transition with $n = -1$. Before comparing the experimental results with this diagram, the dynamic behavior of such a structure was anticipated: immediately after excitation electrons and holes will be distributed over all wells and screen the piezoelectric field. With evolving time the screening of the field will decrease due to the loss of excess carriers by recombination. For coupled quantum wells, the excess carriers will redistribute between the wells, finally accumulating in the lowest energy state.

The energy difference between the transition of an isolated single

quantum well and the transition resulting from this lowest energy state with the transition number n is given by $n \times well\ width \times field$. Thus, the $n = -1$ transition energy of the double quantum well is expected to be about 2.5 eV, close to the emission energy of the 6 nm single quantum well. For the triple quantum well, the lowest-energy line is associated with the $n = -2$ transition and should be at about 2.1 eV. All these expectations are supported by the observations made.

Within this model the electron-hole separation for the lowest-energy state in the double and triple quantum well is comparable to the electron-hole separation in a 9 nm and 15 nm single quantum well. This results in an extremely small overlap of the electron and hole wave functions. Based on the dependence of lifetime on well width, which has been already studied in Chapter 3, it is estimated that the decay times of these low-energy states is in the upper microsecond to millisecond range. This

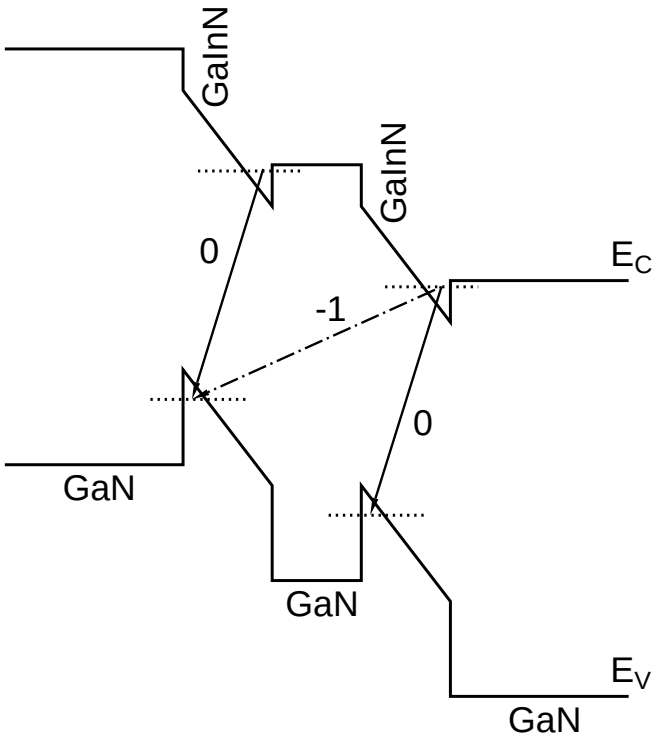

Figure 5.4: *Schematic diagram of a double quantum well with built-in piezoelectric field. The intra- and interwell transition are labeled with 0 and -1.*

expectation is in good agreement with our observation of a constant emission intensity over a time period of 125 μs measured at a feasible repetition rate of 8 kHz.

However, what should be considered now are the optical transitions of the multiple quantum wells at higher energies which we associate with the $n = 0$ and $n = -1$ transition in the case of the triple quantum well. These transitions are observed for short delay times. During this time period redistribution of carriers between the wells takes place and the piezoelectric field is efficiently screened by the high density of excess carriers. The decrease of the screening due to the loss of excess carriers by recombination can be well observed by following the energy shift of the high- and the middle-energy peak in the TRPL spectra of the triple quantum well. As has already been illustrated, the middle-energy line shifts within the same time about twice as much as the high-energy line. This is conclusive with earlier expectations since the potential drop due to the piezoelectric field is twice as large for the $n = -1$ transition than for the $n = 0$ transition.

Taking an even closer look at the decay times, much shorter lifetimes are noticed for the $n = 0$ transitions of the multiple quantum wells than for the 3 nm isolated single quantum well. The optical transitions with low transition number compete with the redistribution of carriers. Obviously, this redistribution takes place on a nanosecond time scale resulting in an effective decay time which is faster than the lifetime of 100 ns for the 3 nm single quantum well.

In fact, the appearance of multiple emission lines depends crucially on the redistribution of excess carriers. Without this redistribution, we would deal with semi-isolated single quantum wells. Since the oscillator strength decreases dramatically with increasing transition number n, we would then observe only the $n = 0$ transition.

The observations made here show that great care has to be taken when analyzing the emission spectra of GaInN/GaN multiple quantum wells. In fact, multiple emission lines from multiple quantum wells have already been reported and were subject to various interpretations [16, 13, 96]. Especially localized states caused by composition fluctuations have been considered. But even if there are such fluctuations in samples of lower

quality, these experimental results clearly rule out a major influence of localized states. The dependence of the lowest-energy line on the number of quantum wells as well as the dramatic increase of the decay time by several orders of magnitude are comparable to the observations in the case of single quantum wells. In both cases an explanation in terms of localized states would require a dramatic localization and a systematic dependence of the localization on the number of wells and on the well width. Both are clearly infeasible.

5.2 GaN/AlGaN asymmetric double quantum well

To investigate the temporal dynamics of the inter- and intrawell transitions in more detail, a double quantum well is studied, which consists of 2 nm and 4 nm GaN quantum wells separated by a 2.5 nm AlGaN barrier layer. The detailed structure diagram is shown in Section 2.2.

5.2.1 Experimental results

Low-temperature photoluminescence spectra of the sample are summarized in Figure 5.5. In the time-integrated spectrum (dotted curve), a main emission line at 3.44 eV is found. This line is neighbored by two lines at 3.34 eV and 3.56 eV. In contrast to two emission lines of the double quantum well studied in Section 5.1, this ADQW structure exhibits three emission lines. It is interesting to note that the energy differences between the main line and the two lines are similar.

Time-resolved measurements reveal a more detailed picture. Figure 5.5 shows normalized photoluminescence time-resolved spectra (solid curves) at increasing delay times. It can clearly be distinguished that three peaks dominate again the spectrum for different delay times. Within approximately 8.7 ns after excitation, the high-energy peak intensity vanishes almost completely and the middle-energy peak dominates the spectrum. With further evolution in time, the low-energy peak takes over the maximum position.

A comparison of the decay times of the emission lines is given in Figure 5.6 The high-energy peak intensity decays with a lifetime of about

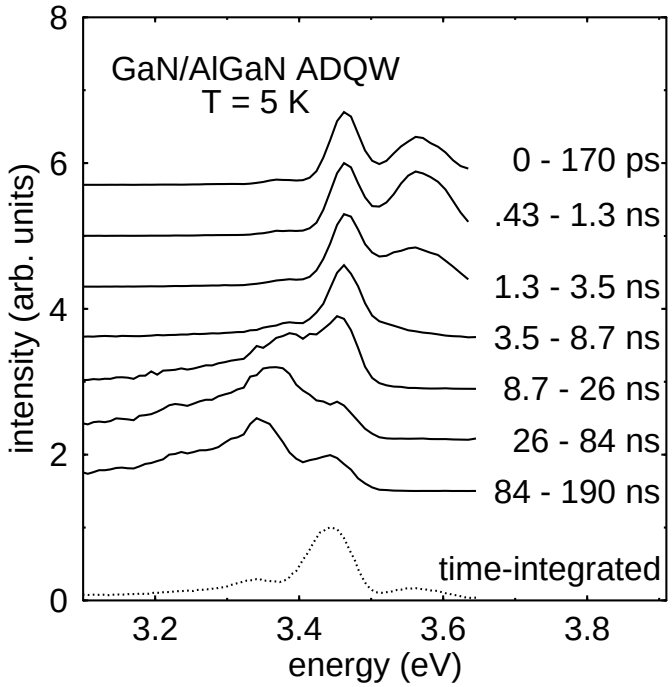

Figure 5.5: *Time-resolved and time-integrated photoluminescence spectra of a GaN/AlGaN asymmetric double quantum well.*

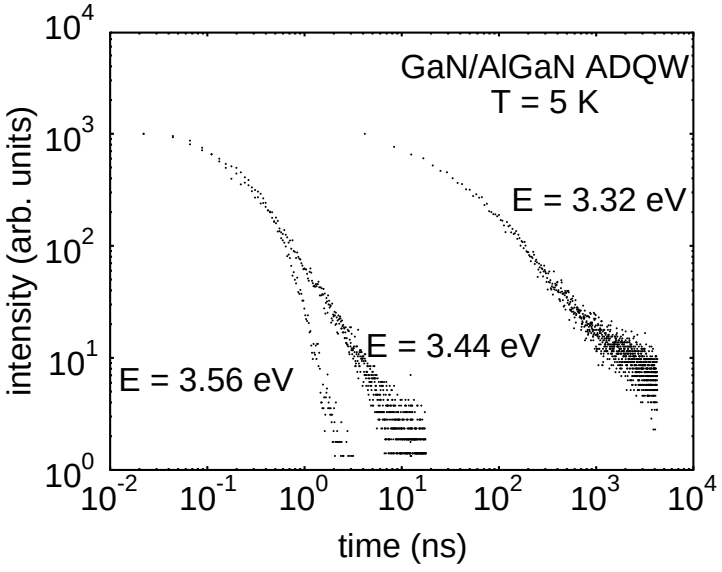

Figure 5.6: *Photoluminescence decay of the emission lines in a GaN/AlGaN asymmetric double quantum well.*

0.3 ns and the middle-energy peak shows a rather increased lifetime of 4 ns. The decay time of the low-energy emission line is dramatically increased up to the microsecond range.

5.2.2 Discussion

The origin of the aforementioned peaks will now be discussed. Guided by the previous results of GaN/AlGaN single quantum wells (see Chapter 3), the high- and middle-energy lines can be interpreted as intrawell transitions in the 2 nm and 4 nm quantum well, respectively.

To explain the low-energy line, a close look is required at the band diagram of a double quantum well with a piezoelectric field, which is depicted schematically in Figure 5.7. In thermal equilibrium, global band bending due to background doping gives rise to a depletion region in the AlGaN barriers below the GaN quantum wells, and electrons are accumulated in the topmost quantum well (see Section 4.1.3). The resulting space charges partially screen the piezoelectric field F_{piezo} in both quantum

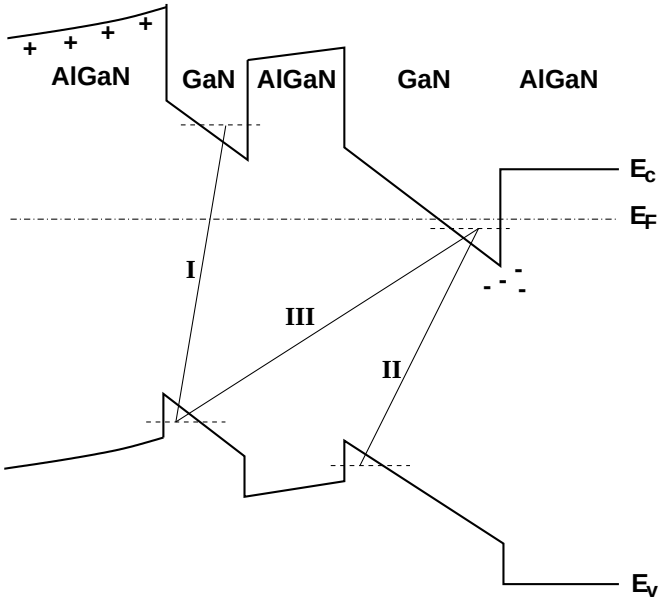

Figure 5.7: *Schematic band diagram of an asymmetric GaN/AlGaN double quantum well with a piezoelectric field. Due to Fermi level alignment, the conduction band of the AlGaN buffer layer is bend upward, and electrons are depleted.*

wells in an almost homogeneous manner. Additionally, the screening field F_{scr} induces an electric field in the AlGaN barrier. The effective field F_{eff} in the quantum wells are given by $F_{\mathrm{eff}} = F_{\mathrm{piezo}} - F_{\mathrm{scr}}$. Since the barrier layer between the two quantum wells is much thinner than the typical Debye length of several 10 nm, the barrier layer does not carry any significant space charge.

The transition energy of quantum wells, which are thicker than 2 nm, varies approximately linearly with the well width as seen in Figure 3.9. Within this approximation, the energy difference between intrawell transitions of the 2 nm and the 4 nm quantum well, denoted respectively by I and II, is given by $\Delta E_{\mathrm{I,II}} = F_{\mathrm{eff}} \times \Delta L$, where ΔL is the well width difference of the GaN quantum wells. On the other hand, we can express the energy difference of the interwell (III) and the intrawell (II) transition as $\Delta E_{II,III} = F_{eff} \times L_{\mathrm{I}} - F_{\mathrm{B}} \times L_{\mathrm{B}}$, where L_{I} and L_{B} is the width of the 2 nm GaN quantum well and of the AlGaN barrier layer, respectively. Our photoluminescence measurements result in $\Delta E_{\mathrm{I,II}}$ of 120 meV and $\Delta E_{\mathrm{II,III}}$ of 100 meV. In comparison with the model, the electric field F_{B}, which is induced by a screening field F_{scr} in the AlGaN barrier, is about 10% of the piezoelectric field F_{piezo}. Furthermore, the electron-hole separation for the interwell transition (III) can be approximated to the electron-hole separation in an 8.5 nm quantum well, which results in a small overlap of electron and hole wave functions. The lifetime in the microsecond range of the low-energy emission complies well with this expectation. Both the energetic position and the lifetime of the low-energy line can be well understood by the model considering an electric field in the double quantum wells. It should be noted that the appearance of the interwell transition depends crucially on the redistribution of excess carriers. Without this redistribution each quantum well would be semi-isolated, and only the intrawell transitions would be observed. The TRPL spectra shows that the intrawell transition peak of the 2 nm quantum well disappears within about 8 ns. This indicates that the excess electrons in the 2 nm quantum well escape to the 4 nm quantum well or recombine with holes on this time scale. In this context, we can expect that the change of the position of the two quantum wells causes a different distribution of excess carriers in the quantum wells. In this case, the excess

electrons in the 4 nm quantum well escape to the 2 nm quantum well and the intrawell transition peak of 4 nm quantum well could disappear much faster in TRPL spectra.

Chapter 6

Critical discussion

6.1 Localization effect vs. polarization field effect

The key optical properties of group-III nitride quantum wells shown in the previous chapters are summarized as follows:

- significant well-width dependence of decay time and emission energy in single quantum wells
- sub-bandgap emission and extremely long decay times in thick quantum wells
- lack of inversion symmetry in single quantum wells verified by study on asymmetric quantum well structures
- splitting of inter- and intrawell transition energy levels in multiple quantum wells

It has been shown that those properties can be most consistently explained by the polarization field effect. The quantum confinement Stark effect (QCSE) explains increasing decay time and a redshift of emission energy with increasing well width. Asymmetric barrier structure and asymmetrically doped structure both have shown consistently that the piezoelectric

field breaks the inversion symmetry in single quantum wells. The piezoelectric field leads to the splitting of the inter- and intrawell transition energy levels in multiple quantum wells.

In the localization model, the emission in quantum wells is explained by the recombination of localized carriers at potential minima developed by compositional inhomogeneity or even phase separation. However, this model cannot explain easily the aforementioned key optical properties. Especially, localization cannot be the origin of the transitions below the bulk GaN bandgap observed in GaN/AlGaN quantum wells. In addition, asymmetry of GaInN/GaN single quantum wells and extremely long decay time in thick layers cannot be clearly understood in context of the localization model. The large Stokes shift, which has been often attributed to the localization effect, can be explained simply by the polarization field, without referring to the localization effect. Furthermore, even moderate composition and well-width fluctuation can lead to the large emission linewidth due to the enhancement by the polarization field. From theoretical consideration [32], the elastic strain in epitaxial GaInN layers coherently grown on GaN layer suppresses phase separation dramatically, which can allow one to improve quality of thin GaInN epitaxial layer. Considering the large critical thickness of strained nitride layers [37, 97, 98], the effect of phase separation in nitride quantum wells can be less significant than expected [29]. In the context of localization effect, the blueshift of the emission of quantum well LEDs for increasing driving current is explained by band filling of the localized states [11, 99], which can also be accounted for by screening of the polarization field [100].

6.2 Piezoelectric constant

As discussed in Section 1.4, the electric field due to the interface discontinuity of spontaneous polarization in GaN/AlGaN quantum well is expected to be comparable with piezoelectric polarization. Optical transitions in GaN/AlGaN quantum wells are influenced by the total electric field, which is the sum of both piezoelectric and spontaneous polarization fields. In contrast, due to similar spontaneous polarization of GaN and

InN, the spontaneous polarization field in GaInN/GaN quantum wells can be neglected. Therefore, the internal fields in GaInN/GaN quantum wells, which have been determined in the previous chapters, originates mostly from the strain-induced piezoelectric field.

It is interesting to note that the determined piezoelectric field in GaInN/GaN quantum wells can be used for estimation of the piezoelectric constant of GaInN alloys. Combining Equations 1.8 and 1.9 the piezoelectric field F_3^{piezo} along the c-axis is expressed via the piezoelectric constant d_{31} as [55]

$$F_3^{\text{piezo}} = -\frac{2\,d_{31}}{\epsilon_0 \epsilon_r}\left(c_{11} + c_{12} - \frac{2\,c_{13}^2}{c_{33}}\right)\epsilon_{xx}. \tag{6.1}$$

The in-plane strain ϵ_{xx} is given by $\epsilon_{xx} = 0.11\,x_{\text{In}}$, where x_{In} is the In content. The piezoelectric field is, consequently, proportional to the In content. Figure 6.1 illustrates the piezoelectric fields, which have been determined in Section 3.2.2 and 4.2.1, as a function of the In content and the strained bandgap. The straight line in Figure 6.1 is a linear

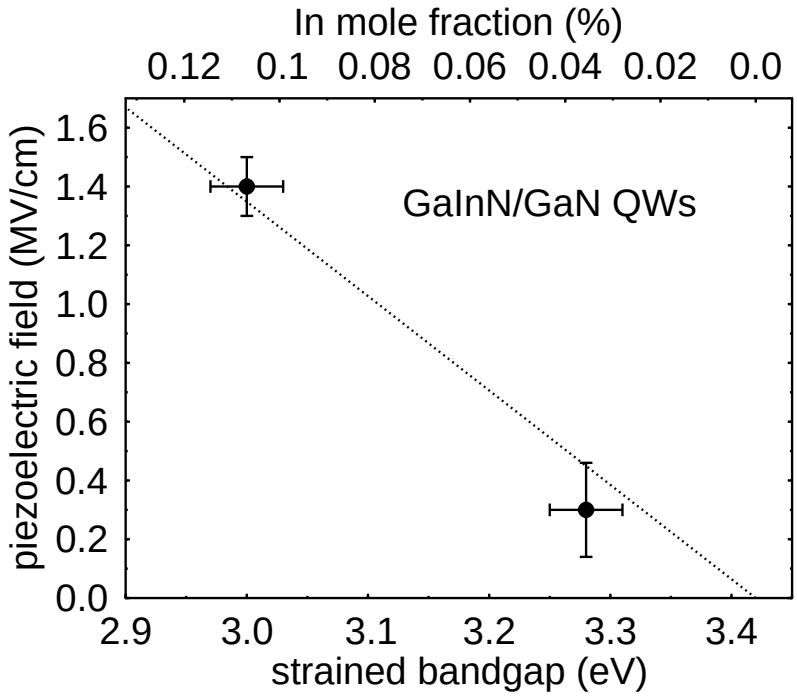

Figure 6.1: *Piezoelectric field vs. strained bulk bandgap in GaInN/GaN quantum wells. The field increases linearly In mole fraction.*

least-squares fit to the data. The relation between the In content and the strained bandgap of GaInN alloys is given by Equation 1.5. Elastic stiffness constants and dielectric constant of InN are not presently available, and the values of GaN is applied. Using ϵ_r(GaN) = 9.5 [101] and elastic constants of GaN determined by Schwarz *et al.* (see appendix A), the slope of the straight line gives $d_{31}(\mathrm{Ga}_{1-x}\mathrm{In}_x\mathrm{N}) = -1.2 \times 10^{-10}$ cm/V for $x < 0.11$, which is comparable with the value of -1.1×10^{-10} cm/V (InN) and -1.7×10^{-10} cm/V (GaN) estimated by Martin *et al.* [102].

6.3 Internal field and quantum efficiency

Surprisingly, the light-emitting efficiencies of nitride-based LEDs were remarkably insensitive to dislocations [7, 103, 99]. It has been argued that the localization of carriers by compositional fluctuations can provide the immunity to non-radiative recombination at threading dislocations and that internal polarization fields are detrimental to the efficiency of light emitting diodes [99]. Within this line of reasoning, it is thought that indeed polarization fields lead to a strongly reduced oscillator strength for radiative transitions and therefore to a reduced quantum efficiency.

However, though it is true that the probability of radiative recombination is reduced by internal fields, we have little knowledge of the effect of internal fields on non-radiative recombination. It is certainly not appropriate to assume that non-radiative transitions are unaffected by strong internal fields.

The physical origin of the reduced radiative oscillator strength is the spatial separation of the electron and hole wave functions. In fact, the very same mechanism may also apply to non-radiative transitions. Figure 6.2 shows a sketch of the situation representative for non-radiative recombination in a piezoelectric quantum well. The recombination proceeds through a deep defect level, whose wave function is localized on an atomic scale. As with conventional two-step recombination involving deep defect states [104, 105], the capture rate for electrons and holes is proportional to the overlap of their respective wave function with that of the defect state. Since the total recombination rate is governed by the smaller of the two capture coefficients, the maximum non-radiative

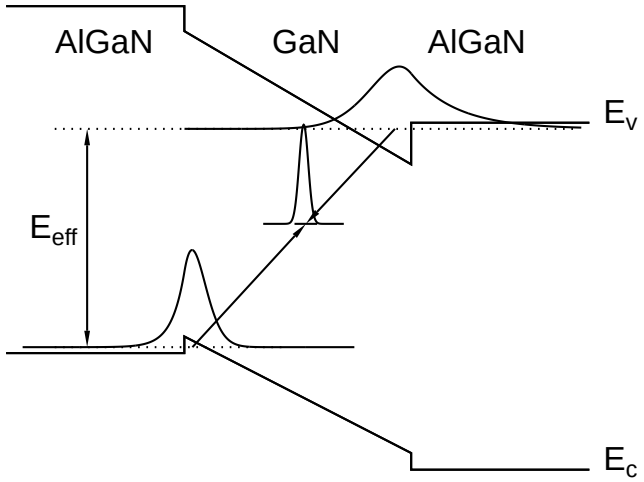

Figure 6.2: *Schematic view of a non-radiative recombination process through a deep defect level in a piezoelectric quantum well.*

rate will be reached if the defect is located such that the two overlaps are equal. Moreover, since the wave functions decay exponentially, the spatial separation of the electron and hole wave functions will lead to a dramatic decrease in the non-radiative recombination rate.

Obviously this scenario is very similar to that applicable to radiative recombination as discussed earlier. Both the radiative and the non-radiative recombination rate can be expected to exhibit a dramatic decrease for large internal fields and for wide quantum wells. Now, the quantum efficiency is given by the ratio of the radiative recombination rate to the total recombination rate. It is extremely difficult to predict its behavior, which will depend on all the details of the specific defect involved. However, it is certainly not justified to assume that internal fields will automatically lead to a reduced quantum efficiency.

Chapter 7

Summary

It is demonstrated that the strain-induced piezoelectric field dominates to a large extent the optical properties of wurtzite group-III nitride quantum wells. The study has been performed using time-integrated and time-resolved photoluminescence spectroscopy as well as photoluminescence excitation spectroscopy. According to the structure of the quantum wells studied, the results are divided into three parts.

First, the optical properties of GaInN/GaN and GaN/AlGaN single quantum wells are studied with emphasis on well-width dependence. The active layers of the quantum wells are thiner than the critical thickness and fully strained. The strain-induced piezoelectric field in quantum wells leads to a Stark shift of the optical transitions and reduction of oscillator strength due to the spatial separation of the electron and hole wave functions. As a result, the emission energies shift toward lower energy even far below the bulk bandgap with increasing well width. Additionally, the decay times increase drastically by several orders of magnitude. The well-width dependence of the emission energy and decay time can be consistently explained by quantitative calculations based on the piezoelectric effect. The redshift of time-resolved photoluminescence spectra with evolving time can be attributed to partial screening of the piezoelectric field due to photoexcited electron-hole pairs. Decreasing carrier density with time evolution results in the recovery of the screened piezoelectric field and in the redshift of emission energy. The piezoelectric

field effect can also explain the large photoluminescence linewidth and the large Stokes shift between absorption and emission, which are both commonly cited as supporting evidence for carrier localization due to compositional fluctuation or phase separation. Numerical calculations show that electrons and holes wave functions are spatially separated by the piezoelectric field, and the remarkably small absorption in lower energy states due to the small overlap of wave functions leads to the large Stokes shift. Significant absorption can occur only in the more highly excited states which provide a large overlap of wave functions. The piezoelectric field enhances the inhomogeneous broadening due to fluctuations of composition and well-width. This leads to the large photoluminescence linewidth in quantum wells, which are subject to moderate fluctuations of composition and well-width.

Secondly, asymmetric quantum well structures are studied to verify the existence of the piezoelectric field which breaks the inversion symmetry of single quantum wells. Samples studied are classified by two groups. In one sample series, an additional AlGaN barrier layer is introduced to GaInN/GaN single quantum well, so that the GaInN active layer is asymmetrically sandwiched by the barrier layers. In the other one, the GaN barrier layers of GaInN/GaN quantum well are selectively doped, and the quantum well is embedded in asymmetrically doped barriers. The study on the asymmetric GaInN/AlGaN/GaN quantum wells reveals that oscillator strength is enhanced when the AlGaN barrier layer is placed on top of the GaInN layer in reference to the growth direction. The emission energy of GaInN/GaN quantum wells with doped GaN barriers shifts towards higher energy than that of undoped samples due to screening of the piezoelectric field, but only when the lower GaN cladding layer below the quantum well is doped. The sample where an upper GaN cap layer above the quantum well is doped shows no blueshift. The results of both studies on asymmetric quantum well structures indicate a lack of inversion symmetry in GaInN/GaN single quantum wells and provides ambiguous evidence for the existence of the piezoelectric field. Furthermore, both asymmetric structures allow us to determine consistently the direction of the piezoelectric field, which points towards the substrate. Similar results are obtained in the asymmetric barrier structure grown on

substrate sapphire and silicon carbide. The relation between the piezoelectric and crystallographic polarity is also discussed. Guided by the theoretical calculation of the piezoelectric constant, it is found that the epilayers grown by MOCVD on sapphire and silicon carbide are both Ga-face, which is consistent with their smooth surface morphology.

Thirdly, the properties of multiple quantum wells are studied. The piezoelectric field leads to the splitting of the inter- and intrawell transition energies in multiple quantum wells. As a result, multiple emission lines are observed in GaInN/GaN double and triple quantum wells and exhibit clearly different temporal behavior. Time-resolved spectra show that there is a combined effect of field screening and carrier redistribution which makes intrawell transitions disappear first and transitions between the outmost quantum wells lasting for an extremely long time. The GaN/AlGaN asymmetric double quantum well structure, which consists of two quantum wells of different thickness, exhibits also intra- and interwell transitions influenced strongly by the piezoelectric field.

The localization effect is critically reviewed on the basis of aforementioned results. Especially, transitions below the bulk GaN bandgap in GaN/AlGaN quantum wells, lack of inversion symmetry in GaInN/GaN single quantum wells, and extremely long decay time in thick layers cannot be clearly explained by the localization model.

The impact of internal polarization fields on LED efficiency is discussed. It is shown that the non-radiative recombination can be subject to reduction by field effects in a similar manner as the radiative one.

Appendix A

Crystal properties and tensors

In this appendix, the tensor presentation of the physical properties such as elasticity and piezoelectricity are outlined [58].

Elasticity

For sufficiently small stresses, the amount of strain ϵ_j is proportional to the magnitude of the applied stress σ_i. This linear relation is known as Hooke's Law and is expressed via the elastic stiffness constant c_{ij} as

$$\sigma_i = c_{ij}\epsilon_j \qquad (i, j = 1, 2, ..., 6), \tag{A.1}$$

where the suffixes follow the Voigt notation.

The elastic stiffness constant of the wurtzite crystal structure, which belongs to a crystal class $6mm$, has five non-vanishing independent com-

ponents as follows:

$$c = \begin{pmatrix} c_{11} & c_{12} & c_{13} & 0 & 0 & 0 \\ c_{12} & c_{11} & c_{13} & 0 & 0 & 0 \\ c_{13} & c_{13} & c_{33} & 0 & 0 & 0 \\ 0 & 0 & 0 & c_{44} & 0 & 0 \\ 0 & 0 & 0 & 0 & c_{44} & 0 \\ 0 & 0 & 0 & 0 & 0 & \frac{1}{2}(c_{11} - c_{12}) \end{pmatrix} \tag{A.2}$$

Table A.1 summarizes the components of the elastic stiffness constant of GaN measured using a resonance ultrasonic spectroscopy (RUS) [106] and a Brillouin scattering measurement [107]. In this work, we use the values from the measurement on a bulk single crystal using the RUS technique [106], which is expected to be more precise. However, it should be noted that two methods exhibit significant disagreement, especially in c_{33}.

	c_{11}	c_{12}	c_{13}	c_{33}	c_{44}
Schwarz *et al.* [106]	377	160	114	209	81.4
Polian *et al.* [107]	390	145	106	398	105

Table A.1: *Elastic stiffness constant of wurtzite GaN, in GPa units.*

Piezoelectricity

If stress is applied to non-cetrosymmertic crystals, they develop an electric moment P_i whose magnitude is proportional to the applied stress. The linear relation is given by

$$P_i = d_{ij}\sigma_j \qquad (i = 1, 2, 3 \quad j = 1, 2, ..., 6), \tag{A.3}$$

where d_{ij} is a constant called a piezoelectric modulus. The piezoelectric modulus of a wurtzite crystal has three non-vanishing independent components as follows:

$$d = \begin{pmatrix} 0 & 0 & 0 & 0 & d_{15} & 0 \\ 0 & 0 & 0 & d_{15} & 0 & 0 \\ d_{31} & d_{31} & d_{33} & 0 & 0 & 0 \end{pmatrix} \tag{A.4}$$

Combing Equation A.1 and A.3 yields a relation between piezoelectric polarization and strain, which expressed as

$$P_i = d_{ik} c_{kj} \epsilon_j = e_{ij} \epsilon_j \qquad (i = 1, 2, 3 \quad j, k = 1, 2, ..., 6), \tag{A.5}$$

where e_{ij} are the piezoelectric constants. In the matrix notation the piezoelectric tensor of a wurtzite crystal is

$$e = \begin{pmatrix} 0 & 0 & 0 & 0 & e_{15} & 0 \\ 0 & 0 & 0 & e_{15} & 0 & 0 \\ e_{31} & e_{31} & e_{33} & 0 & 0 & 0 \end{pmatrix} \tag{A.6}$$

with the piezoelectric constants

$$\begin{aligned} e_{31} &= (c_{11} + c_{12}) d_{31} + c_{13} d_{33} \\ e_{33} &= 2 c_{13} d_{31} + c_{33} d_{33} \\ e_{15} &= c_{44} d_{15}. \end{aligned} \tag{A.7}$$

Appendix B

Self-consistent calculation of Schrödinger and Poisson equations

The calculation of equilibrium band structure of quantum wells requires self-consistent solution of Schrödinger and Poisson equations [108]. The one-dimensional effective mass Schrödinger equation is

$$-\frac{\hbar^2}{2}\frac{d}{dz}\left(\frac{1}{m^*(z)}\frac{d}{dz}\right)\psi(z)+V(z)\psi(z)=E\psi(z), \qquad \text{(B.1)}$$

where ψ is the wave function, E is the energy, V is the potential energy, and m^* is the effective mass. The one-dimensional Poisson equation is

$$\frac{d}{dz}\left(\epsilon_r(z)\frac{d}{dz}\right)\phi(z)=\frac{-q[N^D(z)-n(z)]}{\epsilon_0}, \qquad \text{(B.2)}$$

where ϵ_r is the dielectric constant, ϕ is the electrostatic potential, N_D is the ionized donor concentration, and n is the electron density distribution. In a quantum well, the potential energy V is related to the electrostatic potential ϕ as follows:

$$V(x)=-q\phi(z)+\Delta E_c(z)+qF_{piezo}(z)\times z, \qquad \text{(B.3)}$$

where F_{piezo} is the piezoelectric field and ΔE_c is the pseudopotential energy due to the band offset at the heterointerface. The wave function $\psi(z)$ in Equation B.1 and the electron density $n(z)$ in Equation B.2 are related by

$$n(z) = \sum_{i=1}^{l} \psi_i^*(z)\psi_i(z)n_i, \tag{B.4}$$

where l is the number of bound states, and n_i is the electron occupation for each state. The electron concentration for each state can be expressed by

$$n_i = \frac{m^*}{\pi\hbar^2} \int_{E_i}^{\infty} \frac{1}{1 + e^{(E-E_F)/kT}}\, dE, \tag{B.5}$$

where E_i is the eigenenergy. For non-degenerate quantum wells, we can use the Boltzmann distribution function instead of the Dirac distribution function in Equation B.5.

The electron density distribution $n(z)$ is computed by using the wave functions and their corresponding eigenenergies, which is calculated with a trial potential $V(z)$. The computed $n(z)$ is taken into account to in solving the electrostatic potential $\phi(z)$, which gives a new potential $V(z)$. The iterative procedure will yield self-consistent solutions of Schrödinger and Poisson equations.

To solve the Schrödinger and Poisson equation numerically, the Fourier transformation of the differential equations is performed. Real space with length L is divided into equip-distant discrete N mesh points. $\psi(z)$ and $\phi(z)$ can be expressed by the Fourier series:

$$\psi(z) = \sum_{j=1}^{N} \psi_j e^{-i\frac{2\pi}{L}jz} \quad \text{and} \quad \phi(z) = \sum_{j=1}^{N} \phi_j e^{-i\frac{2\pi}{L}jz} \tag{B.6}$$

If the heterointerface discontinuity of the electron mass and dielectric constant in quantum wells is neglected, the Shrödinger equation is given by

$$\sum_{j'=1}^{N} \left[-\frac{\hbar^2}{2m^*} \left(\frac{2\pi j}{L} \right)^2 \delta_{jj'} + V_{jj'} \right] \psi_{j'} = E\psi_j \qquad (j = 1, 2, ..., N) \tag{B.7}$$

where

$$V(z) = \sum_{j,j'} V_{jj'} e^{-i\frac{2\pi}{L}(j-j')z}, \tag{B.8}$$

and the Poisson equation is obtained as

$$\left(\frac{2\pi}{L}j\right)^2 \phi_j = \frac{-q(N_j^D - n_j)}{\epsilon_r \epsilon_0} \qquad (j = 1, 2, ..., N), \tag{B.9}$$

where N_j^D and n_j are the Fourier coefficient of $N^D(z)$ and $n(z)$, respectively. By solving Equation B.7 and B.9, we obtain the Fourier coefficients of $\psi(z)$ and $\phi(z)$, which can be obtained, in turn, by Equation B.6.

Bibliography

[1] S. M. Sze, *Physics of semiconductor devices* (John Willey & Sons, New York, 1981).

[2] S. Strite and H. Morkoç, *GaN, AlN, and InN: A review*, J. Vac. Sci. Technol. B **10**, 1237 (1992).

[3] S. Nakamura, M. Senoh, N. Iwasa, and S.-I. Nagahama, *High-power InGaN single-quantum-well-structure blue and violet light-emitting diodes*, Appl. Phys. Lett. **67**, 1868 (1995).

[4] S. Nakamura, M. Senoh, N. Iwasa, S.-I. Nagahama, T. Yamada, and T. Mukai, *Superbright green InGaN single-quantum-well-structure light-emitting diodes*, Jpn. J. Appl. Phys. **34**, L1332 (1995).

[5] T. Mukai, H. Narimatsu, and S. Nakamura, *Amber InGaN-based light-emitting diodes operable at high ambient temperatures*, Jpn. J. Appl. Phys. **37**, 479 (1998).

[6] H. Morkoç and S. N. Mohammad, *High luminosity gallium nitride blue and blue green light emitting diodes*, Science **267**, 51 (1995).

[7] F. A. Ponce and D. P. Bour, *Nitride-based semiconductors for blue and green light-emitting devices*, Nature **386**, 351 (1997).

[8] S. Nakamura, *III-V nitride based light-emitting devices*, Solid State Commun. **102**, 237 (1997).

[9] S. Nakamura, M. Senoh, S.-I. Nagahama, T. Matsushita, H. Kiyoku, Y. Sugimoto, T. Kozaki, H. Umemoto, M. Sano, and T. Mukai, *Violet InGaN/GaN/AlGaN-based laser diodes operable at 50 ^{o}C with a fundamental transverse mode*, Jpn. J. Appl. Phys. **38**, L226 (1999).

[10] S. N. Mohammad, A. A. Salvador, and H. Morkoç, *Emerging gallium nitride based devices*, Proc. IEEE **83**, 1306 (1995).

[11] S. Chichibu, T. Azuhata, T. Sota, and S. Nakamura, *Spontaneous emission of localized excitons in InGaN single and multiquantum well structures*, Appl. Phys. Lett. **69**, 4188 (1996).

[12] R. W. Martin, P. G. Middleton, K. P. O'Donnell, and W. V. der Stricht, *Exciton localization and the Stokes' shift in InGaN epilayers*, Appl. Phys. Lett. **74**, 263 (1999).

[13] Y. Narukawa, Y. Kawakami, S. Fujita, S. Fujita, and S. Nakamura, *Recombination dynamics of localized excitons in $In_{0.20}Ga_{0.80}N/In_{0.05}Ga_{0.95}N$ multiple quantum wells*, Phys. Rev. B **55**, R1938 (1997).

[14] K. P. O'Donnell, T. Breitkopf, H. Kalt, W. van der Stricht, I. Moerman, P. Demeester, and P. G. Middleton, *Optical linewidths of InGaN light emitting diodes and epilayers*, Appl. Phys. Lett. **70**, 1843 (1997).

[15] S. Chichibu, D. A. Cohen, M. P. Mack, A. C. Abare, P. Kozodoy, M. Minsky, S. Fleischer, S. Keller, J. E. Bowers, U. K. Mishra, L. A. Coldren, D. R. Clarke, and S. P. DenBaars, *Effects of Si-doping in the barriers of InGaN multiquantum well purplish-blue laser diodes*, Appl. Phys. Lett. **73**, 496 (1998).

[16] Y. Narukawa, Y. Kawakami, M. Funato, S. Fujita, S. Fujita, and S. Nakamura, *Role of self-formed InGaN quantum dots for exiton localization in the purple laser diode emitting at 420 nm*, Appl. Phys. Lett. **70**, 981 (1997).

[17] J. G. Gualtieri, J. Kosinski, and A. Ballato, *Piezoelectric materials for acoustic wave applications*, IEEE Transaction on Ultrasonics, Ferroelectrics, and Frequency Control **41**, 53 (1994).

[18] T. Takeuchi, S. Sota, M. Katsuragawa, M. Komori, H. Takeuchi, H. Amano, and I. Akasaki, *Quantum-confined Stark effect due to piezoelectric fields in GaInN strained quantum wells*, Jpn. J. Appl. Phys. **36**, L382 (1997).

[19] *Properties of group III nitrides (EMIS Data Rewiew Series 11)*, edited by J. H. Edgar (INSPEC, IEE, London, 1994).

[20] M. Suzuki and T. Uenoyama, *Strain effect on electric and optical properties of GaN/AlGaN quantum-well lasers*, J. Appl. Phys. **80**, 6868 (1996).

[21] J. W. Orton and C. T. Foxon, *The electron mobility and compensation in n-type GaN*, Semicond. Sci. Technol. **13**, 310 (1998).

[22] T. L. Tansley and C. P. Foley, *Optical band gap of indium nitride*, J. Appl. Phys. **59**, 3241 (1986).

[23] Q. Guo and A. Yoshida, *Temperature dependence of band gap change in InN and AlN*, Jpn. J. Appl. Phys. **33**, 2453 (1994).

[24] M. Drechsler, D. M. Hofmann, B. K. Meyer, T. Detchprohm, H. Amano, and I. Akasaki, *Determination of the Conduction Band Electron Effective Mass in Hexagonal GaN*, Jpn. J. Appl. Phys. **34**, L1178 (1995).

[25] J. S. Im, A. Moritz, F. Steuber, V. Härle, F. Scholz, and A. Hangleiter, *Radiative carrier lifetime, momentum matrix element, and hole effective mass in GaN*, Appl. Phys. Lett. **70**, 631 (1997).

[26] K. Kim, W. R. L. Lambrecht, B. Segall, and M. van Schilfgaarde, *Effective masses and valence-band splittings in GaN and AlN*, Phys. Rev. B **56**, 7363 (1997).

[27] *Properties, processing and application of gallium nitride and related semiconductors*, edited by J. H. Edgar, S. T. Strite, I. Akasaki, H. Amano, and C. Wetzel (INSPEC, IEE, London, 1999).

[28] O. Gfrörer, T. Schlüsener, V. Härle, F. Scholz, and A. Hangleiter, *Relaxation of thermal strain in GaN epitaxial layers grown on sapphire*, Mat. Sci. Eng. B **43**, 250 (1997).

[29] I. hsiu Ho and G. B. Stringfellow, *Solid phase immiscibility in GaInN*, Appl. Phys. Lett. **69**, 2701 (1996).

[30] N. A. El-Masry, E. L. Piner, S. X. Liu, and S. M. Bedair, *Phase separation in InGaN grown by metalorganic chemical vapor deposition*, Appl. Phys. Lett. **72**, 40 (1998).

[31] R. Singh, R. J. Molnar, M. S. Ünlü, and T. D. Moustakas, *Intensity dependence of photoluminescence in GaN thin films*, Appl. Phys. Lett. **64**, 336 (1994).

[32] S. Y. Karpov, *Suppression of phase separation in InGaN due to elastic strain*, MRS Internet J. Nitride Semicond. Res. **3**, 16 (1998).

[33] G. Parish, S. Keller, P. Kozodoy, J. P. Ibbetson, H. Marchand, P. T. Fini, S. B. Fleischer, S. P. DenBaars, U. K. Mishra, and E. J. Tarsa, *High-performance (Al,Ga)N-based solar-blind ultraviolet pin detectors on laterally epitaxially overgrown GaN*, Appl. Phys. Lett. **75**, 247 (1999).

[34] J. Han, M. H. Crawford, R. J. Shul, J. J. Figiel, M. Banas, L. Zhang, Y. K. Song, H. Zhou, and A. V. Nurmikko, *AlGaN/GaN quantum well ultraviolet light emitting diodes*, Appl. Phys. Lett. **73**, 1688 (1998).

[35] S. Nakamura and G. Fasol, *The blue laser diode* (Spinger-Verlag, Berlin, 1997).

[36] A. Kniest, *Einfluß der Gitterfehlanpassung bei der Epitaxi von GaInN*, Master's thesis, Universität Stuttgart, 1998.

[37] T. Takeuchi, H. Takeuchi, S. Sota, H. Sakai, H. Amano, and I. Akasaki, *Optical properties of strained AlGaN and GaInN on GaN*, Jpn. J. Appl. Phys. **36**, L177 (1997).

[38] M. D. McCluskey, C. G. van de Walle, C. P. Master, L. T. Romano, and N. M. Johnson, *Large band gap bowing of $In_xGa_{1-x}N$ alloys*, Appl. Phys. Lett. **72**, 2725 (1998).

[39] K. Osamura, K. Nakajima, and Y. Murakami, *Fundamental absorption edge in GaN, InN and their alloys*, Solid State Commun. **11**, 617 (1972).

[40] K. Osamura, S. Naka, and Y. Murakami, *Preparation and optical properties of $Ga_{1-x}In_xN$ thins films*, J. Appl. Phys. **46**, 3432 (1975).

[41] S. Nakamura, *InGaN/AlGaN blue light-emitting diodes*, J. Vac. Sci. Tech. A **13**, 705 (1995).

[42] Y. Koide, H. Itoh, M. R. H. Khan, K. Hiramatu, N. Sawaki, and I. Akasaki, *Energy band-gap bowing parameter in an AlGaN alloy*, J. Appl. Phys. **61**, 4540 (1987).

[43] S. Yoshida, S. Misawa, and S. Gonda, *Properties of $Al_xGa_{1-x}N$ films prepared by reactive molecular beam epitaxy*, J. Appl. Phys. **53**, 6844 (1982).

[44] D. K. Wickenden, C. B. Bargeron, W. A. Bryden, and J. Miragliotta, *High-quality self-nucleated $Al_xGaN_{1-x}N$ layers on (001) sapphire by low-pressure metal organic chemical vapor deposition*, Appl. Phys. Lett. **65**, 2024 (1994).

[45] G. Martin, S. Strite, A. Botchkarev, A. Agarwal, A. Rocket, W. R. L. Lambrecht, and B. Segall, *Valence band discontinuity between GaN and AlN measured by x-ray photoemission spectroscopy*, Appl. Phys. Lett. **65**, 610 (1994).

[46] C. G. V. de Walle and J. Neugebauer, *Small valence-band offsets at GaN/InGaN heterojunctions*, Appl. Phys. Lett. **70**, 2577 (1997).

[47] S. Wei and A. Zunger, *Valence band splittings and band offsets of AlN, GaN, and InN*, Appl. Phys. Lett. **69**, 2719 (1996).

[48] F. Bernardini and V. Fiorentini, *Macroscopic polarization and band offsets at nitride heterojunctions*, Phys. Rev. B **57**, R9427 (1998).

[49] C. Wetzel, T. Takeuchi, H. Amano, and I. Akasaki, *Valence band splitting and luminescence Stokes shift in GaInN/GaN thin films and multiple quantum well structures*, J. Crystal Growth **189/190**, 621 (1998).

[50] L. Bellaiche, T. Mattila, L.-W. Wang, S.-H. Wei, and A. Zunger, *Resonant hole localization and anomalous optical bowing in InGaN alloys*, Appl. Phys. Lett. **74**, 1842 (1999).

[51] G. E. Pikus, *A new method of calculating the energy spectrum of carriers in semiconductors. I. neglecting spin-orbit interaction*, Sov. Phys. Jetp. **14**, 898 (1962).

[52] G. E. Pikus, *A new method of calculating the energy spectrum of carriers in semiconductors. II. account of spin-orbit interaction*, Sov. Phys. Jetp. **14**, 1075 (1962).

[53] A. Gavini and M. Cardona, *Modulated piezoreflectance in semiconductors*, Phys. Rev. B **1**, 672 (1970).

[54] H. Amano, K. Hiramatsu, and I. Akasaki, *Heteroepitaxial growth and the effect of strain on the luminescence properties of GaN films on (11$\bar{2}$0 and (0001) sapphire substrates*, Jpn. J. Appl. Phys. **27**, L1384 (1988).

[55] A. Bykhovski, B. Gelmont, and M. Shur, *The influence of strain-induced electric field on the charge distribution in GaN-AlN-GaN structure*, J. Appl. Phys. **74**, 6734 (1993).

[56] F. Bernardini, V. Fiorentini, and D. Vanderbilt, *Spontaneous polarization and piezoelectric constant of III-V nitrides*, Phys. Rev. B **56**, R10024 (1997).

[57] C. Kisielowski, J. Krüger, S. Ruvimov, T. Suski, J. W. Ager III, E. Jones, Z. Liliental-Weber, M. Rubin, E. R. Weber, M. D. Bremser, and R. F. Davis, *Strain-related phenomena in GaN thin films*, Phys. Rev. B **54**, 17745 (1996).

[58] J. F. Nye, *Physical properties of crystals* (Clarendon Press, Oxford, 1995).

[59] O. Gfrörer, C. Gemmer, J. Off, J. S. Im, F. Scholz, and A. Hangleiter, *Direct observation of pyroelectric fields in InGaN/GaN and AlGaN/GaN heterostructures*, phys. stat. sol. (b) **216**, 405 (1999).

[60] V. Fiorentini and F. Bernardini, *Effect of macroscopic polarization in III-V nitride multiple quantum wells*, Phys. Rev. B **60**, 8849 (1999).

[61] *Semiconductors and Semimetals*, edited by R. K. Willardson and A. C. Beer (Academic Press, New York and London, 1972), Vol. 8.

[62] P. Y. Yu and M. Cardona, *Fundamentals of semiconductors* (Springer, Berlin, 1996).

[63] G. Bastard, *Wave mechanics applied to semiconductor heterostructures* (Les Editions de Physique, Les Ulis, 1988).

[64] A. Sohmer, J. Off, H. Bolay, V. Härle, V. Syganow, J. S. Im, V. Wagner, F. Adler, A. Hangleiter, A. Dörnen, and F. Scholz, *GaInN/GaN heterostructures and quantum wells grown by metalorganic vapor-phase epitaxy*, MRS Internet J. Nitride Semicond. Res. **2**, 14 (1997).

[65] F. Scholz, A. Sohmer, J. Off, V. Syganow, A. Dörnen, J. S. Im, A. Hangleiter, and H. Lakner, *In incorporation efficiency and composition fluctuations in MOVPE grown GaInN/GaN hetero structures and quantum wells*, Mat. Sci. Eng. B **50**, 238 (1997).

[66] A. Sohmer, *Herstellung und Untersuchung von GaInN/GaN-Quantenfilmen*, Master's thesis, Universität Stuttgart, 1997.

[67] J. Off, A. Kniest, C. Vorbeck, F. Scholz, and O. Ambacher, *Influence of buffer layers on the In content of GaInN layers*, J. Crystal Growth **195**, 286 (1998).

[68] S. Nakamura, T. Mukai, and M. Senoh, *Candela-class high brightness InGaN/AlGaN double-heterostructure blue-light-emitting diodes*, Appl. Phys. Lett. **64**, 1687 (1994).

[69] S. Nakamura, M. Senoh, S.-I. Nagahama, N. Iwasa, T. Yamada, T. Matsushita, H. Kiyoku, and Y. Sugimoto, *InGaN-based multi-quantum-well-structure laser diodes*, Jpn. J. Appl. Phys. **35**, L74 (1996).

[70] J. S. Im, *Zeitaufgelöste Untersuchungen zur Rekombination von Ladungsträgern in (AlGaIn)N*, Master's thesis, Universität Stuttgart, 1996.

[71] D. G. Thomas, J. J. Hopfield, and W. M. Augustyniak, *Kinetics of radiative recombination at randomly distributed donors and acceptors*, Phys. Rev. **140**, A202 (1965).

[72] A. Satake, Y. Masumoto, T. Miyajima, T. Asatsuma, F. Nakamura, and M. Ikeda, *Localized exciton and its stimulated emission in surface mode from single-layer $In_xGa_{1-x}N$*, Phys. Rev. B **57**, R2041 (1998).

[73] P. Perlin, C. Kisielowski, V. Iota, B. A. Weinstein, L. Mattos, N. A. Shapiro, J. Kruger, E. R. Weber, and J. Yang, *InGaN/GaN quantum wells studied by high pressure, variable temperature, and excitation power spectroscopy*, Appl. Phys. Lett. **73**, 2778 (1998).

[74] D. A. B. Miller, D. S. Chemla, T. C. Damen, A. C. Grossard, W. Wiegmann, T. H. Wood, and C. A. Burrus, *Band-edge electroabsorption in quantum well structures: the quantum-confined stark effect*, Phys. Rev. Lett. **53**, 2173 (1984).

[75] D. A. B. Miller, D. S. Chemla, T. C. Damen, A. C. Grossard, W. Wiegmann, T. H. Wood, and C. A. Burrus, *Electric field dependence of optical absorption near the band gap of quantum-well structures*, Phys. Rev. B **32**, 1043 (1985).

[76] H.-J. Polland, L. Schultheis, and J. Kuhl, *Lifetime enhancement of two-dimensional excitons by the quantum-confined Stark effect*, Phys. Rev. Lett. **55**, 2610 (1985).

[77] D. L. Smith and C. Mailhot, *Optical properties of strained-layer superlattices with growth axis along [111]*, Phys. Rev. Lett. **58**, 1264 (1987).

[78] E. A. Caridi, T. Y. Chang, K. W. Goossen, and L. F. Eastman, *Direct demonstration of a misfit strain-generated electric field in a [111] growth axis zincblende heterostructure*, Appl. Phys. Lett. **56**, 659 (1990).

[79] R. L. Tober and T. B. Bahder, *Determining the electric field in [111] strained-layer quantum wells*, Appl. Phys. Lett. **63**, 2369 (1993).

[80] D. Sun and E. Towe, *Strain-Generated Internal Fields in Pseudomorphic (In, Ga)As/GaAs Quantum Well Structures on $\{111\}$ GaAs Substrates*, Jpn. J. Appl. Phys. **33**, 702 (1994).

[81] M. P. Halsall, J. E. Nicholls, J. J. Davies, B. Cockayne, and P. J. Wright, *CdS/CdSe intrinsic Stark superlattices*, J. Appl. Phys. **71**, 907 (1992).

[82] C. Gemmer, *Ortsaufgelöste Spektrosopie zu Verspannungen und Kompositionsfluktuation in Gruppe-III-Nitriden*, Master's thesis, Universität Stuttgart, 1998.

[83] O. Gfrörer, *Konsequenzen von Verspannung und Symmetrie in Gruppe-III-Nitriden*, Ph.D. thesis, Universität Stuttgart, 2000.

[84] A. Kozanecki, C. Jeynes, B. J. Sealy, W. Jantsch, S. Lanzerstorfer, W. Heiß, and G. Prechtl, in *Silicon carbide, III-nitrides and related materials*, Vol. 264-268 of *Material Science Forum*, edited by G. Pensl, H. Morkoç, B. Monemar, and E. Janzén (Trans Tech Publications, Switzerland, 1998), pp. 501–504.

[85] M. Giehler, M. Ramsteiner, O. Brandt, H. Yang, and K. Ploog, *Optical phonons of hexagonal and cubic GaN studied by infrared transmission and Raman spectroscopy*, Appl. Phys. Lett. **67**, 733 (1995).

[86] Y.-H. Cho, J. J. Song, S. Keller, M. S. Minsky, E. Hu, U. K. Mishra, and S. P. DenBaars, *Influence of Si doping on characteristics of InGaN/GaN multiple quantum wells*, Appl. Phys. Lett. **73**, 1128 (1998).

[87] M. S. Minsky, S. B. Fleischer, A. C. Abare, J. E. Bowers, E. L. Hu, S. Keller, and S. P. DenBaars, *Characterization of high-quality InGaN/GaN multiquantum wells with time-resolved photoluminescence*, Appl. Phys. Lett. **72**, 1066 (1998).

[88] O. Madelung, *Grundlagen der Halbleiterphysik* (Spinger-Verlag, Berlin, 1970).

[89] B. Daudin, J. L. Rouvière, and M. Arlery, *Polarity determination of GaN films by ion channeling and convergent beam electron diffraction*, Appl. Phys. Lett. **69**, 2480 (1996).

[90] F. A. Ponce, C. G. Van de Walle, and J. E. Northrup, *Atomic arrangement at the AlN/SiC interface*, Phys. Rev. B **53**, 7473 (1996).

[91] M. Seelmann-Eggebert, J. L. Weyher, H. Obloh, H. Zimmermann, A. Rar, and S. Porowski, *Polarity of (00.1) GaN epilayers grown on (00.1) sapphire*, Appl. Phys. Lett. **71**, 2635 (1997).

[92] E. S. Hellman, *The polarity of GaN: a critical review*, MRS Internet J. Nitride Semicond. Res. **3**, 11 (1998).

[93] J. L. Rouviere, J. L. Weyher, M. Seelmann-Eggebert, and S. Porowski, *Polarity determination for GaN films grown on (0001) sapphire and high-pressure-grown GaN single crystals*, Appl. Phys. Lett. **73**, 688 (1998).

[94] R. Gaska, J. W. Wang, A. Osinski, A. D. Bykhovski, and M. S. Shur, *Piezoeffect and gate current in AlGaN/GaN high electron mobility transistors*, Appl. Phys. Lett. **71**, 3673 (1997).

[95] R. Gaska, J. W. Wang, A. D. Bykhovski, M. S. Shur, V. V. Kaminski, and S. M. Soloviov, *Piezoresistive effect in GaN-AlN-GaN structures*, Appl. Phys. Lett. **71**, 3817 (1997).

[96] M. Smith, J. Y. Lin, H. X. Jiang, A. Khan, Q. Chen, A. Salvador, A. Botchkarev, W. Kim, and H. Morkoç, *Exciton-phonon interaction in InGaN/Gan and GaN/AlGaN multiple quantum wells*, Appl. Phys. Lett. **70**, 2882 (1997).

[97] C. Wetzel, T. Takeuchi, S. Yamaguchi, H. Katoh, H. Amano, and I. Akasaki, *Optical band gap in* $Ga_{1-x}In_xN$ *(*$0 < x < 0.2$*) on GaN by photoreflection spectroscopy*, Appl. Phys. Lett. **73**, 1994 (1998).

[98] C. A. Parker, J. C. Roberts, S. M. Bedair, M. J. Reed, S. X. Liu, and N. A. El-Masry, *Determination of the critical layer thickness in InGaN/GaN heterostructures*, Appl. Phys. Lett. **75**, 2776 (1999).

[99] T. Mukai, K. Takekawa, and S. Nakamura, *InGaN-based blue light-emitting diodes grown on epitaxially laterally overgrown GaN substrates*, Jpn. J. Appl. Phys. **37**, L839 (1998).

[100] T. Takeuchi, C. Wetzel, S. Yamaguchi, H. Sakai, H. Amano, and I. Akasaki, *Determination of the piezoelectric field in strained GaInN quantum wells using the quantum-confined Stark effect*, Appl. Phys. Lett. **73**, 1691 (1998).

[101] J. W. Orton and C. T. Foxon, *Group III nitride semiconductors for short wavelength light-emitting devices*, Rep. Prog. Phys. **61**, 1 (1998).

[102] G. Martin, A. Botchkarev, A. Rockett, and H. Morkoç, *Valence-band discontinuities of wurtzite GaN, AlN, and InN heterojunctions measured by x-ray photoemission spectroscopy*, Appl. Phys. Lett. **68**, 2541 (1996).

[103] S. D. Lester, F. A. Ponce, M. G. Craford, and D. A. Steigerwald, *High dislocation densities in high efficiency GaN-based light-emitting diodes*, Appl. Phys. Lett. **66**, 1249 (1995).

[104] W. Shockley and W. Read, *Statistics of the recombination of holes and electrons*, Phys. Rev. **87**, 835 (1952).

[105] R. Hall, *Electron-hole recombination in germanium*, Phys. Rev. **87**, 387 (1952).

[106] R. B. Schwarz, K. Khachaturyan, and E. R. Weber, *Elastic moduli of gallium nitride*, Appl. Phys. Lett. **70**, 1122 (1997).

[107] A. Polian, M. Grimsditch, and I. Grzegory, *Elastic constants of gallium nitride*, J. Appl. Phys. **79**, 3343 (1996).

[108] I.-H. Tan, G. L. Snider, L. D. Chang, and E. L. Hu, *A self-consistent solution of Schrödinger-Poisson equations using a nonuniform mesh*, J. Appl. Phys. **68**, 4071 (1990).

Danksagung

An dieser Stelle möchte ich mich bei allen bedanken, die zum Gelingen dieser Arbeit beigetragen haben. Mein Dank gilt:

Prof. Dr. M. Pilkuhn für die Aufnahme am 4. Physikalischen Institut der Universität Stuttgart.

Prof. Dr. A. Hangleiter für die Betreuung, die wertvolle Unterstützung und die vielen Anregungen.

Prof. Dr. E. O. Göbel für die Übernahme des Mitberichts.

Holger Kollmer für die vielen guten Beiträge während seiner Diplomarbeit.

den Mitgliedern der Arbeitsgruppe Optoelektronik für die gute Zusammenarbeit und das freundlichen Arbeitsklima, namentlich Elvira Fehrenbacher, Thomas Forner, Gerd Frankowski, Christian Gemmer, Oliver Gfrörer, Sabine Heppel, Frank Hitzel, Christine Knorr, Peter König, Stephan Krämer, Achim Moritz, Thomas Riedl, Holger Seitz, Tim Schlüsener, Anja Weber, Ulf Wilhelm, Ralf Wirth, Martin Zimmermann.

Dr. Ferdinand Scholz, Jürgen Off, Bertram Kuhn, Volker Härle, Helmut Boley, Arno Kniest, Andreas Sohmer, Frank Steuber, Elli Lux und den übrigen Mitarbeitern im Kristallabor für die hervorragende Kooperation.

allen nicht genannten wissenschaftlichen und technischen Mitarbeitern des 4. Physikalischen Instituts der Universität Stuttgart und des Instituts für Technische Physik der Technischen Universität Braunschweig.

dem Deutschen Akademischen Austauschdienst für das Stipendium während meiner Promotion.

meinen Eltern für die unermüdliche und vielfältige Föderung meiner Ausbildung.